UiT The Arctic University of Norway

Faculty of Health Sciences
Department of Clinical Medicine

Hippocampal plasticity

Development of connectivity and growth hormone modulation of place cells and behavior

–

Kamilla G. Haugland

A dissertation for the degree of Philosophiae Doctor, March 2021

Abstract

The hippocampus has an incredible capacity for plasticity. Adaptation to the ever-changing world is essential for survival, and the brain is tuned to acquire new information and remember events that differ from previous experiences. The developing brain displays the greatest form of plasticity as the numbers of new neurons and projections drastically increase. Nevertheless, the information conducted between synapses can be adjusted by synaptic plasticity throughout the lifetime. In this way, important memories get strengthened while irrelevant memories get weakened. Still, the various mechanisms behind hippocampal plasticity is not fully understood. In this thesis, I present three reports in which I describe factors that cause hippocampal plasticity at three different levels; connections, neural firing and behavior, and during two distinct temporal stages; postnatal development and in the adult. In the first study, I described the development and topography of projections from the hippocampus and the parahippocampus (PHR) to the retrosplenial cortex (RSC) in Long Evans rat pups. Taking advantage of traditional tracing techniques, I showed that the first projections were present at birth, and that the density became adult-like during the second week of age. These projections displayed a stable topography throughout the two postnatal weeks. The results of paper 1 suggest that the projections are experience-independent, depending on genetic factors. In the remaining part of the thesis, I explored the impact of the local neuromodulator growth hormone (GH) in the hippocampus of adult Long Evans rats. To alter the GH levels, I used adeno-associated viruses (AAV)s with GH or antagonizing GH (aGH), the latter to block the GH receptor. In the second paper, utilized behavioral approaches and showed that GH enhanced memory performance in a spontaneous recognition task (SLR), and increased the spine density on apical dendrites of CA1. aGH impaired the performance in the Morris water maze task and reduced the spine density. In the third paper, I recorded single-units and found that GH tended to increase global remapping in the CA1 during exploration of a novel environment, while aGH impaired remapping events. The results from papers 2 and 3 suggest that GH enhances hippocampal plasticity by increasing sensitivity for novel sensory inputs while decreasing interference of similar memories. In summary, I report that hippocampus is a flexible brain structure which utilizes various forms of plasticity approaches. Revealing the factors that causes alteration in the hippocampal plasticity is essential for understanding the mechanisms not only behind memory deficiency, but also for normal development and ageing.

Acknowledgements

This PhD thesis includes three projects. The first project was carried out at the Kavli Institute for Systems Neuroscience and Centre for Neural Computation at the Norwegian University of Science and Technology (NTNU). The second project was performed at the The University of Tromsø (UiT) - The Artic University of Norway, and the third project was conducted at UiT and the University of Bergen (UiB). Vegard H. Brun has been my main supervisor and Kirsten B. Kjelstrup has been my co-supervisor.

First of all I would like to express my gratitude to Vegard and Kirsten for the opportunity to work in this highly intriguing field of research. I am deeply grateful for all the guidance and scientific advices you have given me, and the strong support regardless of unforeseen challenges and for cultivating scientific independence. Thank you Menno Witter and Jørgen Sugar for your guidance and sharing your expertise. I also want to thank Janne Grønli, Anne Marie Kinn Rød and Nina Harkestad for letting me finish my animal experiments at your research facility at UiB when UiT could not provide me one. I further would like to thank all the other co-authors, Anniken Olberg, Andreas Lande and Erik Knutsen. It has been a great joy working with you.

I would like to thank May-Britt and Edward Moser, and Stefan and Jill Leutgeb, for research stays at your respective laboratories and working with your research groups, and Marta Sabariego, Ingvild Ulsaker-Janke and Nenitha Dagslott for technical advises. Also, thank you Marianne Fyhn, Tokrel Hafting and Alexander Stasik, for collaborative work. Thank you, Kii Goosen for kindly providing us with viruses used in the second and third paper. I am very grateful to all the members and alumni associated with the research group for Neurobiology at UiT, including Angel Moldes, Lorenzo Ragazzi, Fanny Stette, Håvard Marsteen, Mathias Greve Johannessen and Roy Heijkoop. Especially thanks to Angel, Fanny and Mathias for your amazing work during additional research projects. I am also grateful for sharing this PhD journey with you, Lorenzo, my PhD colleague, with travels to conferences, summer schools and research stays in Norway and abroad. Also, thank you Olivia Le Moene, it has been a great joy to work in the animal facility in the room next to you, and all the travels for work, or for desperately needed breaks from work, have been very much appreciated. Lastly, I would like to thank my family and friends for your everlasting support, patient and understanding during these years. Especially to you William, this thesis is dedicated to you.

List of papers

Paper 1

Haugland, K.G, Sugar, J., Witter, M.P.
Development and topographical organization of projections from the hippocampus and parahippocampus to the retrosplenial cortex

European Journal of Neuroscience, March 2019, doi: 10.1111/ejn.14395.

Paper 2

Haugland, K.G., Olberg, A., Lande, A., Kjelstrup K.B., Brun, V.H.
Hippocampal growth hormone modulates relational memory and the dendritic spine density in CA1

Learning and Memory, January 2020, doi: 10.1101/lm.050229.119.

Paper 3

Haugland, K.G, Knutsen, E., Kjelstrup, K.B., Brun, V.H.
Growth hormone modulates remapping in the hippocampal area CA1

Manuscript

Abbreviations

Brain regions

- CA, Cornu ammonis
- EC, Entorhinal cortex
- HF, Hippocampal formation
- EC, Entorhinal cortex
- MEC, Medial entorhinal cortex
- LEC, Lateral entorhinal cortex
- RSC, Retrosplenial cortex
- SUB, Subiculum
- PaS, Parasubiculun
- PHR, Parahippocampal region / Parahippocampus
- PER, Perirhinal
- POR, Postrhinal
- PrS, Presubiculum

Molecules and solutions

- AAV, Adeno-associated virus
- ACh, Acetylcholin
- aGH, antagonizing Growth hormone
- AMPA-R, α-amino-3-hydroxy-5-methyl-4-isoxazolepropionic acid receptors
- BDA, Biotinylated dextran amine
- BDNF, Brain-derived neurotrophic factor
- cDNA, complementary deoxyribonnuclei acid
- CMV, Cytomegalovirus
- DA, Dopamine
- DNA, Deoxyribonnuclei acid
- GFP, Green fluorescent protein
- GH, Growth hormone
- NE, Norepinephrine
- IGF, Insulin-like growth factor
- IRES, Internal ribosome entry site
- NMDA-R, N-methyl-D-aspartate receptor
- p-Stat5, phosphorylated Signal and Transducer of activation 5
- PBS, Phosphate-buffered saline
- PFA, Paraformaldehyde
- RNA, Ribonnuclei acid
- 5-HT, Serotonin

Terms and tasks

- LFP, Local field potential
- LTP, Long-term potentiation
- SLR, Spontaneous recognition task
- SWS, Slow wave sleep
- SWR, Sharp wave ripple
- RT-qPCR, Real-time polymerase chain reaction

Morris Water maze, platform positions

- SW, south west
- SE, South east
- NW, North west
- NE, North east

Contents

Introduction

The complexity of the mind has fascinated people for millennia. In the fifteenth century BC, the old Egyptians noticed that brain functions could be encountered based on abnormal behavior of individuals with cognitive impairments [1]. 1100 years later, Hippocrates claimed that the study of the mind begins with the study of the brain [2]. Today, after major advancements in both science and technology, we have a deeper understanding about the brain. During the evolution, the brain has changed dramatically on demands from environmental conditions, resulting in brains of different sizes and functions between species [3, 4]. Although the humans might be proved of having a large brain compared to the body size, one could easily be surprised by the functions of smaller brains, knowing that even a single-cell eukaryote can initiate a complex behavior sequence [5]. The human brain is unsurprisingly more complex, with neural networks of more than 100 billion individual neurons interconnected in systems of neural circuits. The capacity of behavioral sequences in the human brain is therefore enormous, and generated by the interplay of cells with multiple neuronal pathways [6].

As we can imagine, the human brain is different from a rat brain, but still, we share similarities. Critical regions have been conserved in both species during the evolutions, especially the hippocampus. Nevertheless, it does not mean that the hippocampus is identical between humans and rats. Although the intrinsic circuitry remain conserved, the size and extrinsic connectivity have evolved differently [7].

Still, the brain is exceedingly more complex. The evolution is not the only factor contributing to changes in the brain as it keeps developing and refining within each living organism. The brain is exceptionally plastic during development and it retains the ability to modify its processes throughout the lifetime. The brain keeps changing at various levels, including synapses, cells, connections, which in turn can change the behavior [8]. As the hippocampus is critical for memory and learning, the capacity of being plastic is a key mechanism for the hippocampal function. Despite years of research, knowledge about the various factors contributing to hippocampal plasticity remain elusive. In this thesis, I present three reports involving distinct aspects of plasticity in the hippocampus, concerning developing **connections**, and how the adult hippocampal circuits respond to neuromodulation by growth hormone (GH) on a **cellular** and **behavioral** level.

The cognitive map

One of the most influential researchers in cognitive science was the brilliant psychologist, Edward Tolman. Tolman proposed that the complexity an animal's behavior is a result of a cognitive map, an integrative learning system that allows the animal to refine its previous experiences in order to compute prediction about the future [9]. His ideas were quite controversial at the time, as Kant had laid out his theory of the "pre-structured brain organization". It was thus commonly accepted that the behavioral outcome was determined by a single input - output pathway (stimulus-response associations), and not that a stimulus could become associated with other stimuli to form what Tolman called "sign-gestalts" or cognitive maps [10]. Tolman related his findings to human behavior, and argued that cognitive maps required flexibility in order to adapt to changes in the environment [11]. In his paper "Cognitive Maps in Rats and Men", Tolman described a link between the cognitive map and the spatial map. He noticed when rats had learned to traverse a meandering maze route, the animals would find the correct shortcut when presented with several alternative routes, even if the rats had never visited that space before. Tolman argued that the animals managed this task because of the representation of space in their mind, a cognitive map, from which the shortcut could be computed. The rats could therefore find relationships between events and predict the consequences of their actions [11].

Only five years after Tolman published his theories about the cognitive maps, a man known as patient HM (Henry Molaison) underwent an experimental brain surgery that made him one of the most famous patients in the field of neuroscience [12]. HM suffered from severe epileptic seizures and had his medial temporal lobes bilaterally removed. Unexpectedly, the surgery resulted in a striking loss of recent memories, rendering HM unable to remember new information (global anterograde amnesia). HM forgot daily events nearly as fast as they occurred, but without any deficits his intelligence or perception. Although HM could no longer make new memories, he could learn various skills such as mirror drawing and motor skills at a normal rate [13, 14]. The reports of the patient HM intrigued researchers to conduct further studies about the functions of the medial temporal lobe. Several experiments utilizing various model systems, including rodents, non-human primates and human patients, have demonstrated evidence for dense amnesia as a result of medial temporal lobe damage [15, 16].

There are multiple memory systems in the brain which can be divided into declarative (conscious) and non-declarative memory (unconscious) [17]. HM suffered from amnesia due to

impairments in the declarative memory, which includes recall or recognition of places, lists, faces, melodies and other materials. The non-declarative memory system was not affected in HM, which includes probabilistic classification learning, perceptual-motor skill learning, and tasks that assess the ability to gain knowledge based on series of exemplars, like artificial grammar learning [17, 18].

Hippocampus

One particular region of interest in the medial temporal lobe is the hippocampus. Today it is commonly known that the hippocampus is critical for the declarative memory system, with functions such as memory, navigation and cognition [19]. Concerning the memory functions, the hippocampus serves a critical role in encoding, consolidation and retrieval of long-term memories. Studies involving hippocampal lesion patients have revealed the importance of the hippocampus in so-called relational memories, which are memories that stores information about complex combination of stimuli or states [20]. ts long, curved form is present across all mammalian orders and runs along a dorsal (septal)-to-ventral (temporal) axis in rodents, corresponding to a posterior-to-anterior axis in humans

In order to understand the mechanisms behind the hippocampal memory system, the anatomy of the hippocampal region must be kept in mind. The hippocampus is a long, curved structure that runs along the dorsal-to-ventral axis in the rodents, which corresponds to the posterior-to-anterior axis in the humans[7]. In the rodents, the hippocampus consists of the subiculum (SUB), dentate gyrus (DG) and the Cornu Ammonis (CA)1, CA2 and CA3. These subregions are interconnected in a diligent manner (Figure 1). In the traditional and simplified view, the DG granule cells projects by its Mossy fibers to the proximal dendrites of the CA3 pyramidal cells. The CA3 projects to the proximal dendrites of the pyramidal cells of CA1 by its Schaffer collaterals, and in turn, CA1 projects the hippocampal information to cortical and subcortical targets, either directly or indirectly through the SUB[7, 21]. The hippocampus is interconnected with its neighboring region, the parahippocampal region (PHR), consisting of presubiculum (PrS), parasubiculum (PaS), entorhinal cortex (EC), postrhinal cortex (POR) and perirhinal cortex (PER)[22]. EC is the main source of information to the hippocampus, with either inputs to the distal apical dendrites of the CA1, or to the outer two-thirds of the molecular layer of the DG[23]. The medial part of the EC (MEC) is suggested to provide spatial information (*spatial* context of an experience) to the hippocampus, while the lateral EC (LEC)

is believed to send object information (information about the *content* of an experience) to the hippocampus[24]. The information from MEC and LEC target separately parts of DG[23] which together with CA3 integrates the polymodal sensory information[21, 25]. While DG is important for distinguishing similar events or memories[26], the CA3 is suggested to combine the representation about "where" and "what" into an associative network, allowing memories to be recalled and brought to consciousness when represented with only partial cues [27].

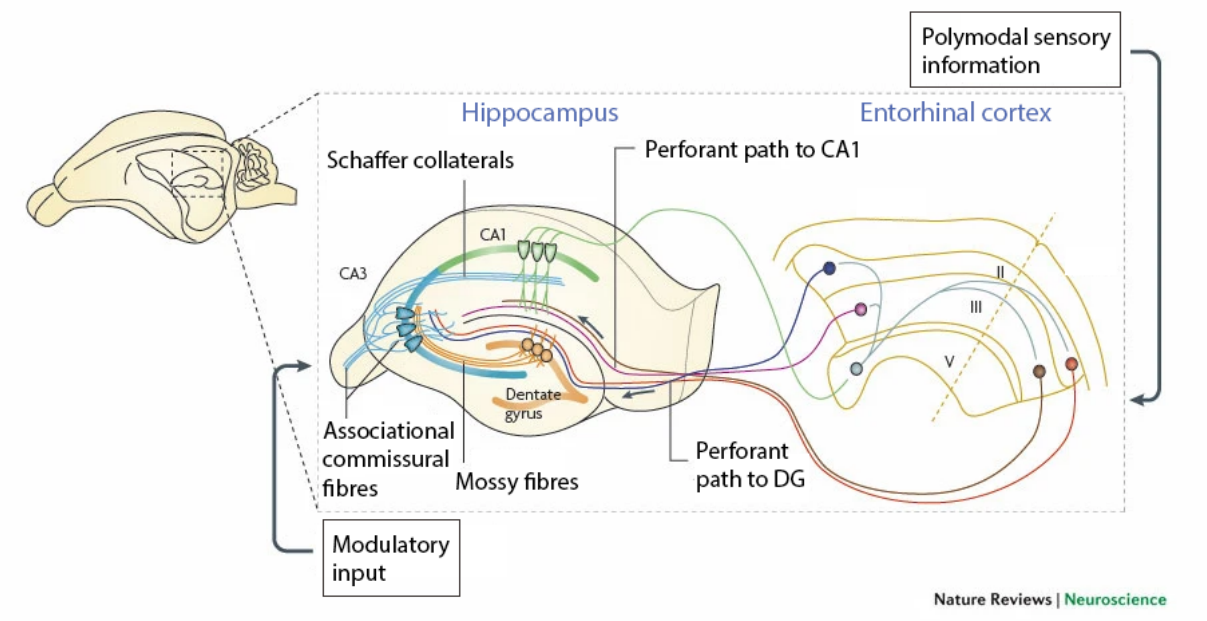

Figure 1. Hippocampal circuitry. The traditional trisynaptic loop consist of the Perforant path carrying polymodal sensory information from entorhinal cortices (EC) layer II to the dentate gyrus (DG) by, which subsequently target CA3 by mossy fibers, and further to CA1 through Schaffer collaterals. Sensory information can also reach CA1 directly from EC layer III. Hippocampus also receives modulatory inputs which modulate the signaling processes (modified from ref[22]).

The retrosplenial cortex (RSC), also known as the Brodmann areas A29 and A30, is one of the major target regions of the hippocampal projections, and in turn, RSC projects information to the PHR [28-31], and share similar functions to the hippocampus, including spatial memory and navigation [32-34]. The function of some of the projections from the hippocampus and PHR to the RSC has recently been studied. Although the MEC-RSC projection do not seem to be involved in remote memory processes[35], recent evidence shows that RSC receives sharp wave ripples (SWR) from SUB. Since SWR is associated with memory consolidation, [36] this projection might be important concerning long-term memory storage.

Developmental connectivity

The development and maturation of hippocampal connections involves different processes, including activity-dependent maturation of synaptic plasticity, local circuitry formation, myelination and the generation of intrinsic and extrinsic connectivity [37]. An important aspect of developmental connectivity is whether the projections are experience-induced or not.

One of the earliest studies concerning experienced-based plasticity was reported by Wesel & Hubel in 1965. The authors described the importance of a functional neural circuit during development using a kitten. They discovered that if they kept one of the eyes closed after birth, and kept it closed for a few months, the vision of the kitten was compromised when the eye was reopened. The loss of spatial vision when the eye did not receive visual stimuli indicates that there is a critical time period during development [38].

Further studies have focused on the development of the memory system. In humans, the development of memories can be investigated using functional resonance imaging (fMRI). In the fMRI, a clear age-related increase in memory formation has been found in the posterior portion of the medial temporal lobe [39], showing that the hippocampal memory is expressed relatively late during the development. Contextual long-term memories can be retained around the age of 3 years in humans, while around postnatal (P) day 21 in rats [40, 41]. The hippocampus undergoes extension of postnatal structures as well as functional maturation [41], which occur in parallel, suggesting that the functional competence of the hippocampal memory and the structural maturation are co-dependent [42].

In the rat, evidence suggests that the hippocampus is interconnected with PHR from birth, and that these connections mature during the first two postnatal weeks [43-45]. The PHR contains spatially modulated cells, like the head direction cells. The presence of functional head-direction cells is in parallel with this structural development of connectivity, as the head-direction cells suggested to be functionally before eye-opening at P14-P15 [46]. The head direction cells are highly specialized neurons that fire only when the animal faces a certain range of directions in the horizontal plane [47], and can be found in the PHR of PrS, PaS and MEC, but also in RSC [48]. Interestingly, the development of projections from the RSC to the PHR is adult-like before eye-opening [29], however, the development of projections from the hippocampus and PHR to the RSC is unknown.

The first paper aim to investigate the development of projections in the hippocampal network, more precisely the projections from the hippocampus and parahippocampus to the RSC.

Modulation by the growth hormone

The neural processes of the hippocampal circuits can be modulated by substances known as neuromodulators [49-51]. Neuromodulation is an important feature of hippocampal plasticity as it assures flexibility in the neural circuit operations. Individual neuromodulators can exert divergent actions on single neurons by targeting multiple physiological mechanisms [50, 52, 53].

Various neuromodulators, like acetylcholine (ACh), serotonin (5-HT), dopamine (DA), and norepinephrine (NE), are known to modulate hippocampal signaling processes [54, 55]. However, a neuromodulator which has received less attention is the GH. GH is a peptide hormone that is commonly known for its effects on somatic growth. The anterior pituitary gland secrets GH into the blood stream to promote growth and metabolism in peripheral tissues [56], but GH can exert functions in the brain too [57-62]. GH is capable of crossing the blood brain barrier [63] and receptors for GH are distributed over the central nervous system, in brain regions such as the hippocampus [58, 59]. Evidence over the past few years has found GH to functionally influence regions such as the hippocampus, amygdala, and hypothalamic areas related to hormone regulation [64-68]. Reports from human research have revealed that patients with GH-deficiency experience memory impairments [69, 70]. In spite of the evidence suggesting that GH modulates critical functions in the central nervous system, GH seems to be overlooked in the literature as a neuromodulator in the hippocampus.

As the secretion of GH from the anterior pituitary decreases with age [71], one might wonder if GH has a role in the memory impairments seen in the elderly population. In agreement with this hypotheses, GH is mainly secreted during the onset of sleep during slow wave sleep (SWS), which is of particular interest when it comes to hippocampal memory with SWR events. During SWR, experiences and memory representations acquired during the encoding are transferred from a temporary state in the hippocampus to a long-term storage in the cortex. This reorganization process is referred to as consolidation, and is essential for stabilizing the memory over time as it gets more resistant to interference or disruption [72]. As sleep and GH secretion is related, Kim et al [66] investigated the impact of GH on memory performance after sleep depression. They described that systemically administrated GH rescued the plasticity in

the hippocampus [66]. Taken together, GH might be involved in the modulation of consolidation processes in the hippocampus.

How GH exerts its action in the hippocampus remain elusive. However, research over the last few years have provided more information about plausible mechanisms of actions [65-67, 73-78]. It is currently known that GH increases the levels of IGF-I and IGF-II, each of them with distinct effects in the hippocampus. IGF-I plays a role in adult neurogenesis [62] while IGF-II mediates spine formation [79]. Furthermore, the mechanisms of GH seems to be related to the N-methyl-D-aspartate (NMDA) receptor and synaptic transmission (Figure 2). Exogenous GH increases the expression of the NMDA subunit NR2B, thereby changing the NR2B/NR2A ratio [80] which impacts the function of the receptor. Acute GH application in CA1 brain slices enhances both the NMDA and the AMPA receptor field excitatory postsynaptic transmission in young and old rats [74-76]. GH seems therefore to be a potent neuromodulator which can modulate synaptic plasticity in the hippocampus.

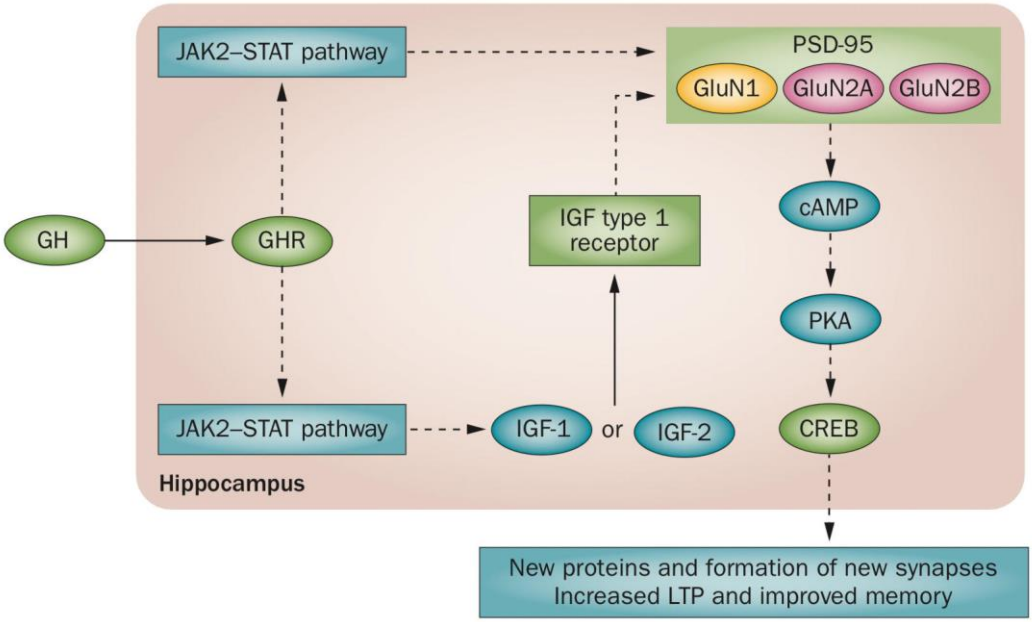

Figure 2. Potential signaling cascades as results of GH receptor activation, leading to increased hippocampal memory. First GH binds to its GH receptor, and then directly or via IGFI or IGFII, JAK2-STAT pathway results in activation of genes related to the NMDA receptor-PSD-95 complex to enhance LTP (From ref [57]).

A key question has been whether the effects of GH has been due to the secretion of GH from the anterior pituitary, or if the effects are caused by a possible local production of GH within the hippocampus. Ground-breaking knowledge came from studies using the Ames Dwarf mice with impaired GH production in the anterior pituitary. These mice do not have GH in the peripheral organs, however, their hippocampi contain high levels of GH, even higher than in normal mice [81]. The Ames Dwarf mice also perform better in a spatial memory task [82]. Consistent with these results, other studies have revealed that the hippocampus encounters its own production of GH [73, 83]. Subsequent experiments have been conducted with the aim to uncover the effects of hippocampal GH on the behavior, but these reports show conflicting results [67, 78, 84-88]. This could be explained by their use of methods, as these studies manipulate the GH concentration systemically, which can lead to numerous side-effects not mediated by the hippocampus.

The second paper aim to address how local GH in the hippocampus affect the memory performance.

The plasticity of place cells

One approach to investigate the hippocampal function is by examining the neural activity. In 1971, O´Keefe placed tetrodes in the rat hippocampus and made the remarkably discovery of so-called place cells, which are specialized neurons that fire at specific locations (place field) in the environment [89]. Following this revelation, other spatially modulated cell types have been revealed, supporting the view that the hippocampus creates a map of physical space and performs subsequent navigational strategies [90]. Still, the hippocampus is not solely dedicated to create spatial maps, as the hippocampal representation is not purely spatial. The hippocampus also represents nonspatial information, including time, events, objects, context and emotional values, suggesting a broader function of the hippocampus. Therefore, the hippocampus is proposed to be involved in learning relations between experiences and nonspatial features [91], which reflects the capacity of plasticity in the hippocampal network.

The hippocampal circuit has been the hub for plasticity studies since the discovery of long-term potentiation (LTP) by Bliss and Lømo[92]. By performing electrophysiological studies in brain slices, they described a putative cellular mechanism for the storage of memories [92]. LTP

is associated with synaptic plasticity at appropriate synapses during memory formation [22]. The direct relationship between LTP and the hippocampus was described in 1998, when Kentros et al [93] showed that the NMDA receptor is not required for the initial formation of the place fields, but was necessary for long-term binding of the place cells map to a given environment [93].

Recent evidence suggests that artificial memory manipulations in rodents can alter hippocampal memories. Memories can be erased and reinstalled, as well as being created [22]. The concept is based on the postulate of Hebb, that cells that "fire together, wire together" [94]. In other words, the synapse between to cells can be strengthened when the cells are coactivated. This mechanism is suggested to be the neural substrate of memory, and has been demonstrated using LFP in pairs of cells in the hippocampus [95]. Studies looking at populations of cells in CA3-CA1 synapses have confirmed that the strongest connections between cells were those of populations of cells that fired together during memory and learning processes. This relationship between memory strength and synaptic connectivity therefore suggests that these factors together are necessary for creating memories [95].

A common approach to investigate the plasticity of hippocampus is to record the neural activity of place cells when the sensory information changes. Place cells can detect such changes and subsequently adjust their neural firing in a processes known as remapping [96]. In remapping, populations of place cells can fire at new locations in the environment, resulting in new positions of their place fields (global remapping). Global remapping can be observed when the environment changes substantially, like when an animal is visiting a novel room. However, if the sensory changes are more subtle, like when an animal is exploring a novel apparatus in the same room, rate remapping can be observed [97]. These remapping processes might be crucial for storing large amounts of similar experiences with minimal interference [98]. Various intrinsic states can adjust remapping, such as changes in sensory, motivational state or behavior context, can be modulated [96].

For instance, ageing can affect the intrinsic state of the hippocampus [99]. he place cells of the aged animals failed to remap (Figure 3)[99]. In other words, although the environment changed, the place cells of the aged rats did not signal the change. This evidence suggests that not only sensory information affects the hippocampal representation.

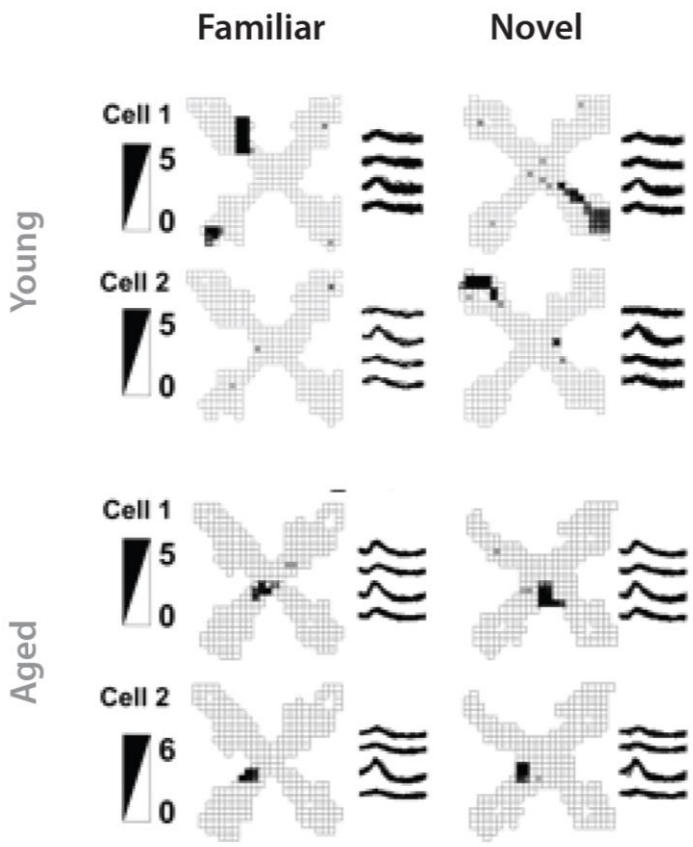

Figure 3. Place cells of young and aged animals recorded in CA3 during exploration of familiar and novel environments. While the place cells in young rats remap in a novel environment, the place cells of aged rats keep firing at the same location, failing to globally remap (modified from ref [99]).

Could then other factors affecting the intrinsic properties of the hippocampus change the neural signaling of the place cells? As reduced levels of GH is associated with ageing[71], could GH impact the place cell activity?

The third paper aim to investigate how the place cells respond to sensory changes when the hippocampal plasticity is modulated by the GH.

Objectives

The hippocampal circuits have remarkable capacity for structural reorganization and synaptic plasticity. New neurons and projections can be created through neurogenesis, and pre-existing circuits can me rewired and modified in their dendritic complexity and number of spines [37]. This ability, known as plasticity, is critical for early development and continues throughout life in response to behavioral conditions. Since the hippocampus is essential for integrating new information onto existing memory traces, deficits in the plasticity can have major consequences, including memory deficits and impaired spatial navigation. In this thesis, I present reports involving structural, cellular and behavioral changes in the hippocampus, investigating factors that causes alteration in the hippocampal circuits. The objectives of this thesis are thus threefold.

1. **Paper 1** aims to describe when the projections from the hippocampus and parahippocampus arrive at the RSC during the first two postnatal weeks. The paper also aims to address the topographical organization of these developing projections. Are the projections experience-dependent or predetermined by the genetics?
2. **Papers 2** aims to reveal the impact of GH on hippocampal memory. Is local GH modulation in the dorsal CA1 is sufficient to alter hippocampal-dependent memory in adult rats?
3. **Paper 3** aims to investigate the impact of local GH on hippocampal place cells in the dorsal CA1. Can place cell firing be modulated by GH when an animal explores a novel environment?

Synopsis of methods

In this thesis, I have used rats of the Long Evans strain. The well-being of the animals were of high concern and daily checked. In paper 1, I used rat pups which lived in a controlled environment (22 ± 1°C; humidity 60%; lights on from 8:00 p.m. to 8:00 a.m.) with their mother and litter mates. Food and water were available ad libitum. For paper 2 and 3, adult rats were used, which were housed pairwise in paper 2 and single-housed in paper 2 due to microdrive implants. The rats were kept in controlled environments (21± 1°C; humidity 55 ± 5 %; lights on from 7:00 p.m. to 7:00 a.m.). In paper 2, the food and water were provided ad libitum, while in paper 3 the animals in experiments received their daily amount of food (to maintain their weight) after the experiments were finished for the day. During the experiments, these animals were freely foraging for biscuits or choco loops. Water was always ad libitum in the home cage.

All of the experimental protocols followed the European Communities Council Directive and the Norwegian Experiments on Animals Act and local directives of the responsible veterinarian at the Norwegian University of Science and Technology (paper 1) / The University of Tromsø - The Artic University of Norway and The University of Bergen (paper 2 and 3).

Paper 1 | **Development and topographical organization of projections from the hippocampus and parahippocampus to the retrosplenial cortex**

In the first paper, a total of 69 female and male Long Evans rats were used, aged between postnatal day 0 (P0) and 15 (P15). In order to investigate the projections from the hippocampus and parahippocampus the RSC, both retrograde and anterograde tracers were used (Figure 4). I injected retrograde tracers in RSC at various rostrocaudal and dorsoventral position according to the age of the animal, manually adjusting the coordinates in parallel with data analysis of the injection sites of previously injected brains. I aimed to cover most of RSC for all the ages, having several injection sites in each age group. The tracers used were Fast Blue, Fluoro Gold, IX Retrobeads and Fluospheres 580/605. The tracers were pressure injected at the identified coordinates using hand-made micropipettes. In addition to retrograde tracers, 11 animals were used for anterograde tracing experiments with Biotinylated dextran amine (BDA) in SUB and PHR. The anterograde tracers were delivered through micropipettes using iontophoresis. After surgery, the pups were returned to their mother for 24 hours before perfusion. The animals were perfused with cold Ringer's solution followed by 4% solution of fresh PFA and 0.1 % glutaraldehyde for pups P0-P2. Brain were cut on a freezing microtome 40 µm thick in horizontal or sagittal sections. One series was used for Nissl staining while the next series were used for the analysis of the tracers. For the anterograde tracers, the sections underwent histochemistry against BDA. The sections were digitalized with a fluorescence and bright-field scanner. The projections were analyzed and illustrated using Panramic viewer and Adobe Photoshop and Illustrator, in addition to the Waxhom space (http://software.incf.org [101]).

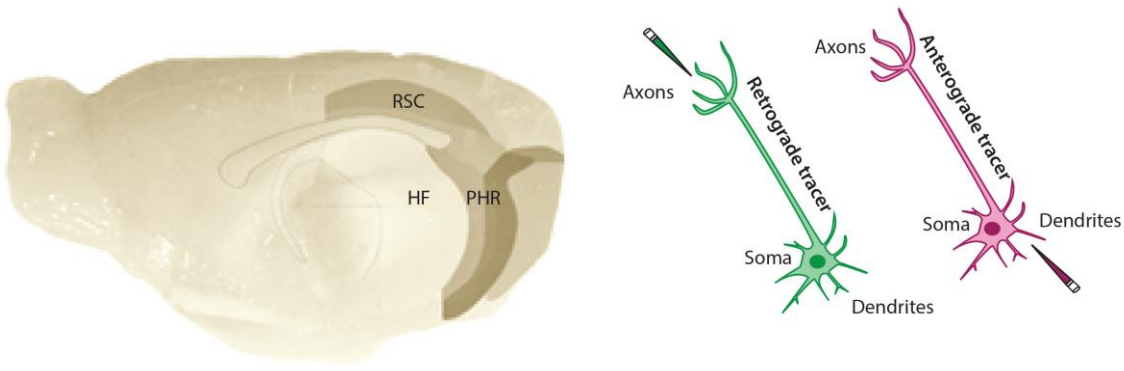

Figure 4. Retrograde and anterograde tracing: To the left, a rat brain in a sagittal view, marked with the regions of interest, the retrosplenial cortex (RSC), hippocampus (HF) and parahippocampal region (PHR), modified from [28]. To the right, neurons receiving either a retrograde tracer (green) or an anterograde tracer (pink).

Paper 2 | **Hippocampal growth hormone modulates relational memory and the dendritic spine density**

In the second paper, I used 44 adult male Long Evans rats to describe the behavioral effect of local GH in the hippocampus. I performed surgery on 37 of the animals and seven rats were left unoperated. 27 of the animals that underwent surgeries were used for behavioral assessments and subsequent phosphorylated Signal and Transducer of activation 5 (p-Stat5) immunohistochemistry, while the remaining 10 animals were devoted for spine analysis. During the surgery, the animal received either recombinant adeno-associated viruses (rAAV)s with GH, aGH or only green fluorescent protein (GFP) as controls (AAV-CMV-GH-IRES-GFP, AAV-CMV-aGH-IRES-GFP, AAV-CMV-IRES-GFP, respectively), in the dorsal CA1. The animals were subjected to behavioral tests after three weeks of incubation time, in order to let the hippocampal cells overexpress the proteins of interest.

During the third week of incubation, the animals were habituated to a 1 x 1 meter black box with a local cue card (15 min sessions for 5 days) while freely foraging for biscuits. Distal cues, like cabinets and doors, remained constant. After habituation, the rats participated in two versions of a hippocampal-dependent task known as the spontaneous recognition task (SLR)[102]. As rats naturally tend to explore novel object locations, and this behavior is hippocampal-dependent, we utilized this approach to assess the effects of GH on the hippocampal memory. In the first version of the SLR, rats explored the familiar box, while the second task involved a circular arena (90 cm in diameter with a local cue). Both of the tasks consisted of a sample phase and a test phase, with a delay of either 3 hours or 24 hours. In the sample phase, the animals were allowed to explore objects secured with blue-tack, while in the test phase the objects were replaced by new identical copies, and one of them placed in new locations.

In the sample phase of the box-version of the task (Figure 5), two identical objects were placed in two randomized corners of the box. In the test phase, one of the object locations was changed to a randomized location (novel location), while the other object was kept in the same corner (familiar location).

In circle-version of the task, the rats were first habituated to the novel circular arena for 10 min before entering the sample phase. The sample phase consisted of the exploration of three identical objects, A, B and C. Object A was located the farthest away from the other two objects, with either 120 or 40 degrees between object A and the other two objects. In the test

phase, only two identical copies of the objects were assessable. The object location for object A remained the same (familiar location), while B and C were merged into one location (novel location).

During the SLR tasks, the movement of the rats were recorded by a camera, and EthoVision XT 11.5 (Noldus) was used to track the animal's position and to manually score the object exploration. The object exploration was defined as the rat directing its nose towards an object with a distance of 2 cm or less, while standing on the object or looking elsewhere were not considered as object exploration. The exploration time with the objects was calculated by the discrimination ratio (difference in time spent with the novel object location and the familiar object location divided on the sum of the time spent with both of them).

Since these SLR tasks consisted of single-learning trials, we also wanted to investigate the impact of GH on the multi-trial Morris water maze task. 27 of the operated animals were trained in the Morris water maze task (in a pool, 2 m in diameter, filled with 50 cm opaque water, about 23 °C). We trained the rats for five consecutive days to find a submerged platform located south west (Figure 5). Each training day consisted of eight trials divided into two session with four trials each with a minimum of 3 hours apart. The first trial of the day was always a reinforcement probe trial, in which the platform location remained unable until 60 sec. For the other seven trials, the platform was kept available 1 cm underneath the opaque water. In the cases when the animals failed to locate the hidden platform within 120 sec, the animals were manually guided to the platform by the experimenter. The rats were put dry under a heating lamp after each training session. The overall memory performance was measured on day 6 during the probe test. All starting positions were counterbalanced across the trials.

To investigate memory flexibility, we put the animals back into the water maze for two more training days (day 12 and 13), after one week of rest (one week after last training). This time the platform location was changed to north east position, the quadrant opposite for the previous goal location. The new learning was assessed on the probe trial on day 14. A camera tracked the positon of the animals during the Morris water maze task, and the data was sampled using Dacq acquisition system (Axona Ltd). The performance in the task was calculated by measuring the mean latency to the platform location (sec), and occupancy maps were plotted as heat maps for visualization of the swimming path using MATLAB (Mathworks, Natick, MA).

The animals were then subjected to a balance test, in which the animals had to balance on a ruler (60 cm long, 3 cm broad) for max 1 minute to rule out possible motor or balance effects that could have affected the swimming in the Morris water maze.

After the experiments, the animals were perfused with physiological PBS and then 4 % PFA (pH 7.4). The brains were dissected and placed first in 4 % PFA before cryoprotective 2 % DMSO. The brains for spine analysis were perfused with ice-cold PBS only, and the brains were sectioned with 100 µm interval, while the rest of the brain sections were cut coronally with 40 µm thickness. I performed immunohistochemistry for GFP and p-Stat5, in addition to Nissl staining. The sections were analyzed and digitalized using bright-field, fluorescence and confocal microscope.

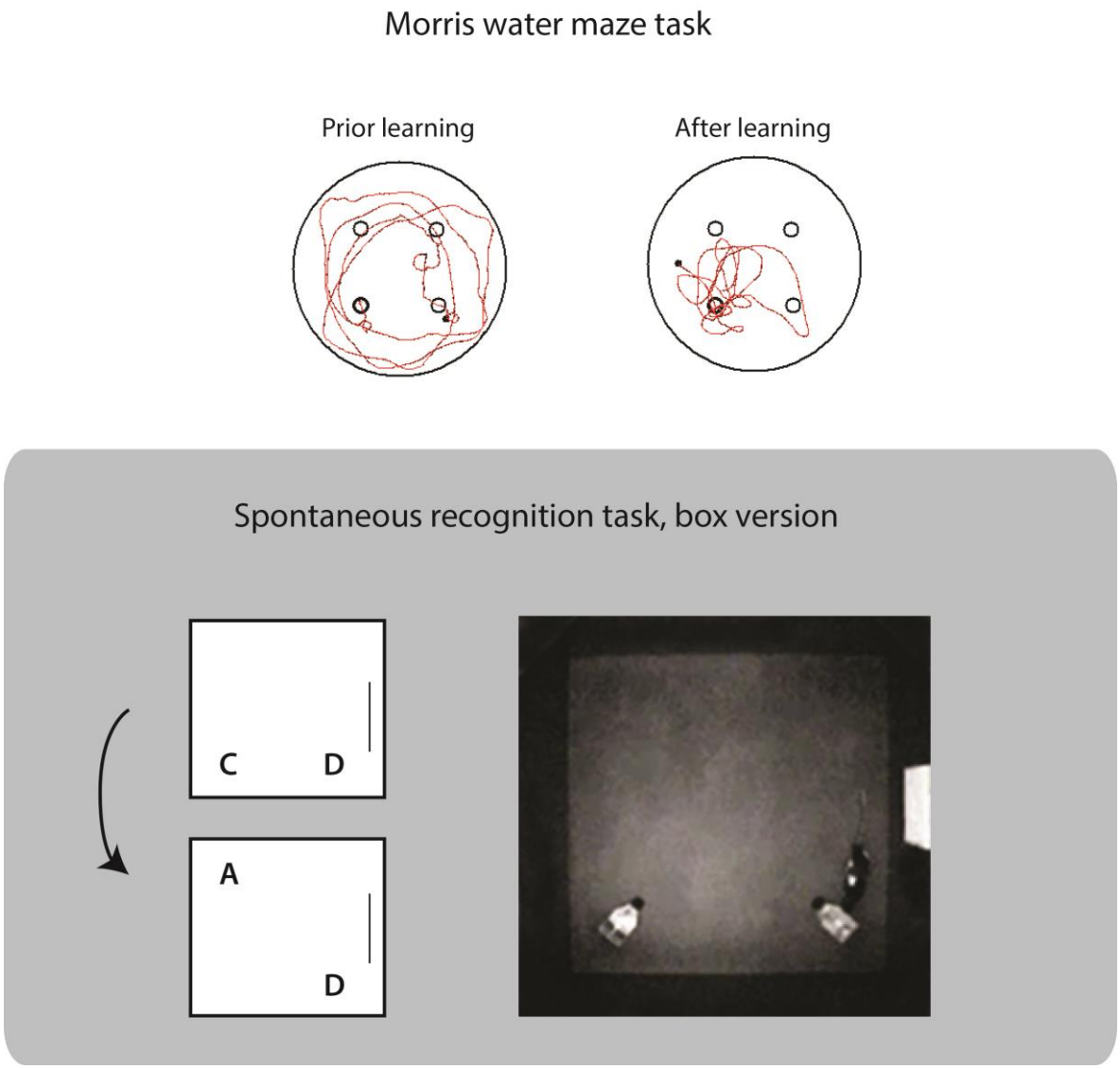

Figure 5. Hippocampal memory tasks. Top panel: Examples of a swimming path in the Morris water maze, prior and after learning, to locate the hidden target platform. Bottom panel: To the left, the design of the box version of the spontaneous recognition task (SLR), first with two randomized object locations (objects in location C and D) in the sample phase, and after a delay, the test phase with an object locations randomly changed (A) while one object was kept in the familiar object location (D). To the right, an example of a rat exploring an object in location D during the sample phase (data from own recordings).

Paper 3 │**Growth hormone modulates remapping in the hippocampal area CA1**

For this study, I used 12 male Long Evans rats for GH manipulations and single-unit recordings. The animals underwent surgeries receiving rAAVs with either GH, aGH or GFP only, in addition to implantation of one to two microdrives, all in the dorsal CA1. I manually assembled the microdrives (Axona Ltd) with cannulas and four tetrodes, and plated the tetrode tips with platinum for the reduction of impedance. One week after the surgery, the rats were habituated to the familiar box (1 x 1 meter with a local cue card). The tetrodes were implanted in the cortex above hippocampus and daily lowered (25-50 µm at a time) to the hippocampal CA1. The animals were ready for experiments when the animals explored all parts of the box and place cells were separable during off-line analysis. The experiments consisted of sessions in the same room, including the familiar box – novel circle – familiar box, each lasting 10 min, starting and ending with pot sessions. During the trials, the animals were freely foraging for choco loops. The position of the animal was recorded by a camera, and the animals were tracked by light-emitting diodes attached to the microdrives (Figure 6). The single-unit activity was recorded using Axona data acquisition system (Axona Ltd). The signals were amplified and filtered as described in the paper. I analyzed the data for each session off-line. The spike-sorting was achieved by manual clustering in two-dimensional parameter space using graphical cluster-cutter software (Axona TINT). MATLAB (Mathworks, Natick, MA) scrips were used for the analysis of the place cells firing.

The tetrodes were not moved after the final recording. To verify the viral transfections and tetrode traces, the animals were perfused with PBS and subsequent 4 % PFA, before the brains were dissected. The brains were sectioned with 40 µm thickness and analyzed in a fluorescence microscope. For analyzing the GH levels in the three groups, another batch of 11 animals were used for Real-time polymerase chain reaction (RT- qPCR) and sequencing. These animals were perfused with ice cold PBS before fast freezing of the dissected brain. The tissue were homogenized and the total RNA was isolated. DNA contamination was removed and cDNA was synthetized. Primers for made for the protein of interest, as described in the paper.

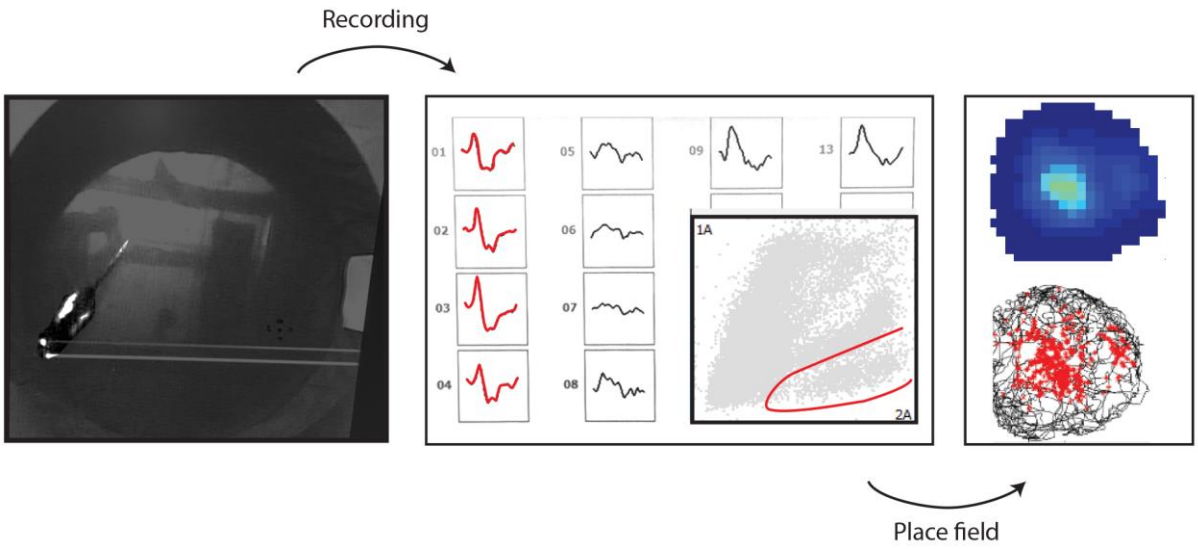

Figure 6. Recording of single-units. During a trial, the rat was freely foraging for choco loops in the recording apparatus. Microdrives implanted in the dorsal CA1 were connected to the recording system via a cable, and the position of the animal was detected by light-emitting diodes attached to the microdrives. During recordings, an oscilloscope showed the electrical activity, with columns representing one tetrode with four electrodes. Only signals with an amplitude exceeding a set threshold were recorded. The signals were then clustered into single-units, sorted according to the actual position of the rat at the time of sampling (data from own recording).

Synopsis of results

Paper 1 │**Development and topographical organization of projection from the hippocampus and parahippocampus to the retrosplenial cortex**

To reveal the developing projections from the hippocampus and PHR to the RSC, we utilized the traditional anatomical approach of retrograde and anterograde tracers. In our study, we found that SUB, PrS and PaS projected strongly to RSC, with SUB as the main source of projections to the RSC. We also observed some projections from MEC, LEC and POR, while only a few from PER. Both SUB and PrS projected to RSC in P1-P3 animals, in addition to a few projections arriving from CA1, MEC and LEC. The projections in the P1-P3 animals were only targeting the caudal RSC. The rostral RSC only received projections from the hippocampus and PHR in the second half of the first postnatal week. All of the projections in the animals regardless of age were topographically organized, suggesting that the first axons arriving to the RSC display a mature topographical organization.

We further investigated the topographical organization of the projections (Figure 7). Using retrograde tracers to reveal CA1-RSC projections, we located labelled cells in the most anterior part of dorsal CA1, in stratum radiatum, stratum lacunosum moleculare, which projected to the entire RSC.

Also retrograde injections in SUB uncovered a distinct topography of the SUB-RSC projections. Dorsoventrally, caudal injections within A30 resulted in labelled cells in the entire dorsoventral SUB, whereas progressively more rostral and ventral injections in A30 and A20 resulted in labelled cells in more dorsal parts of SUB. Proximodistally, injections in A30 resulted in labelled cells in distal SUB, while A29 injections gave labelled neurons in intermediate proximodistal SUB. Anterograde injections in distal SUB labelled cells in A30 layer I and IV, and a few cells in layer V and VI.

Retrograde injections in RSC revealed labelled cells in PrS and PaS layer V, as well as some cells in layer VI. Injections in caudal A30 provided labelled cells in more ventrally parts of PrS and PaS, while more rostral injections in A30 resulted in labelled cells the most dorsal parts of PrS. Anterograde injection in the deep layers of intermediate dorsal dorsoventral PrS labelled fibers mainly in caudal A30 layer IV, in addition to some fibers in layer I.

For EC, we found after retrograde experiments that EC projected to RSC through the superficial layer V of MEC and LEC, while a few projections arrived from layer III. The more dorsal parts of MEC projected more strongly to RSC and ventral MEC. We found that rostral A29 and A30 received projections from lateral MEC projects, while caudal RSC received projections from medial MEC. Anterograde tracing described fibers in caudal RSC originating from dorsolateral MEC. These results provide new insight into both development and topographical organization from hippocampus and PHR to RSC.

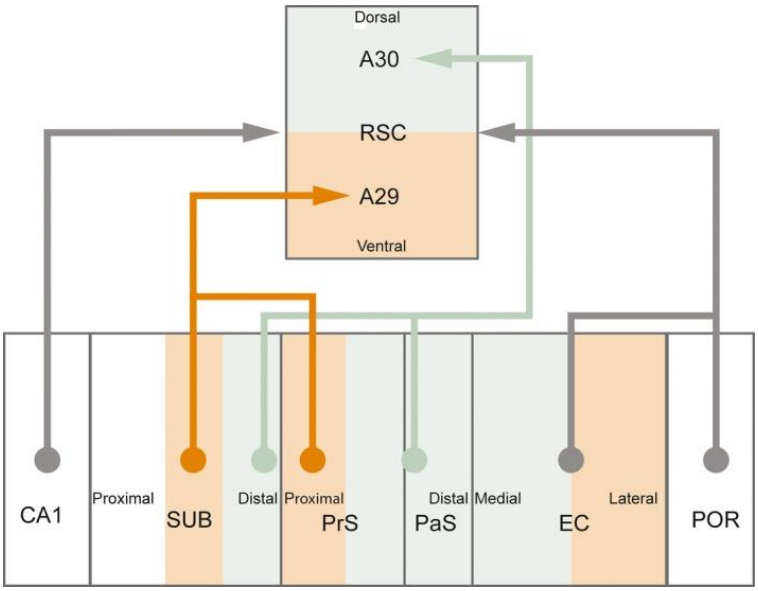

Figure 7. Topographical organization of projections from hippocampus and parahippocampus to retrosplenial cortex (RSC). The intermediate proximodistal subiculum (SUB) and proximal presubiculum (PrS) projected to RSC A29, whereas distal sub and distal parasubiculum (PaS) projected to A30 (illustration from paper 1).

Paper 2 | **Hippocampal growth hormone modulates relational memory and the dendritic spine density**

Not much is known about the GH as a neuromodulator in the hippocampus, but evidence suggests that GH could be involved in hippocampal plasticity [75, 76]. By locally manipulating the levels of GH using rAAVs in the dorsal CA1, we assessed the impact of GH on the hippocampal memory. In the Morris water maze tasks, we found that the blockage of the GH receptor by aGH impaired the memory performance on day 6. When the rats were trained to find a novel platform location after one week of rest, the aGH rats kept swimming toward the former platform location (Figure 8). However, the aGH animals remembered the novel platform location after receiving one additional day of training. We found no effect after the elevation of the GH levels in the Morris Water maze task. However, when the GH animals were subjected to a single-trial learning task, they performed significantly better than controls in a SPR task. The histology revealed that the hippocampal neurons in CA1 were transfected with the virus, and immunohistochemistry for p-Stat5 resulted in significant higher levels of p-Stat5 in the GH group, indicating increased GH-receptor activation in this group. In addition, spine analysis described a significant difference in the spine density. The increased GH resulted in higher spine density while the aGH reduced the spine density. These combined approaches of behavior tasks and morphological examinations after GH manipulations provide a strong argument for GH as a neuromodulator in the hippocampus.

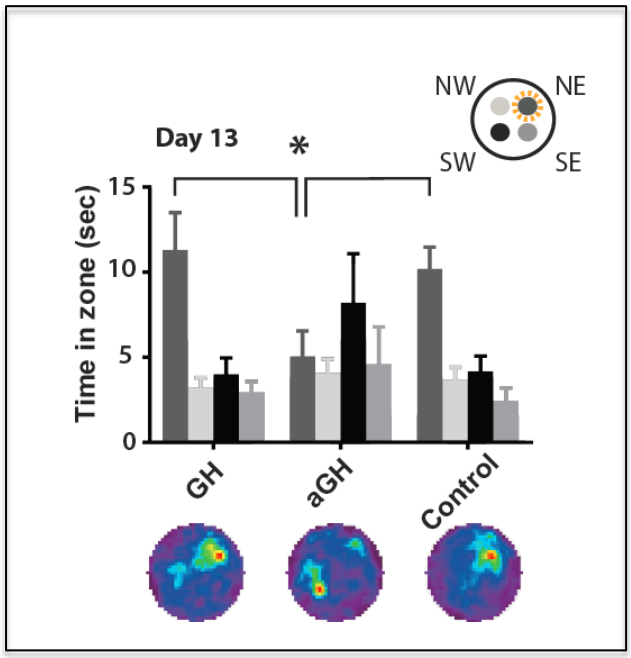

Figure 8: aGH impaired the hippocampal memory during new learning in the Morris water maze. After trained for locating the hidden platform at the position south west (SW), the platform location was changed to north east (NE). The aGH animals failed to remember the new platform location after one day of training and searched for the former platform location. The histogram represents the amount of time spent in the targets zones, while the occupancy maps bellow illustrates the swimming paths in a heat maps (illustration from paper 2).

Paper 3 | **Growth hormone modulates remapping in the hippocampal area CA1**

Place cells represent spatial maps for individual environments. When the environment changes, the neural activity of the place cells can change too (i.e. remapping). Although the hippocampus is influenced by neuromodulators, there are no reports about the effects of GH on the place cell activity. After changing the GH levels in dorsal hippocampus with the overexpression of either GH or aGH, we recorded place cells as the animals explored familiar and a novel environments. The animals had intact and stable place fields in the familiar environment, although the aGH animals showed changed place cell firing, including peak firing, and bursting, field size and sparseness. In the novel environment, the aGH treated animals displayed further changes in average firing rate, peak rate and information density, and sparseness in the novel arena. Comparing the place cell firing between the environments, we found that only control rats rate remapped. The GH animals tended to globally remap with no spatial correlation between the place fields of the familiar and novel environment (Figure 9). This paper reveal new effects of GH as GH can modulate remapping of the place cells.

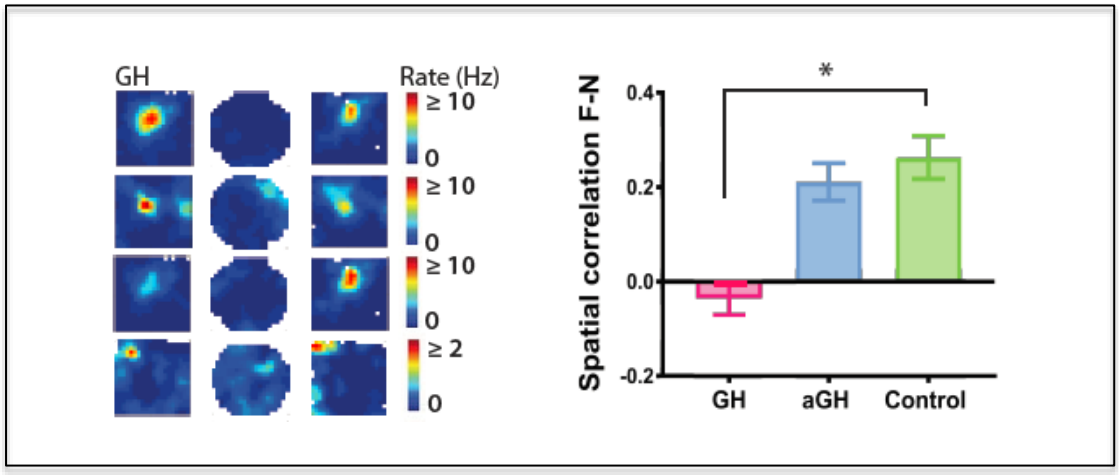

Figure 9. Growth hormone (GH) tended to enhance global remapping. To the left, examples of place cells with their respective place fields in the familiar (F) box and the novel (N) circle. To the right, the histogram showing no spatial correlation of the place fields between F and N in the GH animals (from paper 3).

Discussion

In this thesis, hippocampal plasticity was investigated at two distinct temporal stages, first during early development with concern to developing **connections**, followed by changes in neural **activity** and **behavior** in the adult by the neuromodulator GH. In paper I, we report that the first projections from the hippocampus and PHR to the RSC were present at birth and continued to develop until the time of eye-opening. The topography remained stable throughout the development which suggests that the projections keep a stable topographical organization. In the second paper, we showed that GH enhanced the hippocampal memory and increased the spine density on apical dendrites of CA1, while blocking the GH receptor by aGH impaired the hippocampal memory and decreased the spine density. The GH increased the production of immature spines, suggesting that GH enhanced synaptic plasticity. With these effects of GH in mind, we investigated the neural signaling in the hippocampal with the overexpression of GH or aGH. The third paper describe changed neural firing when the GH levels were altered. While aGH changed the general firing activity and the proportion of bursting, the GH tended to enhance global remapping events. As global remapping is suggested to increase pattern separation processes, enabling the hippocampus to distinguish between to similar events, GH could utilize such mechanism to enhance hippocampal functions.

Methodological considerations

Anatomical tracing in rat pups

In paper 1, traditional anterograde and retrograde tracers were used to study the developing connections from hippocampus and PHR to the RSC. By using both tracer techniques we could get more laminar information of the projections. As the injection sites were usually not constrained to one layer only, it would be difficult to describe which layers the injections were made in using retrograde tracers only. Nevertheless, by injecting retrograde tracers in the RSC we could see exactly where the cell bodies were located in the hippocampus and PHR. Anterograde injections in hippocampus and/or PHR provides detailed information of where the projections were targeted in the RSC.

Various retrograde tracers were used, which are taken up by the dendrites and somata. However, possible uptake by damaged fibers passing through the area of the injection site that do not project to the injection site could be challenge. To avoid this we used micropipettes with the outer tip-diameter at the minimum of 20 µm to avoid brain damage. This was most likely not an issue as we did not observe anterograde transport of the retrograde tracers. Anterograde tracers are taken up by the neural dendrites and/or the neural somata, and the tracers are transported toward the axonal terminals[103]. BDA 10 KD is the most broadly used anterograde tracer as it is reliable, providing clear a background, can be visualized after an efficient two-step immunohistochemistry, and is compatible with fixatives like PFA and glutaraldehyde. A limitation of anterograde tracers is that retrograde uptake can occur by cells that that project to the site of injections[104]. Precautions were used to minimize such retrograde uptake. We used 10 KD BDA, which is the molecular weight version of BDA with the lowest retrograde component[104, 105]. Micropipettes with outer tip-diameter at the minimum of 20-25 µm were used to minimize damage to the brain tissue. We found very little retrograde transport in our samples. Lastly, the survival time of the animals was put to 24 hours due to earlier developmental studies showing that such survival time is sufficient with developing projections [44].

Comparing the previously known projections from the hippocampus and PHR in the adults with our findings, we see that we have found a few projections from PER that have not been described before. This could be because of differences in these projections between postnatal, adolescent and adult rats, as there are structural differences in the young and adult hippocampus[42]. However, as the topography of the other projections we describe in paper 1 displayed an adult-like pattern, this seems unlikely. Another explanation could be that these PER-RSC projections were overlooked at they are only a few and very sparse.

Furthermore, as our dataset is not exhaustive as we did not inject the entire extent of RSC with retrograde tracers for each age, or the entire hippocampus and PHR with anterograde tracers, we may have missed some projections. However, as we aimed to look into the topography of the projections, we aimed to have several but smaller injections in the target regions. Moreover, a limitation of the trace approaches is that we cannot rule out potential pruning events based on our results. Although we did not observe any change in the topographical organization of the developing projections, other higher resolution techniques, like super-resolution microscope with in vivo recording, would be beneficial for such purpose.

A major challenge in this study was the use of new-born rat pups (P0-P15). The coordinates of the target regions had to be adjusted manually in parallel with the experiments. In some of the youngest animals, when we did not observe retrogradely labelled cells in hippocampus or in the PHR, we investigated other brain regions to look for tracer transport. If we found retrogradely labelled cells in other regions, we knew that the tracers were working. In such cases, we concluded that there were no projections to the area of that injections site. Another challenge with using pups was that the histology was not adult-like. After Nissl staining, the cell bodies were located more sparsely to each other, making delineating more challenging. However, I feel confident that out delineating was optimal as all the authors of the papers were analyzing and delineating the most challenging cases.

GH manipulating in hippocampus

In the second and third paper, we looked at the effects of GH in the hippocampus. In order to do so, we used rAAVs to overexpress GH or GH. We chose to utilize rAAV as it provides both a local and chronic overexpression of the proteins of interest. AVV is a well-established method to insert genes into cells with little toxicity and with long-lasting effects. Given that the AVV cannot be replicated without a helper-virus, AAV is useful to infect only one node of a neural circuit, with little concern of the virus jumping across synapses to infect neighboring cells[106].

However, a major concern with using the rAAVs was that we could neither precisely predict how much of the viral particles that were taken up by the cells, nor know how much GH that were overexpressed, released or were taken up by the neurons. To improve the transduction efficiency of the virus, we utilized a pseudotyped ½ chimeric rAAV[107]. However, overexpressing GH could lead to downregulating of GH receptors to counteract for the increased GH levels[108]. In our pilot study with 10-times higher virus titer, we found major necrosis in the tissue surrounding the injection sites. For the second and third paper, we therefore suspended the virus in sterile PBS to titer of 2.46×10^{12} vg/mL for the control GH and 2.46×10^{12} for aGH. We found no necrosis and no or very little tissue damage in the rats included in paper 2 and 3.

Furthermore, to minimize damage to the brain we used a small Hamilton needle (2µL) and small injection volumes (each injection of 0.4 µL). Each injection covered only small parts of the CA (about 500 µm), so although we used four injections in the CA1 in each hemisphere anterior-posteriorly and proximolaterally, we only covered parts of the CA1. Therefore, the

effects of GH on the hippocampal memory in paper 2 and 3 could be underestimated. For paper 3, the microdrive implantation was placed in the middle of the two most anterior coordinates, to optimize the recording of cells that were overexpressing the GH or the aGH. However, the GH modulation of the recorded cells may vary is the virus injections or microdrive implant were located differently. Nevertheless, I verified the histology for both injection sites and tetrode traces in all the animals, thus I feel confident that the recorded CA1 neurons overexpressed the proteins of interests.

To verify the changes in GH levels after the virus injections, I first performed immunohistochemistry for p-Stat5. Stat5 is a small protein underneath the cell membrane associated with the GH receptor. When the GH receptor gets activated, Stat5 gets phosphorylated. Although we found significant changes in p-Stat expression after increased GH, we did not observe significant changes after aGH. However, around some injection sites, the cells looked damaged and they highly expressed p-Stat5. Although p-Stat5 is a common marker for GH receptor activation, also other processes can induce p-Stat5. In paper 3, we analyzed the tissue by RT-qPCR and found major differences in the GH, aGH and control. Sequencing revealed the mutation between aGH and GH, thereby verifying that all both the two viruses provided significant changes in the GH level.

Behavioral assessments

For testing how GH affects the hippocampal memory, we used the Morris water maze task, which is one of the most utilized behavioral task to assess spatial memory[109, 110]. Animals with hippocampal lesions are unable to learn and remember the hidden platform location and swim around randomly. Nevertheless, if the hippocampus is only partly lesioned, animals can learn and perform well in this task. Evidence suggests that only relative small segments of the hippocampus are required to encode spatial memory [111]. Still, in paper 2, we found that the aGH animals had impaired memory performance in the Morris water maze. In contrast, we did not observe any effects of the GH in the water maze task. We believe this is because of a ceiling effect. However, in the box version of the SLR task with 24 hours of delay, we found differences between GH and control. In the SLR task, the exploration time with novel object-locations was assessed after a single learning trial, which could be easier to detected more subtle changes in the memory. Interestingly, the GH effects were seen after 24 hours only and not 3 hours, indicating long-term mechanism of GH in the hippocampus. A concern in this task was whether the animals were interested in the objects we used in the SLR tasks. We

calculated the exploration time with all of the objects we used in the tasks and found no differences. I therefore feel confident that the types of objects did not bias our results.

Single-unit recording

A concern in the third paper was whether the difference between the familiar and novel environments were sufficient for the animals to signal changes in the location or not. We only changed the shape of the apparatus, from a square box to a circle, while the room, colors, floor and distal cues remained the same. If the changes in the environments are too subtle, pattern completion processes in the hippocampal CA3 will make animal perceive these distinct environments as the same environment. Although it has previously been reported that changes in the apparatus can lead to rate remapping[97], the rate remapping of the CA1 place cells is associated with task demand[112]. Since we knew that GH modulation of CA1 cells enhanced hippocampal memory from paper 2, I recorded place cells from the CA1 region. The CA1 received a variety of inputs, with both direct and indirect inputs from EC, which would be good candidate for the GH modulation. Although the CA3 place cells rate remap more strongly when the shape of the apparatus changes than the CA1 cells[97], we observed rate remapping in our control animals. I therefore believe that the changes in the environment were sufficient to make the control animals aware of the change, although the impact of the rate remapping could have been underestimated due to recordings in the CA1 and not the CA3.

Potential projection for spatial information to the retrosplenial cortex

During development, the hippocampal network is highly plastic as new cells are being born and the connections between the neurons are taking form. In the first paper of this thesis, we described the postnatal development of the hippocampal/PHR-RSC projections. An important aspect of studying developmental changes is to uncover potential functional associations [33]. The hippocampus sends information to the neocortex, and RSC is one of the main targets[30]. The hippocampus and RSC share functional attributes, which could be mediated by the strong SUB-RSC connections. Human studies have revealed simultaneously activation of RSC and the hippocampus during navigation in virtual environments[113]. Further evidence has described spatially modulated cells in these brain regions, in particular grid cells in MEC[114], place cells

in the hippocampus[89], border cells in MEC[115], and head-directional cells in RSC[116], PrS[47], PaS[46] and MEC[117].

In this study, we report that the hippocampal/PHR-RSC projections are present at birth in a topographical organized manner, suggesting that the targets in the RSC are predetermined before the axons arrive at their final destination. However, due to the resolution of our approach, we cannot rule out that the earliest axons are precisely organized as the adult projects. Our paper could nonetheless reveal that the projections became adult-like around the time when the pups open their eyes. This is also the same time period as functional head-directional cells have been recorded [46]. While head-direction cells and place cells are functionally mature around P15-P16, the grid cells require three weeks before their signaling pattern is mature[118]. It has been suggested that head-direction cells modulate grid cell firing[119]. This may imply a functional importance of the hippocampus-PHR to RSC during postnatal development. To reveal the functional significance of the RSC for the grid cell firing in MEC, inactivation of RSC could be performed while simultaneously recording the neural activity in the PHR, when an animal is exploring an environment.

Furthermore, in paper, 1 we found distinct topographical patterns of the projections from the hippocampus/PHR to RSC. There seems to be two main information routes reaching the RSC, which is in particular apparent in the projections originating from the SUB. The distal SUB is suggested to process spatial information and seems to projects to A30 (Figure 10), while intermediate proximodistal seems to projects to A29, which is in agreement with the literature [28, 120], especially since the distal SUB contains more spatially modulated cells than the proximal SUB[121]. As we did not observe much projections from proximal SUB, LEC or POR, it might suggests that RSC do not receive much object-based information from the hippocampus/PHR. However, this in contrast to a behavioral study which found that RSC has a role in object information in addition to spatial information[122].

Based on paper 1 and the previously reported study concerning the projections from RSC to PHR[29], we can conclude that A30 is connected to the distal SUB, distal PrS, PaS and medial MEC, while A29 is connected to more intermediate proximodistal SUB, proximal PrS, and lateral parts of MEC and not to PaS. These distinct patterns are related to the parallel processing in the hippocampus and PHR and in accordance with previous literature.

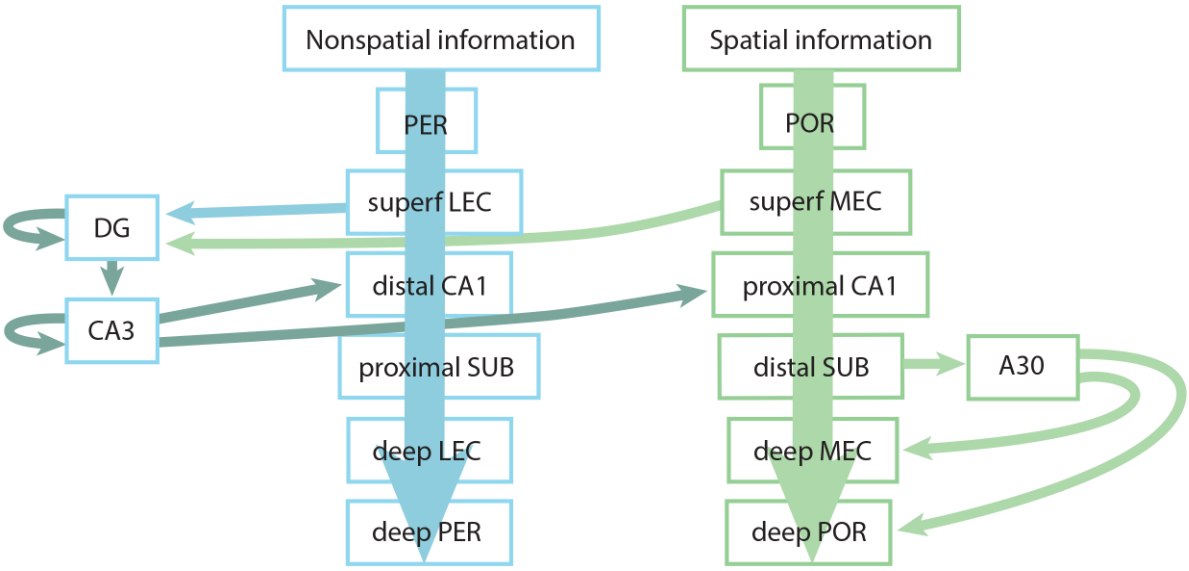

Figure 10. Parallel processing streams in the medial temporal lobe. The main inputs to the hippocampus arrives from the medial entorhinal cortex (MEC) and lateral entorhinal cortex (LEC) carry spatial information and nonspatial information, respectively. Hippocampal dentate gyrus (DG) and CA3 presumably integrate these sensory inputs into conjunctive representations, and update the parallel streams. Retrosplenial cortex A30 receive presumed spatially information from distal subiculum (SUB) and could update the deep layers of MEC and postrhinal (POR; Modified from ref [25]).

Growth hormone modulates hippocampal information

Although major neural changes are associated with early development, synaptic changes continue to occur during the adolescence and aging[37]. Evidence claims that maturational processes of adult-generated neurons follow stages characteristic of the ones described during the development[123]. It has been suggested that synaptic mechanisms responsible for de novo synapse formation during development are recruited again in the adult brain to support structural synaptic plasticity underlying long-term memory formation. During adulthood, new dendritic spines and spine synapses form and regress on CA1 pyramidal neurons, and existing spines exhibit rapid change in size and shape, and can regress [124]. In paper 2 and 3, we looked further into the hippocampal circuits and assessed how the hippocampus responded to the modulation of the GH.

Very little is known about the mechanisms exerted by the GH in the hippocampus, which was a major challenge for paper 2 and 3. GH is locally expressed in the hippocampus[73] and can exert both autocrine and paracrine effects[125]. Evidence also shows that GH affects the excitatory transmission in the CA1[75, 76]. However, its remains unknown which synapses the GH modulates. By looking into the mechanisms of other neuromodulators we might get some clues (Figure 11). In general, neuromodulators like ACh, NE, 5-HT and DA can alter information processes mediated by fast transmitters such as glutamate and GABA. Although the neuromodulators may differ in modulating signaling processes, the primary mechanisms shared by them is altering the dynamics of excitatory and inhibitory synaptic transmission, changing synaptic modification processes, and changing the resting membrane potential [49-51]. Neuromodulators influence the signaling processes by volume transmission to diffusely target synapses, which makes the influence less specific than neurotransmitters. In the CA1, the common modulator effects are suppression of excitatory potential from EC afferents and/or Schaffer collaterals from CA3, suppression of inhibitory potential from inhibitory interneurons, selective suppression of excitatory potential from intrinsic fibers, and suppression of adaptation [51].

Neuromodulators can only target cells when the proper neuromodulator receptor is present. GH targets the GH receptor, which has been located in the hippocampus [58, 59]. Although the mechanism behind GH receptor activation in the hippocampus is unknown, in paper 2 we described the activation of a signaling protein, p-Stat5, which increased after GH modulation. As illustrated in figure 2, the JAK2-STAT pathway can potentially activate transcriptions for genes related to LTP to improve memory processes [57]. Our findings are in line with the literature, relating p-Stat5 to GH receptor activation [126]. Nevertheless, to my knowledge we are the first to describe increased p-Stat5 after local modulation of GH in the hippocampus, which rules out the plausible contribution of GH from the circulation.

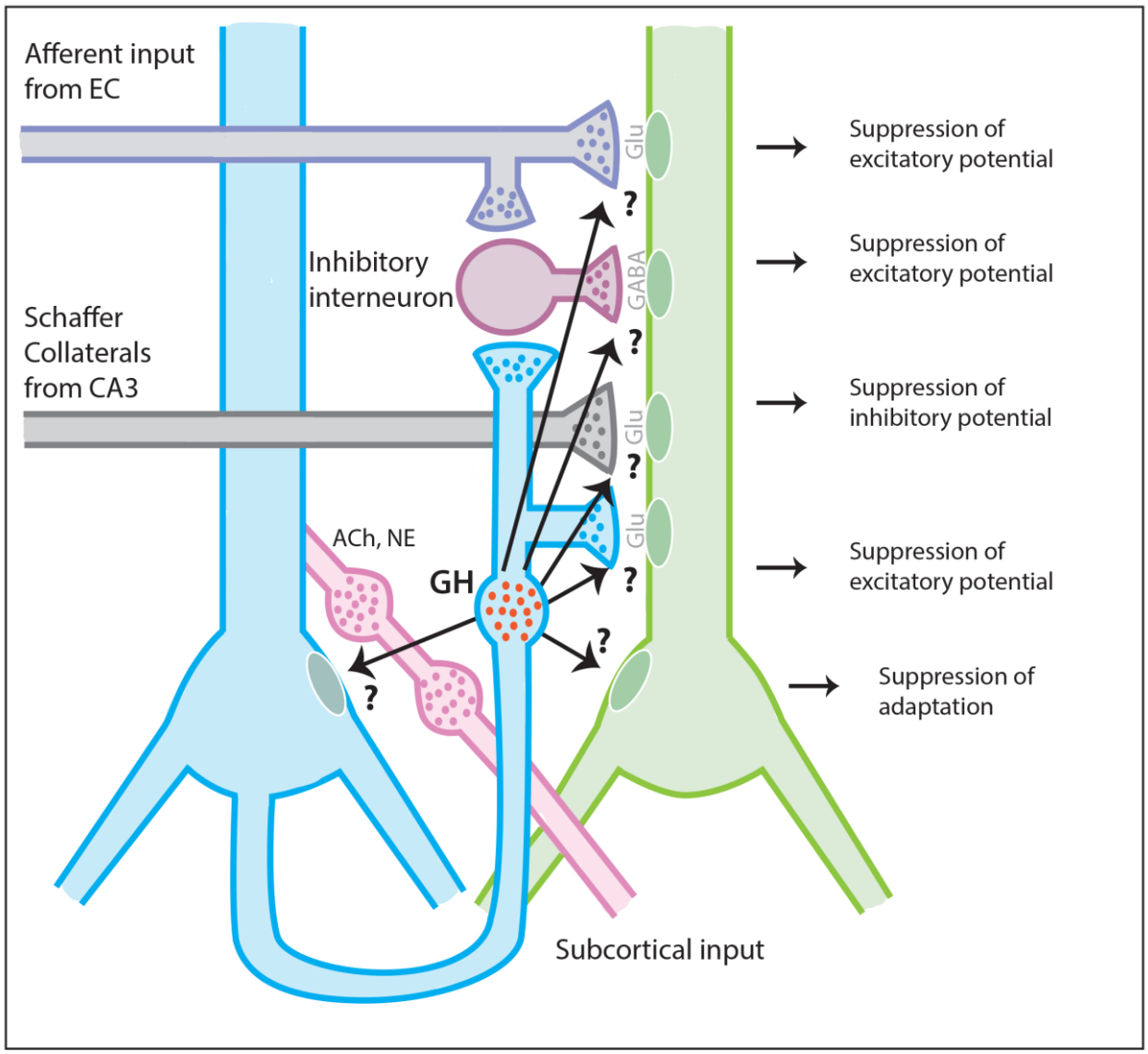

Figure 11. Potential mechanisms of local GH neuromodulation in the hippocampus by volume transmission. GH is known to influence information processes of neighboring neurons, as well as itself, but the mechanism remain elusive. Neuromodulatory innervations usually influence the circuits by volume transmission, released from axonal varicosities without postsynaptic densities, affecting both inhibitory and excitatory potentials (figure modified from ref[51]).

In paper 2, we addressed the behavioral effects of GH in the hippocampus. We found that GH increased memory performance in a one-trial learning task with 24 hours of delay, but not with a delay of only 3 hours. This suggest that the effects of GH requires more than 3 hours to be observed behaviorally, which could be due to activation of genes. Since our GH manipulation was chronic, the animals had high levels of GH before, during and after the task,

which makes us unable to pinpoint exactly at what stage the GH enhanced the memory. Optogenetic approach to inactive or activate the GH-responding cells at specific time intervals could be used to determine this.

In paper 2, we described an intriguing effect of the aGH in the Morris water maze task. After reversal training to a novel platform location the animals failed to locate the hidden platform, but after one extra day of training, they managed. This impairment in memory performance might be related deficits in pattern separation processes, as this tests requires the hippocampus to distinguish between similar events. To successfully perform this reversal training in the Morris water maze, the hippocampus must distinguish between the two similar tasks, either to locate the novel platform location or to locate the former platform location. As a neuromodulator, GH could impact the CA1 place cells by enhancing novel sensory inputs to the hippocampus, making the hippocampus more sensitive to changes in the environment. Our hypothesis is in line with a previous study using the GH-releasing peptide ghrelin to enhance pattern separation [102]. In our study, we also assessed the impact of GH on a hippocampal task suggested to be dependent on pattern separation functions. For this purpose, the circle version of the SLR task were used, described in the methods. However, we did not observe any significant effects of GH, although there was a clear trend that GH animals performed better. Although we could not confirm a relation between the GH and pattern separation in paper 2 we addressed this further in paper 3.

Can changes in remapping reflect hippocampal plasticity?

Building on the findings from paper 2, knowing that local GH can enhance hippocampal memory, we decided to look into the effects of local GH on the hippocampal place cells. Place cells represent the hippocampal activity[127], with inputs of both sensory and internal information[128, 129]. In paper 3, we wanted to investigate if GH modulation could impact the firing of place cells in a novel environment. In our experimental design (box-circle-box, in the same room), we discovered that aGH impaired rate remapping in the novel environment. The observed impairment in the CA1 place cells might be due to reduced sensitivity to novel sensory information. I speculate if this can be related to deficits in NMDA-signaling, as the NMDA receptor is associated with GH function[65, 130]. Impaired remapping in animals has been related to impairments in the NMDA receptor in the DG [131].

While aGH impaired the rate remapping, the GH tended to increase global remapping. Although we did not observe rate remapping in the GH animals, we cannot conclude that the GH increased global remapping. Global remapping is the greatest form of remapping, involving the change of locations of place fields. Global remapping is thought to be important for the separation of similar experiences, as global remapping increases the differences between the experiences[96]. Although global remapping is commonly observed when an animal explores a novel room, and not just to changes to the shape of the apparatus, GH could modulate the CA1 place cells to be more sensitive to new information.

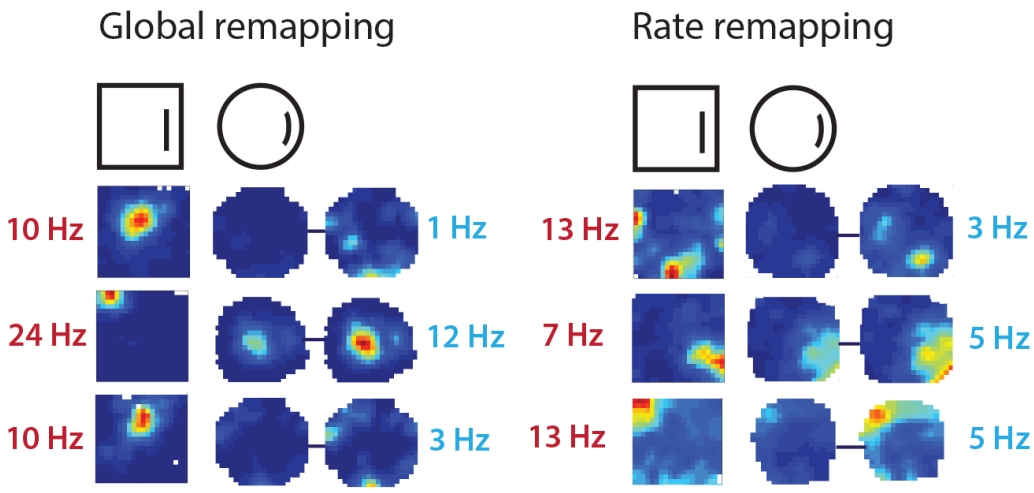

Figure 12. Two types of remapping events; rate remapping and global remapping. When there is a subtle change in sensory information to the place cells, like changing the shape or color of the apparatus, rate remapping can be observed. In rate remapping, the firing of the place cells changes in the novel environment. If there is a greater change in sensory information, like changing the rooms, the place cells can globally remap. In this case, the place fields change their locations in the novel environment. For all the illustrated place cells: To the left, place fields from box recordings with max firing rates shown in red, followed by recordings in a circular arena to the right. The recordings in the circle are shown in two figures, first plotted with the same max rate as in the box, then with individual firing rates, as described in blue to the right (data from own recordings).

It is a delicate balance between encoding novel information and consolidating the information. Other neuromodulators have been found to increase the novelty encoding and at the same time decrease the consolidation processes[51]. High levels of ACh result in enhanced attention and encoding for new memories, while low levels of ACh result in weaker influence of afferent input on the spiking activity relative to the magnitude of excitatory feedback, providing stronger internal dynamics for consolidation[132, 133]. Furthermore, also NE and DA initiate global remapping events[134, 135], which may share similarities with the GH actions. Further experiments are required to assess the mechanism of GH modulation on the place cell activity, in addition to revealing the identity of the synapses affected, and where GH is released from (see future directions for more details).

As addressed in paper 2, GH might play a part in pattern separation processes. In paper 3 we found that GH tended to induce global remapping although the changes to the environmental only were subtle. In global remapping, the experiences in each environment become organized in separate spatial maps such that smaller changes to features within an environment can be detected [136]. Our results in paper 3 therefore suggest a role of GH in pattern separation processes. Since pattern separation functions are associated with the DG and CA3 regions of the hippocampus[98], this hypotheses leads to some concerns. Firstly, how did GH affect the DG when GH was only overexpressed in the CA1? An explanation for this could be that GH is most likely secreted in by volume transmission, which makes the GH diffuse over long distances in the extracellular space. Still, since there are no information about such varicosities releasing GH in the hippocampus, or the locations of these varicosities, further experiments are needed to answer this question. I speculate if the GH manipulations were directed towards the DG instead of the CA1, we would have seen stronger effects of GH on the pattern separation processes, including pattern separation in the circle version of the SLR task in paper 2, global remapping during single-unit recordings when the animals explored the novel environment in paper 3.

Since MEC is associated with global remapping and sensory information, I speculate if GH might modulate these inputs. MEC sends input both directly to CA1 by MEC and indirectly through the DG and CA3. Taken into the account of the mechanisms and effect of ACh, which also modulates the novelty information processes in the hippocampus, these MEC projections might be modulated by GH. Increased GH might enhance these inputs while decreased GH might reduce MEC information, and instead enhance CA3 consolidation processes. Another input that could be modulated by GH is therefore the CA3-CA1

connection[21]. CA3 is theorized to be essential for the integration of spatial and nonspatial elements that comprise an individual episode. Because of its extensively interconnected recurrent collateral system, CA3 is thought to associate arbitrary inputs [137]. As a region involved in pattern completion, CA3 might give rise to memory interference when two different environments seems to be similar [96]. In paper 3, aGH impaired the rate remapping, which might suggest such memory interference. This could be due to increased information coming from CA3. However, as we do not know the identity of the GH receiving cells, or which synapses GH modulate, I can only speculate which projections or regions that were affected by the GH modulation.

Taken together, paper 2 and 3 reveal previously unknown effects of the GH in the hippocampus. While GH enhanced hippocampal plasticity and memory performance, blocking the GH receptor by aGH decreased the plasticity and impaired memory performance. These effects might be related to the balance of memory transience (forgetting) and persistence (remembering). Although some people may believe that a memory with the highest form of persistence would be beneficial for memory performance, without transience, such memory would be absolute rigid and without the capability of updating or in generalizing events. Therefore, transience is crucial for letting the memory being flexible, promote generalization, and by reducing the influence of outdated information on memory-guided decision making [138]. In other words, although enhanced levels of GH seems beneficial for the hippocampal memory, the hippocampus would need the right balance between plasticity and rigidity for healthy neural processes.

Future directions

The present thesis has explored the plasticity in the hippocampal circuits by developmental connections (paper 1) and neuromodulations by GH (paper 2 and 3). The results from these papers raise numerous further question.

In paper 1, we described the development and topography of the projections from the hippocampus and PHR to the RSC. As the structural developmental seems to be correlated with functional development, it still remains to be explored whether these postnatal projections are functional at the early temporal stages or not. This could for instance be achieved by recording from RSC cells while stimulating projecting regions, like the distal SUB to the A30, as this projection is string and these regions might share functional

attributes. Furthermore, to assess the developmental importance of the hippocampus/PHR-RSC projections, the distal SUB-A30 projections could be inactivated from birth. Recording from grid cells in the MEC could reveal a plausible role of RSC on grid cell firing, as head directional cells are known to modulate grid cells, knowing that head directional cells mature before grid cells.

In paper 2, we described enhanced memory performance after increased GH in CA1. Since we used rAAVs to overexpress the GH, the levels of GH were chronically high throughout the experiments. In order to assess exactly when GH impacts the memory, like encoding and consolidation processes, the modulation of GH should be temporally specific. By using chemogenetics or optogenetic, the GH manipulation could be specific to the distinct phases of the memory processes. Optogenetics utilizes light-sensitive ion-channels called opsins to active target receptors with a far better temporal precision with light pulses than chemogenetics, with designer receptor activated for hours after a single administration of designer drugs [139]. Using optogenetic would therefore be a preferred option.

Due to recent development in recording approached, neural firing in multiple regions can be recorded simultaneously. In particular, by using high-density silicon probes placed at various positions in the hippocampus [140], the hippocampal circuit effects of GH could be explored. This would be of high interest as in our model system, we find increased spine density and enhances remapping events in CA1, while we suspect enhanced pattern separation processes, which would be detected in DG. Therefore, by recording in DG as well as in CA1, we would reveal more of the mechanism of GH actions in the hippocampus. In this case, it would be interesting to investigate the effects of GH if also the neurons in the CA3 and DG were transfected with the rAAV-GH as when exploring a novel environment, in order to see if this could lead to enhanced pattern separation effects of the GH. By combining high-density silicon probes and optogenetic stimulation, the impact of GH on the hippocampal circuit could be described in more detail [141].

Furthermore, as GH is secreted from the anterior pituitary during the onset of sleep, during the SWS, it would be highly interesting to see whether GH impacts the sharp wave ripples (SWR). A possible approach is to manipulate the GH locally in the hippocampus, like using our viral approach described in paper 2 and 3. If GH enhances SWR, this might be reflected in increased numbers of SWR and/or longer ripple events. If GH affects the SWR, this could suggest that GH modulates memory consolidation processes. To verify possible findings,

optogenetic could be used to inactivate GH receptor cells to assess whether this disrupt the SWR or not.

In paper 2, we detected activated GH receptor by p-Stat5 signals, but the identity of the cells containing the GH receptors, and which synapses GH affects, remain unknown. Revealing the identity of cells with the GH receptor cells could be achieved by immunohistochemistry for specific cell types combined with p-Stat5. In addition, it is still unclear how and where GH is released, which is important for understanding the mechanism of GH. In addition, information about the GH receptor itself in the hippocampus is lacking, which prevents a specific targeting approach for detecting the GH receptor.

Moreover, to understand the signaling processes of the GH receptor activation, further experiments are required. In paper 2, we revealed that GH increased the spine density, which could be due to IGF-2 signaling, as GH can increase IGF-2, and in turn, IGF-2 can increase spine formation [79]. For instance, q-PCR could reveal if local GH in hippocampus can increase IGF-2. In addition, GH could affect IGF-1 as well, which is involved in neurogenesis [62]. Whether GH affected the neurogenesis in paper 2 and 3 or not remains unknown. This could be addressed by BRDU staining. If GH affects neurogenesis this could play a role in memory flexibility. For instance, animals with ablation of new neurons show impaired memory in the water maze when the platform location changes[142].

Lastly, as the GH levels in the circulation drop dramatically with age [143], the reduced memory performance in the elderly could be associated with the reduction of the GH levels. However, it remains elusive if the local levels of GH drops in the hippocampus too. Interestingly, Wilson (2005) described place cell firing in aged animals and reported that the place cells exhibit increased firing rate, the same as we find in the aGH animals of paper 3. In addition, the place cells of the aged animals failed to remap in a novel environment [99], which can be related to our findings as the aGH animals failed to rate remap as the controls. This might suggest that low GH concentration can be associated with memory deficits seen in aged individuals. Contradictory to this, in the Ames Dwarf mice, which have abolished circulating GH, the levels of GH in the hippocampus is enhanced. Further studies are required to address the impact of the local production of GH in the hippocampus during ageing.

Concluding remarks

The hippocampal network has the abilities to change its neural connectivity and activity in response to intrinsic factors and experiences to update both the memories and behavior. In this thesis, I have explored factors that contributes to hippocampal plasticity at three levels; connectivity, neural firing and behavior. I showed that the first hippocampal/ PHR-RSC projections were already present at birth, and the topography was adult-like in the earliest projections. These findings suggest that these projections are experience-independent. Furthermore, in the adult brain, I showed that the hippocampal plasticity can be modulated by local GH. GH enhanced the spine density, hippocampal memory, and tended to reduce interference of similar memories by global remapping. These results suggest that GH is a neuromodulator with a strong impact on hippocampal function. GH might modulate the hippocampal representation by changing the balance between encoding novelty information and consolidation processes. However, more extensive studies are needed to reveal how GH exerts its functions. Revealing factors and mechanisms contributing to hippocampal plasticity is important for understanding not only memory deficiency but also the hippocampal functions throughout the lifetime.

References

1. Minagar A, Ragheb J, Kelley RE. The Edwin Smith surgical papyrus: description and analysis of the earliest case of aphasia. J Med Biogr. 2003;11(2):114-7.
2. Crivellato E, Ribatti D. Soul, mind, brain: Greek philosophy and the birth of neuroscience. Brain Res Bull. 2007;71(4):327-36.
3. Gomez-Robles A, Hopkins WD, Sherwood CC. Increased morphological asymmetry, evolvability and plasticity in human brain evolution. Proc Biol Sci. 2013;280(1761):20130575.
4. Hofman MA. Evolution of the human brain: when bigger is better. Front Neuroanat. 2014;8:15.
5. Dexter JP, Prabakaran S, Gunawardena J. A Complex Hierarchy of Avoidance Behaviors in a Single-Cell Eukaryote. Curr Biol. 2019;29(24):4323-9 e2.
6. Bassett DS, Gazzaniga MS. Understanding complexity in the human brain. Trends Cogn Sci. 2011;15(5):200-9.
7. Strange BA, Witter MP, Lein ES, Moser EI. Functional organization of the hippocampal longitudinal axis. Nat Rev Neurosci. 2014;15(10):655-69.
8. Sweatt JD. Neural plasticity and behavior - sixty years of conceptual advances. J Neurochem. 2016;139 Suppl 2:179-99.
9. Schiller D, Eichenbaum H, Buffalo EA, Davachi L, Foster DJ, Leutgeb S, et al. Memory and Space: Towards an Understanding of the Cognitive Map. J Neurosci. 2015;35(41):13904-11.
10. Binder et al. Cognitive Map Theory. In: Binder MD, Hirokawa N, Windhorst U, editors. Encyclopedia of Neuroscience. Berlin, Heidelberg: Springer Berlin Heidelberg; 2009. p. 794-5.
11. Tolman EC. Cognitive maps in rats and men. Psychol Rev. 1948;55(4):189-208.
12. Squire LR. The legacy of patient H.M. for neuroscience. Neuron. 2009;61(1):6-9.
13. Scoville WB, Milner B. Loss of recent memory after bilateral hippocampal lesions. J Neurol Neurosurg Psychiatry. 1957;20(1):11-21.
14. Milner B, Corkin S, Teuber HL. Neuropsychologia. 1968(6):215–34.
15. Eichenbaum H. Hippocampus: cognitive processes and neural representations that underlie declarative memory. Neuron. 2004;44(1):109-20.
16. Cohen NJ, Squire LR. Preserved learning and retention of pattern-analyzing skill in amnesia: dissociation of knowing how and knowing that. Science. 1980;210(4466):207-10.
17. Squire LR, Zola SM. Structure and function of declarative and nondeclarative memory systems. Proc Natl Acad Sci U S A. 1996;93(24):13515-22.
18. Squire LR, Wixted JT. The cognitive neuroscience of human memory since H.M. Annu Rev Neurosci. 2011;34:259-88.
19. Lisman J, Buzsaki G, Eichenbaum H, Nadel L, Ranganath C, Redish AD. Viewpoints: how the hippocampus contributes to memory, navigation and cognition. Nat Neurosci. 2017;20(11):1434-47.
20. Konkel A, Cohen NJ. Relational memory and the hippocampus: representations and methods. Front Neurosci. 2009;3(2):166-74.
21. Amaral DG, Witter MP. The three-dimensional organization of the hippocampal formation: a review of anatomical data. Neuroscience. 1989;31(3):571-91.
22. Neves G, Cooke SF, Bliss TV. Synaptic plasticity, memory and the hippocampus: a neural network approach to causality. Nat Rev Neurosci. 2008;9(1):65-75.
23. Canto CB, Wouterlood FG, Witter MP. What does the anatomical organization of the entorhinal cortex tell us? Neural Plast. 2008;2008:381243.
24. Knierim JJ, Neunuebel JP, Deshmukh SS. Functional correlates of the lateral and medial entorhinal cortex: objects, path integration and local-global reference frames. Philos Trans R Soc Lond B Biol Sci. 2014;369(1635):20130369.
25. Knierim JJ, Lee I, Hargreaves EL. Hippocampal place cells: parallel input streams, subregional processing, and implications for episodic memory. Hippocampus. 2006;16(9):755-64.

26. Leutgeb JK, Moser EI. Enigmas of the dentate gyrus. Neuron. 2007;55(2):176-8.
27. Bennett MR, Gibson WG, Robinson J. Dynamics of the CA3 pyramidal neuron autoassociative memory network in the hippocampus. Philos Trans R Soc Lond B Biol Sci. 1994;343(1304):167-87.
28. Sugar J, Witter MP, van Strien NM, Cappaert NL. The retrosplenial cortex: intrinsic connectivity and connections with the (para)hippocampal region in the rat. An interactive connectome. Front Neuroinform. 2011;5:7.
29. Sugar J, Witter MP. Postnatal development of retrosplenial projections to the parahippocampal region of the rat. Elife. 2016;5.
30. Wyss JM, Van Groen T. Connections between the retrosplenial cortex and the hippocampal formation in the rat: a review. Hippocampus. 1992;2(1):1-11.
31. Aggleton JP, Wright NF, Vann SD, Saunders RC. Medial temporal lobe projections to the retrosplenial cortex of the macaque monkey. Hippocampus. 2012;22(9):1883-900.
32. Mitchell AS, Czajkowski R, Zhang N, Jeffery K, Nelson AJD. Retrosplenial cortex and its role in spatial cognition. Brain Neurosci Adv. 2018;2:2398212818757098.
33. Vann SD, Aggleton JP, Maguire EA. What does the retrosplenial cortex do? Nat Rev Neurosci. 2009;10(11):792-802.
34. Milczarek MM, Vann SD, Sengpiel F. Spatial Memory Engram in the Mouse Retrosplenial Cortex. Curr Biol. 2018;28(12):1975-80 e6.
35. Kim JI, Choi DI, Kaang BK. Strengthened connections between engrams encode specific memories. BMB reports. 2018;51(8):369-70.
36. Nitzan N, McKenzie S, Beed P, English DF, Oldani S, Tukker JJ, et al. Propagation of hippocampal ripples to the neocortex by way of a subiculum-retrosplenial pathway. Nat Commun. 2020;11(1):1947.
37. Leuner B, Gould E. Structural plasticity and hippocampal function. Annu Rev Psychol. 2010;61:111-40, C1-3.
38. Wiesel TN, Hubel DH. Comparison of the effects of unilateral and bilateral eye closure on cortical unit responses in kittens. J Neurophysiol. 1965;28(6):1029-40.
39. Ofen N, Shing YL. From perception to memory: changes in memory systems across the lifespan. Neurosci Biobehav Rev. 2013;37(9 Pt B):2258-67.
40. Callaghan BL, Li S, Richardson R. The elusive engram: what can infantile amnesia tell us about memory? Trends Neurosci. 2014;37(1):47-53.
41. Ramsaran AI, Schlichting ML, Frankland PW. The ontogeny of memory persistence and specificity. Dev Cogn Neurosci. 2019;36:100591.
42. Travaglia A, Bisaz R, Cruz E, Alberini CM. Developmental changes in plasticity, synaptic, glia and connectivity protein levels in rat dorsal hippocampus. Neurobiol Learn Mem. 2016;135:125-38.
43. Deng JB, Yu DM, Wu P, Li MS. The tracing study of developing entorhino-hippocampal pathway. Int J Dev Neurosci. 2007;25(4):251-8.
44. O'Reilly KC, Gulden Dahl A, Ulsaker Kruge I, Witter MP. Subicular-parahippocampal projections revisited: development of a complex topography in the rat. J Comp Neurol. 2013;521(18):4284-99.
45. O'Reilly KC, Flatberg A, Islam S, Olsen LC, Kruge IU, Witter MP. Identification of dorsal-ventral hippocampal differentiation in neonatal rats. Brain Struct Funct. 2015;220(5):2873-93.
46. Bjerknes TL, Langston RF, Kruge IU, Moser EI, Moser MB. Coherence among head direction cells before eye opening in rat pups. Curr Biol. 2015;25(1):103-8.
47. Taube JS, Muller RU, Ranck JB, Jr. Head-direction cells recorded from the postsubiculum in freely moving rats. I. Description and quantitative analysis. J Neurosci. 1990;10(2):420-35.
48. Taube JS. The head direction signal: origins and sensory-motor integration. Annu Rev Neurosci. 2007;30:181-207.
49. Edelmann E, Cepeda-Prado E, Lessmann V. Coexistence of Multiple Types of Synaptic Plasticity in Individual Hippocampal CA1 Pyramidal Neurons. Front Synaptic Neurosci. 2017;9:7.
50. Palacios-Filardo J, Mellor JR. Neuromodulation of hippocampal long-term synaptic plasticity. Curr Opin Neurobiol. 2019;54:37-43.

51. Giocomo LM, Hasselmo ME. Neuromodulation by glutamate and acetylcholine can change circuit dynamics by regulating the relative influence of afferent input and excitatory feedback. Mol Neurobiol. 2007;36(2):184-200.
52. Hasselmo ME. Neuromodulation: acetylcholine and memory consolidation. Trends Cogn Sci. 1999;3(9):351-9.
53. Atherton LA, Dupret D, Mellor JR. Memory trace replay: the shaping of memory consolidation by neuromodulation. Trends Neurosci. 2015;38(9):560-70.
54. Nadim F, Bucher D. Neuromodulation of neurons and synapses. Curr Opin Neurobiol. 2014;29:48-56.
55. Marder E, Thirumalai V. Cellular, synaptic and network effects of neuromodulation. Neural Netw. 2002;15(4-6):479-93.
56. Thorner MO, Hartman ML, Vance ML, Pezzoli SS, Ampleford EJ. Neuroendocrine regulation of growth hormone secretion. Neurosci Biobehav Rev. 1995;19(3):465-8.
57. Nyberg F, Hallberg M. Growth hormone and cognitive function. Nat Rev Endocrinol. 2013;9(6):357-65.
58. Nyberg F. Growth hormone in the brain: characteristics of specific brain targets for the hormone and their functional significance. Front Neuroendocrinol. 2000;21(4):330-48.
59. Nyberg F, Burman P. Growth hormone and its receptors in the central nervous system--location and functional significance. Horm Res. 1996;45(1-2):18-22.
60. Ashpole NM, Sanders JE, Hodges EL, Yan H, Sonntag WE. Growth hormone, insulin-like growth factor-1 and the aging brain. Exp Gerontol. 2015;68:76-81.
61. Wasinski F, Frazao R, Donato J, Jr. Effects of growth hormone in the central nervous system. Arch Endocrinol Metab. 2019;63(6):549-56.
62. Aberg D. Role of the growth hormone/insulin-like growth factor 1 axis in neurogenesis. Endocr Dev. 2010;17:63-76.
63. Pan W, Yu Y, Cain CM, Nyberg F, Couraud PO, Kastin AJ. Permeation of growth hormone across the blood-brain barrier. Endocrinology. 2005;146(11):4898-904.
64. Meyer RM, Burgos-Robles A, Liu E, Correia SS, Goosens KA. A ghrelin-growth hormone axis drives stress-induced vulnerability to enhanced fear. Mol Psychiatry. 2014;19(12):1284-94.
65. Le Greves M, Zhou Q, Berg M, Le Greves P, Fholenhag K, Meyerson B, et al. Growth hormone replacement in hypophysectomized rats affects spatial performance and hippocampal levels of NMDA receptor subunit and PSD-95 gene transcript levels. Exp Brain Res. 2006;173(2):267-73.
66. Kim E, Grover LM, Bertolotti D, Green TL. Growth hormone rescues hippocampal synaptic function after sleep deprivation. Am J Physiol Regul Integr Comp Physiol. 2010;298(6):R1588-R96.
67. Li E, Kim DH, Cai M, Lee S, Kim Y, Lim E, et al. Hippocampus-dependent spatial learning and memory are impaired in growth hormone-deficient spontaneous dwarf rats. Endocr J. 2011;58(4):257-67.
68. Bhattarai JP, Kim SH, Han SK, Park MJ. Effects of human growth hormone on gonadotropin-releasing hormone neurons in mice. Korean J Pediatr. 2010;53(9):845-51.
69. Bengtsson BA, Eden S, Lonn L, Kvist H, Stokland A, Lindstedt G, et al. Treatment of adults with growth hormone (GH) deficiency with recombinant human GH. J Clin Endocrinol Metab. 1993;76(2):309-17.
70. van Nieuwpoort IC, Drent ML. Cognition in the adult with childhood-onset GH deficiency. Eur J Endocrinol. 2008;159 Suppl 1:S53-7.
71. Bartke A. Growth Hormone and Aging: Updated Review. World J Mens Health. 2019;37(1):19-30.
72. Walker MP. The role of slow wave sleep in memory processing. J Clin Sleep Med. 2009;5(2 Suppl):S20-6.
73. Donahue CP, Kosik KS, Shors TJ. Growth hormone is produced within the hippocampus where it responds to age, sex, and stress. Proc Natl Acad Sci U S A. 2006;103(15):6031-6.
74. Mahmoud GS, Grover LM. Growth hormone enhances excitatory synaptic transmission in area CA1 of rat hippocampus. J Neurophysiol. 2006;95(5):2962-74.

75. Molina DP, Ariwodola OJ, Linville C, Sonntag WE, Weiner JL, Brunso-Bechtold JK, et al. Growth hormone modulates hippocampal excitatory synaptic transmission and plasticity in old rats. Neurobiol Aging. 2012;33(9):1938-49.
76. Molina DP, Ariwodola OJ, Weiner JL, Brunso-Bechtold JK, Adams MM. Growth hormone and insulin-like growth factor-I alter hippocampal excitatory synaptic transmission in young and old rats. Age (Dordr). 2013;35(5):1575-87.
77. Vander Weele CM, Saenz C, Yao J, Correia SS, Goosens KA. Restoration of hippocampal growth hormone reverses stress-induced hippocampal impairment. Front Behav Neurosci. 2013;7:66.
78. Basu A, McFarlane HG, Kopchick JJ. Spatial learning and memory in male mice with altered growth hormone action. Horm Behav. 2017;93:18-30.
79. Pascual-Lucas M, Viana da Silva S, Di Scala M, Garcia-Barroso C, Gonzalez-Aseguinolaza G, Mulle C, et al. Insulin-like growth factor 2 reverses memory and synaptic deficits in APP transgenic mice. EMBO Mol Med. 2014;6(10):1246-62.
80. Le Greves M, Steensland P, Le Greves P, Nyberg F. Growth hormone induces age-dependent alteration in the expression of hippocampal growth hormone receptor and N-methyl-D-aspartate receptor subunits gene transcripts in male rats. Proc Natl Acad Sci U S A. 2002;99(10):7119-23.
81. Sun LY, Al-Regaiey K, Masternak MM, Wang J, Bartke A. Local expression of GH and IGF-1 in the hippocampus of GH-deficient long-lived mice. Neurobiol Aging. 2005;26(6):929-37.
82. Sharma S, Haselton J, Rakoczy S, Branshaw S, Brown-Borg HM. Spatial memory is enhanced in long-living Ames dwarf mice and maintained following kainic acid induced neurodegeneration. Mech Ageing Dev. 2010;131(6):422-35.
83. Donahue CP, Jensen RV, Ochiishi T, Eisenstein I, Zhao M, Shors T, et al. Transcriptional profiling reveals regulated genes in the hippocampus during memory formation. Hippocampus. 2002;12(6):821-33.
84. Zhao Z, Liu H, Xiao K, Yu M, Cui L, Zhu Q, et al. Ghrelin administration enhances neurogenesis but impairs spatial learning and memory in adult mice. Neuroscience. 2014;257:175-85.
85. Albarran-Zeckler RG, Brantley AF, Smith RG. Growth hormone secretagogue receptor (GHS-R1a) knockout mice exhibit improved spatial memory and deficits in contextual memory. Behav Brain Res. 2012;232(1):13-9.
86. Schneider-Rivas S, Rivas-Arancibia S, Vazquez-Pereyra F, Vazquez-Sandoval R, Borgonio-Perez G. Modulation of long-term memory and extinction responses induced by growth hormone (GH) and growth hormone releasing hormone (GHRH) in rats. Life Sci. 1995;56(22):PL433-41.
87. Diano S, Farr SA, Benoit SC, McNay EC, da S, I, Horvath B, et al. Ghrelin controls hippocampal spine synapse density and memory performance. Nat Neurosci. 2006;9(3):381-8.
88. Gronbladh A, Johansson J, Nostl A, Nyberg F, Hallberg M. GH improves spatial memory and reverses certain anabolic androgenic steroid-induced effects in intact rats. J Endocrinol. 2013;216(1):31-41.
89. O'Keefe J, Dostrovsky J. The hippocampus as a spatial map. Preliminary evidence from unit activity in the freely-moving rat. Brain Res. 1971;34(1):171-5.
90. Moser EI, Moser MB. A metric for space. Hippocampus. 2008;18(12):1142-56.
91. Eichenbaum H. Hippocampus: mapping or memory? Curr Biol. 2000;10(21):R785-7.
92. Bliss TV, Lomo T. Long-lasting potentiation of synaptic transmission in the dentate area of the anaesthetized rabbit following stimulation of the perforant path. J Physiol. 1973;232(2):331-56.
93. Kentros C, Hargreaves E, Hawkins RD, Kandel ER, Shapiro M, Muller RV. Abolition of long-term stability of new hippocampal place cell maps by NMDA receptor blockade. Science. 1998;280(5372):2121-6.
94. Hebb DO. The Organization of Behavior. Wiley, New York. 1949.
95. Choi JH, Sim SE, Kim JI, Choi DI, Oh J, Ye S, et al. Interregional synaptic maps among engram cells underlie memory formation. Science. 2018;360(6387):430-5.
96. Colgin LL, Moser EI, Moser MB. Understanding memory through hippocampal remapping. Trends Neurosci. 2008;31(9):469-77.

97. Leutgeb S, Leutgeb JK, Barnes CA, Moser EI, McNaughton BL, Moser MB. Independent codes for spatial and episodic memory in hippocampal neuronal ensembles. Science. 2005;309(5734):619-23.
98. Leutgeb JK, Leutgeb S, Moser MB, Moser EI. Pattern separation in the dentate gyrus and CA3 of the hippocampus. Science. 2007;315(5814):961-6.
99. Wilson IA, Ikonen S, Gallagher M, Eichenbaum H, Tanila H. Age-associated alterations of hippocampal place cells are subregion specific. J Neurosci. 2005;25(29):6877-86.
100. O'Shea A, Cohen RA, Porges EC, Nissim NR, Woods AJ. Cognitive Aging and the Hippocampus in Older Adults. Front Aging Neurosci. 2016;8:298.
101. Papp EA, Leergaard TB, Calabrese E, Johnson GA, Bjaalie JG. Waxholm Space atlas of the Sprague Dawley rat brain. Neuroimage. 2014;97:374-86.
102. Kent BA, Beynon AL, Hornsby AK, Bekinschtein P, Bussey TJ, Davies JS, et al. The orexigenic hormone acyl-ghrelin increases adult hippocampal neurogenesis and enhances pattern separation. Psychoneuroendocrinology. 2015;51:431-9.
103. Lanciego JL, Wouterlood FG. A half century of experimental neuroanatomical tracing. J Chem Neuroanat. 2011;42(3):157-83.
104. Chen S, Aston-Jones G. Axonal collateral-collateral transport of tract tracers in brain neurons: false anterograde labelling and useful tool. Neuroscience. 1998;82(4):1151-63.
105. Reiner A, Veenman CL, Medina L, Jiao Y, Del Mar N, Honig MG. Pathway tracing using biotinylated dextran amines. J Neurosci Methods. 2000;103(1):23-37.
106. Haggerty DL, Grecco GG, Reeves KC, Atwood B. Adeno-Associated Viral Vectors in Neuroscience Research. Mol Ther Methods Clin Dev. 2020;17:69-82.
107. Howard DB, Powers K, Wang Y, Harvey BK. Tropism and toxicity of adeno-associated viral vector serotypes 1, 2, 5, 6, 7, 8, and 9 in rat neurons and glia in vitro. Virology. 2008;372(1):24-34.
108. Frank SJ, Fuchs SY. Modulation of growth hormone receptor abundance and function: roles for the ubiquitin-proteasome system. Biochim Biophys Acta. 2008;1782(12):785-94.
109. Nunez J. Morris Water Maze Experiment. J Vis Exp. 2008(19).
110. Morris R. Developments of a water-maze procedure for studying spatial learning in the rat. J Neurosci Methods. 1984;11(1):47-60.
111. Moser MB, Moser EI, Forrest E, Andersen P, Morris RG. Spatial learning with a minislab in the dorsal hippocampus. Proc Natl Acad Sci U S A. 1995;92(21):9697-701.
112. Sanders H, Ji D, Sasaki T, Leutgeb JK, Wilson MA, Lisman JE. Temporal coding and rate remapping: Representation of nonspatial information in the hippocampus. Hippocampus. 2019;29(2):111-27.
113. Iaria G, Chen JK, Guariglia C, Ptito A, Petrides M. Retrosplenial and hippocampal brain regions in human navigation: complementary functional contributions to the formation and use of cognitive maps. Eur J Neurosci. 2007;25(3):890-9.
114. Hafting T, Fyhn M, Molden S, Moser MB, Moser EI. Microstructure of a spatial map in the entorhinal cortex. Nature. 2005;436(7052):801-6.
115. Solstad T, Boccara CN, Kropff E, Moser MB, Moser EI. Representation of geometric borders in the entorhinal cortex. Science. 2008;322(5909):1865-8.
116. Cho J, Sharp PE. Head direction, place, and movement correlates for cells in the rat retrosplenial cortex. Behav Neurosci. 2001;115(1):3-25.
117. Sargolini F, Fyhn M, Hafting T, McNaughton BL, Witter MP, Moser MB, et al. Conjunctive representation of position, direction, and velocity in entorhinal cortex. Science. 2006;312(5774):758-62.
118. Wills TJ, Barry C, Cacucci F. The abrupt development of adult-like grid cell firing in the medial entorhinal cortex. Front Neural Circuits. 2012;6:21.
119. Gerlei K, Passlack J, Hawes I, Vandrey B, Stevens H, Papastathopoulos I, et al. Grid cells are modulated by local head direction. Nat Commun. 2020;11(1):4228.
120. Honda Y, Ishizuka N. Topographic distribution of cortical projection cells in the rat subiculum. Neurosci Res. 2015;92:1-20.

121. Sharp PE, Green C. Spatial correlates of firing patterns of single cells in the subiculum of the freely moving rat. J Neurosci. 1994;14(4):2339-56.
122. Powell AL, Vann SD, Olarte-Sanchez CM, Kinnavane L, Davies M, Amin E, et al. The retrosplenial cortex and object recency memory in the rat. Eur J Neurosci. 2017;45(11):1451-64.
123. Overstreet-Wadiche LS, Westbrook GL. Functional maturation of adult-generated granule cells. Hippocampus. 2006;16(3):208-15.
124. Bonhoeffer T, Yuste R. Spine motility. Phenomenology, mechanisms, and function. Neuron. 2002;35(6):1019-27.
125. Gisabella B, Farah S, Peng X, Burgos-Robles A, Lim SH, Goosens KA. Growth hormone biases amygdala network activation after fear learning. Transl Psychiatry. 2016;6(11):e960.
126. Furigo IC, Metzger M, Teixeira PD, Soares CR, Donato J, Jr. Distribution of growth hormone-responsive cells in the mouse brain. Brain Struct Funct. 2017;222(1):341-63.
127. Moser MB, Rowland DC, Moser EI. Place cells, grid cells, and memory. Cold Spring Harb Perspect Biol. 2015;7(2):a021808.
128. Kajiwara R, Wouterlood FG, Sah A, Boekel AJ, Baks-te Bulte LT, Witter MP. Convergence of entorhinal and CA3 inputs onto pyramidal neurons and interneurons in hippocampal area CA1--an anatomical study in the rat. Hippocampus. 2008;18(3):266-80.
129. Carr MF, Frank LM. A single microcircuit with multiple functions: state dependent information processing in the hippocampus. Curr Opin Neurobiol. 2012;22(4):704-8.
130. Ramis M, Sarubbo F, Sola J, Aparicio S, Garau C, Miralles A, et al. Cognitive improvement by acute growth hormone is mediated by NMDA and AMPA receptors and MEK pathway. Prog Neuropsychopharmacol Biol Psychiatry. 2013;45:11-20.
131. McHugh TJ, Jones MW, Quinn JJ, Balthasar N, Coppari R, Elmquist JK, et al. Dentate gyrus NMDA receptors mediate rapid pattern separation in the hippocampal network. Science. 2007;317(5834):94-9.
132. Hasselmo ME, McGaughy J. High acetylcholine levels set circuit dynamics for attention and encoding and low acetylcholine levels set dynamics for consolidation. Prog Brain Res. 2004;145:207-31.
133. Dannenberg H, Young K, Hasselmo M. Modulation of Hippocampal Circuits by Muscarinic and Nicotinic Receptors. Front Neural Circuits. 2017;11:102.
134. Grella SL, Neil JM, Edison HT, Strong VD, Odintsova IV, Walling SG, et al. Locus Coeruleus Phasic, But Not Tonic, Activation Initiates Global Remapping in a Familiar Environment. J Neurosci. 2019;39(3):445-55.
135. Tran AH, Uwano T, Kimura T, Hori E, Katsuki M, Nishijo H, et al. Dopamine D1 receptor modulates hippocampal representation plasticity to spatial novelty. J Neurosci. 2008;28(50):13390-400.
136. Solstad T, Yousif HN, Sejnowski TJ. Place cell rate remapping by CA3 recurrent collaterals. PLoS Comput Biol. 2014;10(6):e1003648.
137. Treves A, Rolls ET. Computational constraints suggest the need for two distinct input systems to the hippocampal CA3 network. Hippocampus. 1992;2(2):189-99.
138. Richards BA, Frankland PW. The Persistence and Transience of Memory. Neuron. 2017;94(6):1071-84.
139. Vlasov K, Van Dort CJ, Solt K. Optogenetics and Chemogenetics. Methods Enzymol. 2018;603:181-96.
140. Ulyanova AV, Cottone C, Adam CD, Gagnon KG, Cullen DK, Holtzman T, et al. Multichannel Silicon Probes for Awake Hippocampal Recordings in Large Animals. Front Neurosci. 2019;13:397.
141. Buzsaki G, Stark E, Berenyi A, Khodagholy D, Kipke DR, Yoon E, et al. Tools for probing local circuits: high-density silicon probes combined with optogenetics. Neuron. 2015;86(1):92-105.
142. Garthe A, Behr J, Kempermann G. Adult-generated hippocampal neurons allow the flexible use of spatially precise learning strategies. PLoS One. 2009;4(5):e5464.
143. Bartke A. Growth hormone and aging: a challenging controversy. Clin Interv Aging. 2008;3(4):659-65.

Papers 1-3

Paper 1

Haugland, K.G, Sugar, J., Witter, M.P.

Development and topographical organization of projections from the hippocampus and parahippocampus to the retrosplenial cortex

European Journal of Neuroscience, March 2019, doi: 10.1111/ejn.14395.

Received: 5 September 2018 | Revised: 30 January 2019 | Accepted: 15 February 2019

DOI: 10.1111/ejn.14395

RESEARCH REPORT

WILEY EJN European Journal of Neuroscience FENS

Development and topographical organization of projections from the hippocampus and parahippocampus to the retrosplenial cortex

Kamilla G. Haugland* | **Jørgen Sugar*** | **Menno P. Witter**

Kavli Institute for Systems Neuroscience, Centre for Neural Computation, Egil and Pauline Braathen and Fred Kavli Center for Cortical Microcircuits, NTNU Norwegian University for Science and Technology, Trondheim, Norway

Correspondence
Menno P. Witter, Kavli Institute, The Faculty of Medicine and Health Sciences, NTNU, Trondheim, Norway.
Email: menno.witter@ntnu.no

Present Address
Department of Clinical Medicine, University of Tromsø—The Arctic University of Norway, Tromsø, Norway

Funding information
Kavli Foundation; Centre for Neural Computation, Grant/Award Number: 223262; NORBRAIN1, Grant/Award Number: 197467; The Arctic University of Norway, Grant/Award Number: 227769

Abstract

The rat hippocampal formation (HF), parahippocampal region (PHR), and retrosplenial cortex (RSC) play critical roles in spatial processing. These regions are interconnected, and functionally dependent. The neuronal networks mediating this reciprocal dependency are largely unknown. Establishing the developmental timing of network formation will help to understand the emergence of this dependency. We questioned whether the long-range outputs from HF-PHR to RSC in Long Evans rats develop during the same time periods as previously reported for the intrinsic HF-PHR connectivity and the projections from RSC to HF-PHR. The results of a series of retrograde and anterograde tracing experiments in rats of different postnatal ages show that the postnatal projections from HF-PHR to RSC display low densities around birth, but develop during the first postnatal week, reaching adult-like densities around the time of eye-opening. Developing projections display a topographical organization similar to adult projections. We conclude that the long-range projections from HF-PHR to RSC develop in parallel with the intrinsic circuitry of HF-PHR and the projections of RSC to HF-PHR.

KEYWORDS

connectivity, entorhinal cortex, parasubiculum, presubiculum, subiculum

1 | INTRODUCTION

The hippocampal formation (HF) and the parahippocampal region (PHR) play critical roles in spatial processing (Jarrard, 1978; Maguire, Nannery, & Spiers, 2006). In both regions, spatially modulated neurons are found. Place cells, located in HF, fire at specific locations in the environment (O'Keefe & Dostrovsky, 1971), whereas grid cells, head direction cells, border cells, and speed cells have been reported in various subdivisions of PHR, such as the medial entorhinal cortex (MEC), presubiculum (PrS), and parasubiculum (PaS; Taube, Muller, & Ranck, 1990; Fyhn, Molden, Witter, Moser, & Moser, 2004; Solstad, Boccara, Kropff, Moser, & Moser, 2008; Boccara et al., 2010; Kropff, Carmichael, Moser, & Moser, 2015). It is currently thought that the HF-PHR interaction is necessary to maintain proper place cell and grid cell modulation (Bonnevie et al., 2013; Renno-Costa & Tort, 2017; Solstad, Moser,

Abbreviations: BDA, biotinylated dextran amine; EC, entorhinal cortex; FB, fast blue; HF, hippocampal formation; LEC, lateral entorhinal cortex; MEC, medial entorhinal cortex; PaS, parasubiculum; PB, phosphate buffer; PER, perirhinal cortex; PHR, parahippocampal region; POR, postrhinal cortex; P, postnatal; PrS, presubiculum; RSC, retrosplenial cortex; SUB, subiculum.

*These authors contributed equally to this study.

Edited by Dr. Yoland Smith. Reviewed by: Kathleen Rockland and Ricardo Insausti.

All peer review communications can be found with the online version of the article.

& Einevoll, 2006). In the classical model of HF-PHR circuitry, neurons in superficial layers of EC are the main source of cortical input to HF. Output from the HF originates in Cornu Ammonis fields CA2, and CA1, and the subiculum (SUB), targeting several subcortical and cortical structures including the deep layers of EC as well as PrS and PaS. Neurons in the deep layers of EC originate a main output of the HF-PHR, reaching several subcortical and cortical structures (Cappaert, Van Strien, & Witter, 2015).

Several of HF and PHR subdivisions, in particular, SUB, PrS, PaS, and MEC share connectivity with the retrosplenial cortex (RSC; Finch, Derian, & Babb, 1984; Agster & Burwell, 2009; Honda, Furuta, Kaneko, Shibata, & Sasaki, 2011; Honda & Ishizuka, 2015). Located dorsal to HF and PHR, RSC forms the most caudal portion of the cingulate cortex, and has been suggested to form a continuum with PrS in the monkey (Berger, Alvarez, & Pelaprat, 1997). A close functional relationship between HF-PHR and RSC is evident as RSC also contains spatially modulated neurons (Alexander & Nitz, 2015; Cho & Sharp, 2001; Mao, Kandler, McNaughton, & Bonin, 2017). Malfunction of the RSC results in diminished spatial memory, like the outcome of a dysfunctional HF-PHR (Iaria, Bogod, Fox, & Barton, 2009; Maguire, 2001; Sutherland, Whishaw, & Kolb, 1988). Given that both HF-PHR and RSC are important for spatial cognitive functions, it has been suggested that these areas are reciprocally dependent on each other for proper processing of spatial information (Ranganath & Ritchey, 2012; Vann, Aggleton, & Maguire, 2009). However, the neuronal networks and mechanisms mediating this reciprocal dependency are largely unknown.

In recent years, we and others have used analyses of brain development as a way to study the functional interactions and respective dependencies between neurons and networks in the HF-PHR (Bjerknes, Langston, Kruge, Moser, & Moser, 2015; Canto, Koganezawa, & Witter, 2011; Donato, Jacobsen, Moser, & Moser, 2017; Langston et al., 2010; Muessig, Hauser, Wills, & Cacucci, 2015; O'Reilly, Gulden Dahl, Ulsaker Kruge, & Witter, 2013; O'Reilly et al., 2014; Sugar & Witter, 2016; Wills, Cacucci, Burgess, & O'Keefe, 2010). Our data suggest that the HF-EC interconnectivity and long-range inputs to HF-PHR start to develop around birth, and display adult-like topographical organizations before eye-opening and before the animal starts active exploration of the environment (O'Reilly et al., 2013, 2014; Sugar & Witter, 2016). In view of the close functional relationship between HF-PHR and RSC, we aimed to investigate whether long-range outputs from HF-PHR develop during the same time periods as the intrinsic HF-PHR connectivity and long-range inputs to the region. In this study, we describe the postnatal development of HF-PHR projections to RSC based on a series of retrograde and anterograde tracing experiments in rats of different postnatal ages.

2 | MATERIALS AND METHODS

2.1 | Surgeries and perfusion

In this study, we used a total of 69 female and male Long Evans rats aged between postnatal day 0 (P0) and 15 (P15). The pups were bred in-house and housed in enriched cages together with their parents and littermates. Cages were checked for pups every morning and evening, and the day pups were observed was considered P0. In the paper, we describe data related to the age of the animal, meaning data derived from animals perfused at that particular day. Litters with more than 10 pups were culled to 10 at P0 or P1 to avoid unnecessary stress for the animals. The animals lived in a controlled environment (22 ± 1°C; humidity 60%; lights on from 8:00 p.m. to 8:00 a.m.). Food and water were available ad libitum. The experimental protocols followed the European Communities Council Directive and the Norwegian Experiments on Animals Act and local directives of the responsible veterinarian at the Norwegian University of Science and Technology.

All surgeries were conducted under isoflurane gas anesthesia. Animals were placed in an induction chamber and fully anesthetized before they were moved to a stereotaxic frame where the head was fixed using a neonatal mask and mouthpiece (model 973-B; Kopf, Tujunga, CA, USA) and zygoma ear cups (model 921; Kopf). Before incision, the skin was disinfected with 2% iodine in 65% ethanol, and as a local analgesic, Bupivacain (0.2 ml per 100 g bodyweight of a 0.5 mg/ml solution; Marcain, Astra Zeneca, London, UK) was injected subcutaneously at the place of incision. The skin was opened with a small-sized and sharp tipped scissor. After incision, the mouthpiece and ear cups were adjusted so that bregma and lambda were aligned horizontally. The bone over the injection site and over the posterior extreme of the sagittal sinus was then removed. The exact place of injection was determined using the junction of the transverse and sagittal sinus as a reference for the anteroposterior coordinate, the lateral edge of the midsagital sinus as a reference for the mediolateral coordinate, and the level of the dura as a reference for the dorsoventral coordinate. The retrograde tracers Fast Blue (FB; 1% in 0.125 M PB, EMS Chemie, Domat, Switzerland), Fluoro Gold (2.5% in H_20, Fluorochrome, Denver, CO, USA), DiI (1.5% in EtOH, Paisley, UK), IX retrobeads (Red and Green, Lumafluor, Durham, NC), FluoSpheres 505/515 (0.04 μm, 5%, F8795 Thermo Fischer Scientific [TMS], Waltham, MA, USA), and FluoSpheres 580/605 (0.02 μm, 2%, F8786, TMS) were pressure injected at the identified coordinates. Before injection, the dura was punctured, and glass micropipettes with an outer tip-diameter of 30–60 μm (30-0044, Harvard Apparatus, MA. Pulled with a PP-830 puller, Narishige, Japan) or Hamilton syringes (1 μl, 25 ga, 7001, Sigma-Aldrich, St. Louis, MO,

USA) were used to deliver the tracer. For the majority of the experiments, we used glass micropipettes connected to a pneumatic pump. To avoid dehydration during surgery, appropriate amounts of sterile saline (room temperature) were administered subcutaneously. Animals received carprofen during surgery, which acted as an analgesic during surgery and the first 24 hr after surgery (1 ml per 100 g bodyweight of a 0.5 mg/ml solution; Rimadyl, Pfizer, NY, USA). After surgery, the incision was sutured and the pups were allowed to recover under a heating lamp. When fully awake, the pups were returned to maternal care until the time of kill. In addition to the retrograde tracer injections, we injected, in a subset of animals ($n = 11$), the anterograde tracer biotinylated dextran amine (BDA; 5% in phosphate buffer (PB; 0.125 M in H_20; pH 7.4), 10,000 MW, D1956, Invitrogen, Eugene, OR, USA) into SUB and PHR. The tracer was delivered through micropipettes with an outer tip-diameter of 20–25 μm, using iontophoresis (4–6 μA, alternating currents, 6 s on/6 s off, for 5–15 min current source 51595; Stoelting, Wood Dale, IL, USA).

We euthanized the animals 18–30 hr after surgery under terminal anesthesia with isoflurane. The thorax was opened with a small-sized scissor and cold Ringer's solution was perfused through the body by inserting the needle in the left ventricle and opening the right auricle. When the liver turned pale (~30 s), the perfusion solution was changed to a 4% solution of freshly depolymerized paraformaldehyde in PB (pH 7.4). In the case of P0–P2 animals, 0.1% glutaraldehyde was added to the fixative. The brain was removed from the skull and postfixed overnight at 4°C in the same fixative. Twenty-four hours after perfusion, the brains were transferred to PB containing 2% DMSO (VWR) and 20% glycerol (VWR).

2.2 | Tissue processing

Brains were cut on a freezing microtome (HM-430 Thermo Scientific, Waltham, MA) in 40 or 50 μm thick horizontal or sagittal sections. Depending on the age of the animal, sections were collected in 4–6 equally spaced series. For experiments using retrograde tracers, two of the series were mounted directly on superfrost slides (Thermo Scientific). For experiments using anterograde tracers, one of the series was mounted directly on superfrost slides. Another series was stained to visualize the anterograde tracer biotinylated dextran amine as previously described (O'Reilly et al., 2013). The remaining sections were collected in vials containing 2% DMSO and 20% glycerol in PB and stored at −20°C until further processing. One of the mounted series was Nissl stained. The sections were dehydrated in ethanol, cleared in xylene (VWR), and rehydrated before placed in cresyl violet (0.1% in water, C5042, Sigma) for 2–6 min. Subsequently, the sections were rinsed quickly in water, before placing them in 50% ethanol containing acetic acid to differentiate the staining. The stained sections were dehydrated in ethanol, cleared in xylene and finally coverslipped with Entellan (107961, Merck, Darmstadt, Germany).

In experiments with retrograde tracers, the second mounted series was cleared in toluene and coverslipped with Entellan for microscopic visualization using fluorescence illumination at the appropriate excitation wavelengths (Zeiss Axio Imager M1/2). Digital images of successful injections, retrogradely labeled neurons in PHR or Nissl-stained tissue were obtained using a slide scanner equipped for either brightfield or fluorescence imaging (Zeiss Mirax Midi; objective 20X; NA 0.8). Next, two independent persons assessed all digital images. In the few cases when there were discrepancies between the two observers, we returned to the actual sections to resolve any discrepancies. For illustrative purposes, images of sections were exported using Panoramic Viewer software (3DHistech, Budapest, Hungary) and processed in Adobe Photoshop and Illustrator (CS6, Adobe Systems, San Jose, CA, USA).

2.3 | Location of injections

As brains of different ages have different sizes, we aimed to normalize the position of the injections in RSC. For this purpose, we took advantage of a reference 3D-atlas brain (Papp, Leergaard, Calabrese, Johnson, & Bjaalie, 2014, 2015). First, we identified regularly spaced coordinates of the dorsal, ventral, rostral, and caudal borders of, respectively, A29 and A30 in the atlas brain. The lines between the respective coordinates were smoothed using local regression. Next, we calculated the cutting angle of our experimental brains relative to the atlas brain, and generated matching sections of the standard atlas brain with the same cutting angle. To identify the best matching atlas sections, we used landmarks and cytoarchitectonic borders present in the section containing the center of each injection as selection criteria. The atlas coordinate of the center of each injection was obtained and represented as an age-normalized 3D point-measure of the injection site within RSC. For illustrative purposes, the injections were plotted within the 3D volume (Figure 1a, ITK-SNAP, NIH). As caudal RSC is curved both along the dorsoventral and rostrocaudal axis, we flattened RSC and transposed each injection into a 2D plane (Figure 1b). We divided the surface area of A29 and A30 into multiple triangles (for methodological details, see Sugar & Witter, 2016). In short, the coordinates of the corners of these triangles were obtained from the coordinates of the dorsal and ventral borders of A29 and A30. For each injection, we calculated the shortest vector between the injection and the cortical surface within any of the triangles. Thereafter, we calculated the coordinate of the intersection of the vector with the plane within the triangle. This coordinate represented the "transposed" location onto the cortical surface of each injection and effectively flattened the 3D coordinates of the injections into a 2D plane of RSC (Figure 1b). Next, we normalized the dorsoventral and rostrocaudal

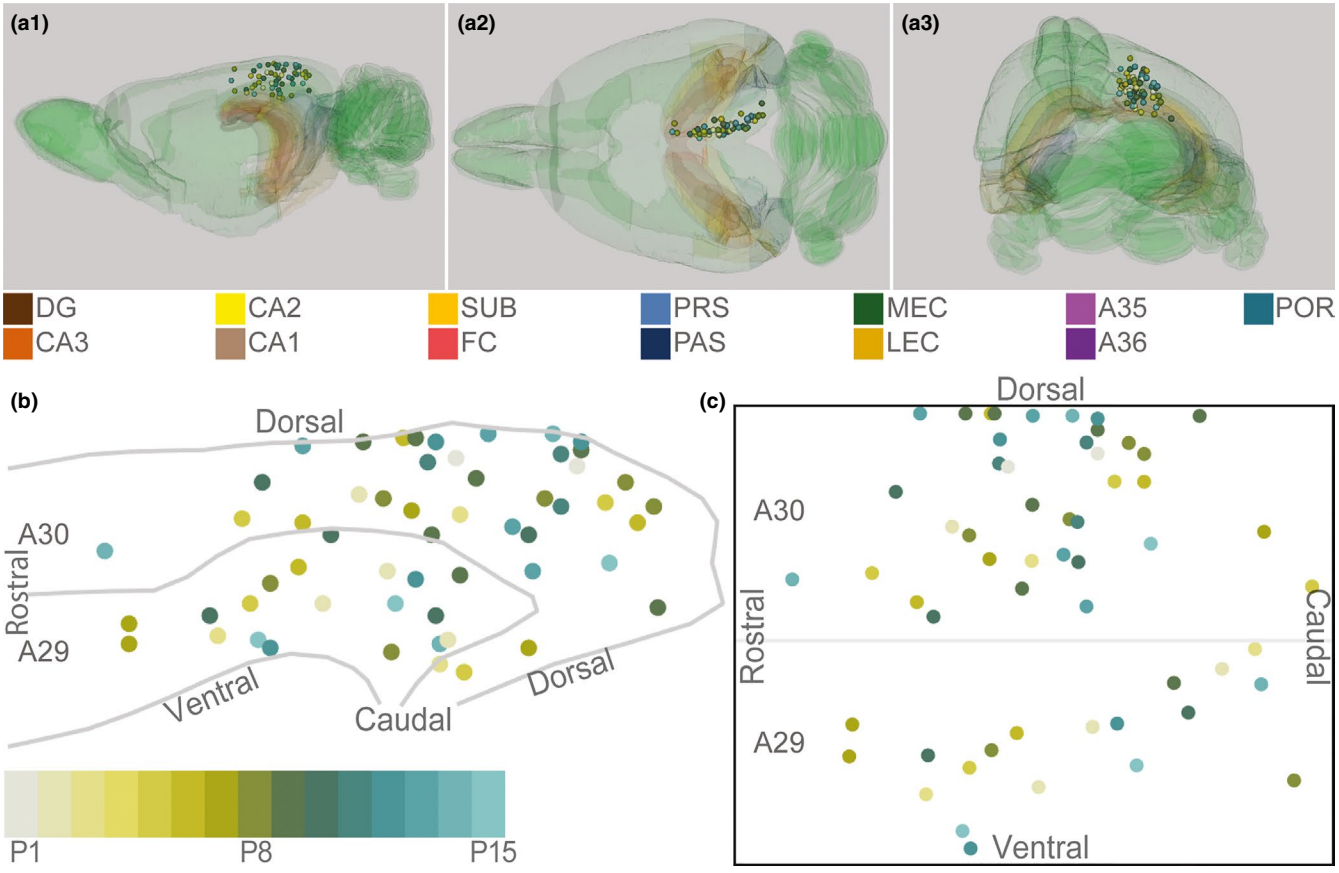

FIGURE 1 Schematic representation of injections in RSC. (a) The location of the center of each injection was normalized to a standard 3D atlas of the rat brain (Waxhom space, http://software.incf.org; Papp et al., 2014). Sagittal (a1), dorsal (a2), and caudal view (a3) of the 3D brain with the center of each injection (colored spheres). Para(hippocampal) structures are color-coded, and the rest of the brain is colored green. In all panels, each injection is color-coded according to the bottom left color scheme; light gray colored injections represent injections in pups aged P1, green colored injections represent injections in pups aged P8, whereas cyan colored injections represent injections in pups aged close to P15. (b) Midsagital view of the center of the injections projected to the pial surface. The mediolateral position was disregarded to allow the injections to be plotted in 2D. Gray lines depict dorsal and ventral borders of RSC and the border between A29 and A30 of RSC. (c) Flatmap of the injections (see methods for details). The 3D RSC was converted to a 2D normalized flatmap to represent the relative rostrocaudal and dorsoventral positions of all injections. The figure is oriented with rostral RSC (left), caudal RSC (right), dorsal RSC (top) ventral RSC (bottom) to each of the sides of the rectangle. Gray line depicts the border between A29 and A30 in RSC. [Colour figure can be viewed at wileyonlinelibrary.com]

coordinates of all injections (Figures 1c and 2). The normalized dorsoventral coordinate was defined as the ratio of the distance from the injection to the ventral border of RSC divided by the distance from the dorsal to the ventral border of RSC. The normalized rostrocaudal coordinate was defined as the ratio of the distance from the injection to the rostral pole of RSC divided by the distance from the rostral to the caudal pole of the injection. From this, we derived the normalized rostrocaudal and dorsoventral positions of each injection (Figure 1c).

3 | RESULTS

3.1 | Injection sites

To investigate the development of HF and PHR to RSC projection patterns, we injected retrograde tracers in different locations within RSC of differently aged pups. We analyzed 56 injections of retrograde tracers in 38 animals (Figures 1 and 2; Table 1, female $n = 20$; male $n = 18$), providing us with 37 injections in A30 and 19 injections in A29. We regarded each of these injections as independent experiments. Following nine of these injections, we did not observe retrogradely labeled cells in HF-PHR, although in other areas, such as the thalamus, labeled cells were present. The observation of retrogradely labeled neurons in other brain structures implied that the lack of retrogradely labeled neurons in HF-PHR probably reflected the absence of HF-PHR-to-RSC projections rather than failure of dye transport. More than half of these experiments were performed in animals younger than P3, however a few older animals also showed similar patterns of retrograde transport (P1, P3, P10 and P14; $n = 1$, P2; $n = 3$, P9; $n = 2$). Most of these injections ($n = 8$) were located in the rostral half of RSC.

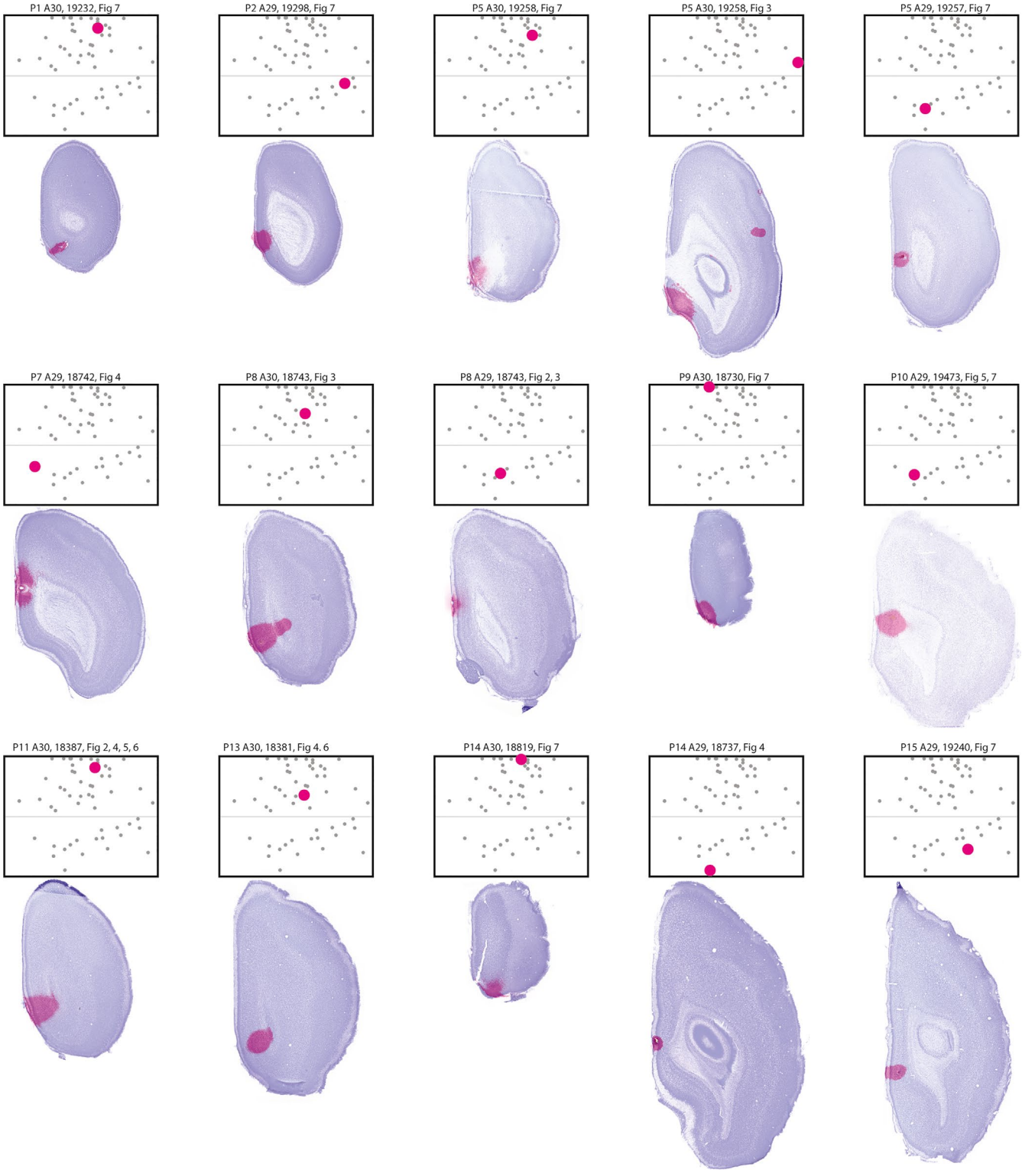

FIGURE 2 Injections used in figures. Images of the section containing the center of the injection overlaid on the image of the neighboring Nissl-stained section are shown together with the flatmaps indicating the normalized position of the respective injection (large dot). Smaller dots depict the normalized position of other injections used for analysis. Heading depicts age of the animal at perfusion, area injected, animal identity, and in which figure retrogradely labeled neurons of the injection were displayed. [Colour figure can be viewed at wileyonlinelibrary.com]

3.2 | General distribution patterns

In accordance with previous studies in the adult, we observed retrogradely labeled neurons in the anterior nuclei of the thalamus, anterior cingulate cortex, prelimbic cortex, orbitofrontal cortex, parietal and visual cortices, in the claustrum, and the septal complex (van Groen & Wyss, 1990, 1992, 2003; Jones, Groenewegen, & Witter, 2005).

TABLE 1 All injections used in analysis

				Injection size	Injection site			Labeled neurons observed					
Animal	**Age**	**Sex**	**Dye**	**Vertical and Horizontal**	**Area**	**R-C**	**Layers**	**CA1**	**Sub**	**PrS/PaS**	**EC**	**POR**	**PER**
19232	P1	F	DiI	600 and 400 µm	A30	I	Sup + deep	–	+	+	+	+	–
19470	P1	M	DiI	600 and 670 µm	A30	I	Sup + deep	–	–	–	–	–	–
19297	P2	F	DiI	915 and 630 µm	A29	I	Sup + deep	–	–	–	–	–	–
19297	P2	F	FB	615 and 555 µm	A29	I	Sup + deep	–	–	–	–	–	–
19298	P2	F	DiI	930 and 710 µm	A30	I	Deep	–	–	–	–	–	–
19298	P2	F	FB	920 and 670 µm	A29	C	Sup + deep	–	+	+	+	–	–
19049	P3	F	FB	380 and 450 µm	A29	C	Sup + deep	–	++	+	–	–	–
19299	P3	F	DiI	300 and 270 µm	A29	R	Sup	–	+	+	+	–	–
19299	P3	F	FB	240 and 310 µm	A30	I	Sup + deep	–	–	–	–	–	–
19257	P5	M	DiI	500 and 450 µm	A30	R	Sup + deep	–	+	++	+	+	–
19257	P5	M	FB	600 and 570 µm	A29	R	Sup + deep	–	+++	+	–	–	–
19258	P5	M	DiI	200 and 510 µm	A30	C	Sup + deep	–	++	++	+	+	–
19258	P5	M	FB	900 and 1,100 µm	A30	C	Sup + deep	+	+++	+++	+	+	–
18810	P6	M	FB	400 and 370 µm	A30	I	Sup + deep	–	+++	++	+	–	–
18810	P6	M	DiI	210 and 610 µm	A30	I	Sup + deep	–	+++	++	+	–	–
19259	P6	M	FB	700 and 740 µm	A29	I	Sup + deep	–	+	+	–	–	–
18379	P6	F	FB	920 and 1,000 µm	A30	C	Deep	–	+++	+++	+++	+++	–
18391	P7	M	FB	800 and 1,200 µm	A30	C	Sup + deep	–	+++	+++	+++	+++	–
18742	P7	M	DiI	340 and 400 µm	A29	R	Sup + deep	–	+++	+++	+	–	–
18742	P7	M	FG	300 and 450 µm	A29	R	Sup	+	+++	+++	++	–	–
19260	P7	M	DiI	100 and 510 µm	A30	I	Sup + deep	–	+++	+++	+	–	–
18743	P8	F	DiI	400 and 250 µm	A29	R	Sup	+	+++	++	+	–	–
18743	P8	F	FB	1,400 and 1,200 µm	A30	I	Sup + deep	–	+++	+++	++	+++	–
18943	P8	F	IX 488	300 and 450 µm	A30	I	Sup	+	+++	++	+	+++	–
19127	P8	M	DiI	315 and 250 µm	A29	C	Sup + deep	–	++	+	+	+	–
19127	P8	M	FB	360 and 550 µm	A30	C	Deep	+	+++	+++	+	++	–
19235	P8	M	DiI	1,300 and 580 µm	A30	C	Sup + deep	+	+++	+++	++	++	–
18385	P9	F	DiI	90 and 130 µm	A30	I	Deep	–	–	–	–	–	–
18385	P9	F	FB	1,400 and 1,200 µm	A30	C	Sup + deep	+	+++	+++	+++	+++	–
18730	P9	F	FB	950 and 780 µm	A30	I	Sup + deep	+	++	++	++	++	–

(Continues)

TABLE 1 (Continued)

				Injection size	Injection site			Labeled neurons observed					
Animal	**Age**	**Sex**	**Dye**	**Vertical and Horizontal**	**Area**	**R-C**	**Layers**	**CA1**	**Sub**	**PrS/PaS**	**EC**	**POR**	**PER**
18730	P9	F	DiI	300 and 450 µm	A30	I	Sup	–	++	++	+	+	–
19051	P9	M	DiI	200 and 390 µm	A29	I	Deep	–	+++	+	–	–	–
19236	P9	M	FB	910 and 1,050 µm	A30	I	Sup + deep	+	+++	+++	+++	++	–
19236	P9	M	DiI	270 and 200 µm	A30	I	Deep	–	–	–	–	–	–
18380	P10	F	FB	2,030 and 980 µm	A30	R	Deep	–	+++	+++	+++	+++	+
19237	P10	F	DiI	340 and 390 µm	A30	I	Deep	–	+	+	–	+	–
19237	P10	F	FB	370 and 320 µm	A30	I	Deep	–	–	–	–	–	–
19473	P10	F	FB	520 and 510 µm	A29	R	Deep	+	+++	++	+	–	–
19473	P10	F	DiI	220 and 250 µm	A29	C	Deep	–	+++	+	–	–	–
18387	P11	F	FB	1,300 and 940 µm	A30	I	Sup + deep	+	+++	+++	+++	+++	–
19239	P11	F	DiI	360 and 520 µm	A30	I	Sup + deep	–	+++	+	–	–	–
19455	P11	F	FB	780 and 610 µm	A30	I	Sup + deep	–	+++	+++	–	++	–
19053	P12	M	DiI	780 and 610 µm	A29	R	Sup + deep	+	+++	+	+	–	–
19053	P12	M	FB	130 and 140 µm	A29	I	Sup	–	+	–	–	–	–
19215	P12	M	FB	440 and 560 µm	A30	I	Deep	+	+++	+++	++	++	–
19216	P12	F	FB	310 and 290 µm	A30	I	Sup + deep	+	+	+	–	–	–
18381	P13	F	FB	820 and 870 µm	A30	I	Deep	–	+++	+++	+++	+++	–
19210	P13	M	FB	580 and 660 µm	A30	I	Sup + deep	+	+	+	+	+	–
19210	P13	M	DiI	1,100 and 930 µm	A30	C	Sup + deep	–	+++	+	+	–	–
19217	P13	M	FB	290 and 320 µm	A30	I	Deep	+	+	+	–	+	–
18746	P14	F	FB	630 and 700 µm	A30	R	Sup + deep	–	–	–	–	–	–
18746	P14	F	DiI	300 and 450 µm	A29	C	Sup + deep	+	+++	+	–	–	–
18819	P14	M	DiI	700 and 800 µm	A30	I	Sup + deep	–	+	+	+	++	–
18737	P15	F	FB	400 and 560 µm	A29	R	Sup	+	+++	+++	+++	+	+
19240	P15	M	DiI	340 and 340 µm	A30	C	Sup + deep	+	+	+	+	+	–
19240	P15	M	FB	580 and 650 µm	A29	I	Sup + deep	–	+++	++	+	+	–

List of all injections used in experiments including the animal identity, age at perfusion, sex, dye injected, size of the injection (diameter in the horizontal and vertical plane), area containing the center of the injection (A29 or A30), the rostrocaudal level of the injection (R: rostral, I: intermediate rostrocaudal and C: caudal levels of RSC), and whether injection covered deep and/or superficial layers of RSC. Columns to the right include information of whether we observed labeled cells (+: <5, ++: 5–10 cells in a section, +++: more than 10 cells in a section) in CA1, subiculum (Sub), pre- and parasubiculum (Prs/PaS), entorhinal cortex (EC), postrhinal cortex (POR), or perirhinal cortex (PER).

However, a detailed assessment of these projections was outside the scope of this paper. Within HF-PHR, we observed a few retrogradely labeled neurons in CA1 after some of the injections. In SUB, as well as in PrS and PaS, we observed many retrogradely labeled neurons. In PrS and PaS, most labeled neurons were located in layers V–VI. Some of the injections resulted in a moderate number of retrogradely labeled neurons in layers III and V–VI of MEC and in layers II–VI of postrhinal cortex (POR), whereas in only a few cases, we observed a few retrogradely labeled neurons in layers V–VI of perirhinal cortex (PER).

3.3 | Labeling in CA1

Nineteen of the injections (34%) resulted in a few retrogradely labeled neurons (typically 1–5 neurons in each section) in stratum radiatum and/or in stratum lacunosum moleculare of the most anterior part of dorsal CA1 (Figure 3a,b). The retrogradely labeled neurons generally had a non-pyramidal-shaped soma with several dendrites leaving the soma in several directions. In four of these cases (7% of the injections), we additionally observed single retrogradely labeled neurons (typically 1–3 neurons within a section) in the pyramidal layer

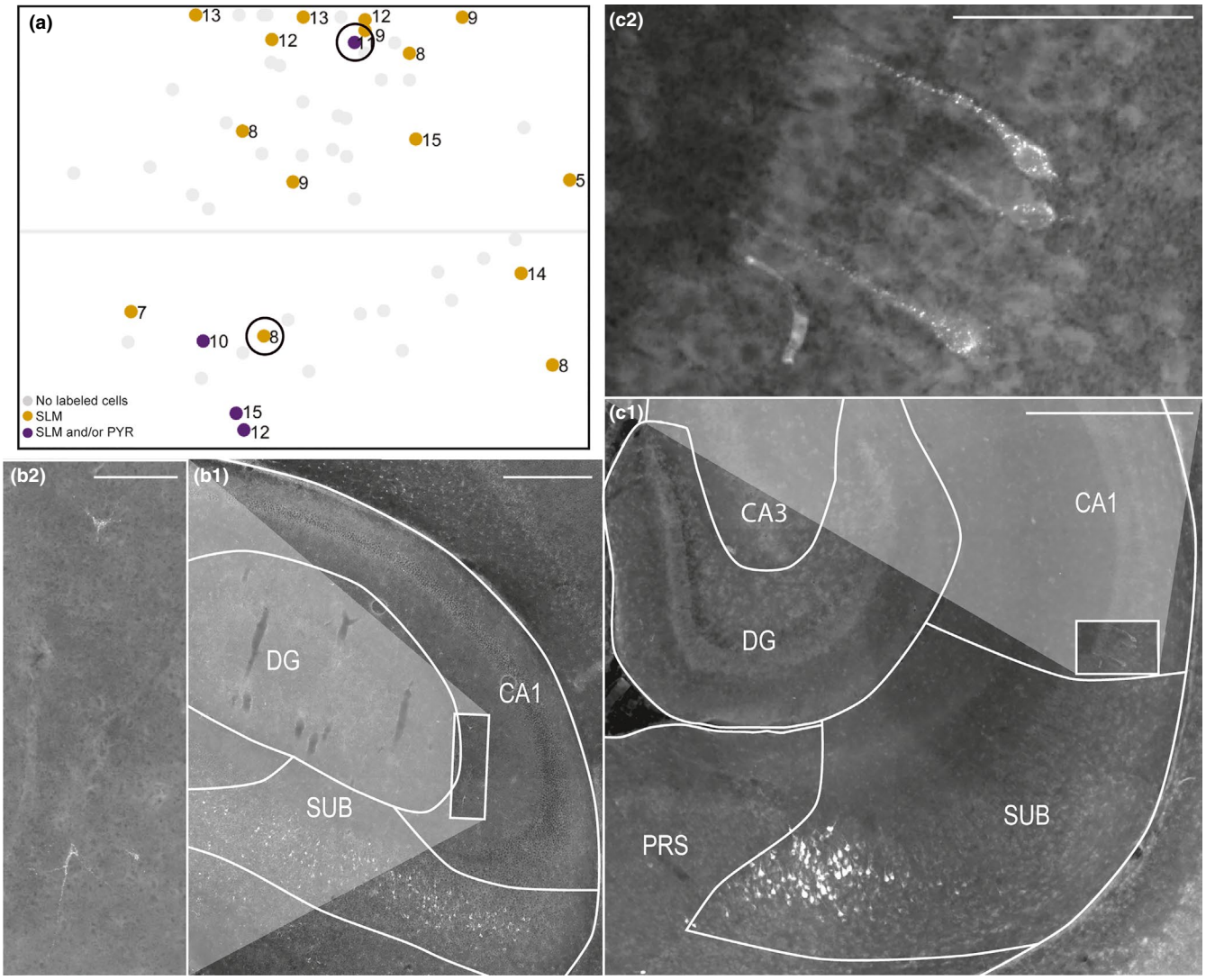

FIGURE 3 Labeled neurons in CA1. (a) Normalized flatmap of RSC. Dots represent injections resulting in retrogradely labeled neurons in the pyramidal layer and/or the stratum lacunosum moleculare and/or stratum radiatum of CA1. Light gray dots represent injections not resulting in retrogradely labeled neurons in CA1. Black circles indicate examples used in the figure (b) and (c). (b) A representative example of retrogradely labeled neurons in stratum radiatum of CA1 after an injection in A29 (animal 18743 P8, DiI). White square in B1 depicts the area shown in high power in B2. The retrogradely labeled neurons had a non-pyramidal-shaped soma and several dendrites leaving the soma in several directions. Scale bar: 500 µm (b1) and 100 µm (b2). (c) A representative example of retrogradely labeled neurons in the pyramidal layer of CA1 after an injection in A30 (animal 18387 P11, FB). White square in c1 depicts the area shown in high power in c2. The retrogradely labeled neurons had a pyramidal-shaped soma and a thick apical dendrite. Many retrogradely labeled neurons could also be seen in distal SUB. Scale bar: 500 µm (c1) and 100 µm (c2). White lines in B and C depict borders of hippocampal and parahippocampal subregions. [Colour figure can be viewed at wileyonlinelibrary.com]

of dorsal and/or intermediate dorsoventral CA1 (Figure 3a,c). The neurons generally had a pyramidal-shaped soma with a thick clearly visible apical dendrite. Such neurons were observed after three injections in A29 located close to the corpus callosum, and after one injection very dorsally in A30.

3.4 | Labeling in SUB

All injections resulting in retrogradely labeled neurons within HF-PHR, displayed retrogradely labeled neurons in the pyramidal layer of SUB. Additionally, SUB was the HF-PHR subregion that in every such experiment contained the highest number of retrogradely labeled neurons. We observed a marked topographical distribution of the labeled neurons in SUB, depending on the location of the injection. First, caudal injections within A30 resulted in retrogradely labeled neurons in the entire dorsoventral SUB, whereas progressively more rostral and ventral injections in A30 and A29 resulted in retrogradely labeled neurons, preferentially in more dorsal parts of SUB (Figure 4a). As illustrated, an injection in

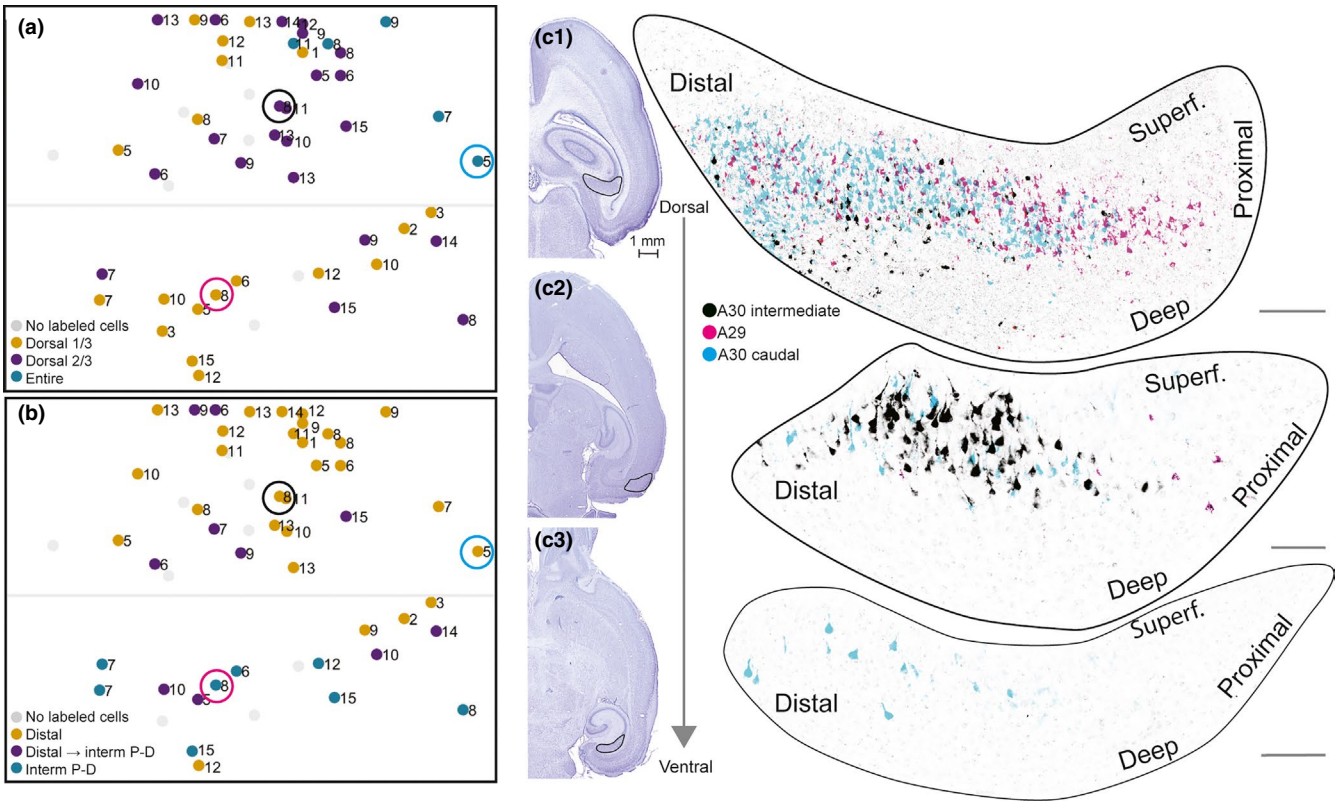

FIGURE 4 Labeled neurons in SUB. (a) Normalized flatmap of RSC illustrating the dorsoventral organization of the origin in SUB of projections to RSC. Injections resulting in retrogradely labeled neurons in the dorsal one-third of SUB (yellow dots), the dorsal two-thirds of SUB (purple dots), and the entire SUB (green dots). Gray dots depict injections not resulting in labeled neurons in SUB. Injections in the caudal A30 resulted in retrogradely labeled neurons in the entire SUB, whereas progressively more rostral and ventral injections resulted in retrogradely labeled neurons in more dorsal parts of SUB. (b) Normalized flatmap of RSC illustrating the proximodistal organization of the origin in SUB of projections to RSC. Injections were color-coded based on the distribution of the retrogradely labeled neurons: in the distal one-third of SUB (yellow dots), in distal SUB dorsally and progressively more proximal SUB at more ventral levels (purple dots), and in intermediate proximodistal SUB (green dots). Gray dots depict injections not resulting in labeled neurons within SUB. Injections in dorsal RSC resulted in retrogradely labeled neurons in distal SUB and progressively more ventral injections resulted in retrogradely labeled neurons in more proximal parts of SUB. (c) Representative examples of the distribution of retrogradely labeled neurons shown in three horizontal sections (c1–c3), taken at different dorsoventral levels after three injections. The distributions of the three cases were merged into one representation in order to illustrate the complex topography along the dorsoventral and proximodistal axes of the subiculum. Retrogradely labeled neurons after a caudal injection in A30 (cyan, 19258 P5, FB), an intermediate rostrocaudal A30 injection (black, 18743 P8, FB), and a ventral and more rostral A29 injection (magenta, 18743 P8, DiI). Circles in (a) and (b) depict the location of each injection in RSC. High-power images (right) of dorsal (top) and more ventral levels of SUB (bottom) are shown. Black contours in adjacent Nissl-stained sections (left) depict location of high-power images. Injections in A30 resulted in retrogradely labeled neurons in distal SUB (cyan and black), whereas injections in A29 resulted in retrogradely labeled neurons in more proximal SUB (magenta). Injections in caudal A30 (cyan) resulted in retrogradely labeled neurons along most of the dorsoventral level of distal SUB, whereas rostral injections resulted in labeled neurons in only the dorsal SUB (magenta and black). Scale bar: 100 μm. [Colour figure can be viewed at wileyonlinelibrary.com]

caudal A30 (cyan) resulted in retrogradely labeled neurons along the entire dorsoventral extent of SUB (Figure 4c1–3). In contrast an intermediately positioned injection in A30 (black), like most of the caudal injections in A29, resulted in retrogradely labeled neurons in the dorsal two-thirds of SUB (Figure 4c1–2). An injection in the rostral half of A29, like most of the rostral injections in A30, resulted in retrogradely labeled neurons in only the dorsal one-third of SUB (Figure 4a,c1, magenta).

The distribution of retrogradely labeled neurons also showed a clear topography along the proximodistal axis of SUB (Figure 4b,c). Injections in A30 resulted in retrogradely labeled cells in the distal extreme of SUB. Injections in A29 resulted in retrogradely labeled neurons in intermediate proximodistal SUB. We never found retrogradely labeled neurons in the proximal extreme of SUB. A few injections located in A29 and adjacent A30 resulted in retrogradely labeled cells in both distal and intermediate proximodistal SUB. The retrogradely labeled cells in distal SUB were always positioned at dorsal levels of SUB, whereas the retrogradely labeled cells in intermediate proximodistal parts were located in more ventral levels of SUB. This mixed pattern suggests that A29 and the directly adjacent parts of A30 receive input from both distal parts of dorsal SUB and intermediate proximodistal parts of more ventral SUB. In general, both young and older rats displayed similarly organized topographical distribution patterns, indicating the absence of clear effects of age, both with respect to the dorsoventral and the proximodistal location of retrogradely labeled cells in SUB.

3.5 | Labeling in PrS and PaS

All injections resulting in retrogradely labeled neurons within HF-PHR resulted in retrogradely labeled neurons in PrS and PaS. We observed retrogradely labeled neurons in superficial parts of layer V of PrS and PaS, directly deep to the lamina dissecans. The labeled neurons were positioned in a "band" of cells often in direct continuation with the retrogradely labeled neurons in distal SUB. Some injections also labeled neurons in deep parts of layer VI. In PrS, we rarely observed retrogradely labeled cell in layers II–III, whereas in PaS, we observed retrogradely labeled cells in superficial layers after nine injections (16% of all injections). All of these latter injections were located in the caudal half of A30 (Figure 5a).

The labeled neurons in PrS and PaS displayed a distinct topography dependent on the location of the injection within RSC (Figure 5b–f). Injections located caudally in A30 tended to result in retrogradely labeled cells more ventrally in PrS and PaS, covering the dorsal two-thirds of PrS and PaS. Injections in more rostral parts of A30 and the complete extend of A29 preferentially resulted in retrogradely labeled cells in only the most dorsal one-third of PrS. As illustrated, an injection centered in A30 (cyan, Figure 5b,e), like most of the caudal injections in A30 resulted in retrogradely labeled neurons in the

FIGURE 5 Labeled neurons in PrS and PaS. (a) Normalized flatmap of RSC illustrating the superficial-to-deep organization of the origin of RSC projections in PaS. Injections were color-coded based on the distribution of the retrogradely labeled neurons: in only layer V of PaS (yellow dots), or layer V and layers II–III of PaS (purple dots). Gray dots depict injections with no labeled neurons in PaS. Injections resulting in retrogradely labeled neurons in layers II–III of PaS (purple dots) are located in caudal A30. In PrS, labeled neurons were only seen in deep layer V and VI. No retrogradely labeled neurons were observed in superficial layers of PrS. Color-coded circles in A–C depict the location of injections in RSC, shown in figures (e,f). (b) Normalized flatmap of RSC illustrating the dorsoventral organization of the origin of RSC projections in PrS and PaS. Injections resulting in retrogradely labeled neurons in the dorsal one-third (yellow dots) and dorsal two-thirds of layer V of PrS and PaS (purple dots) are indicated. Gray dots depict injections with no labeled neurons in PrS or PaS. (c) Normalized flatmap of RSC illustrating the proximodistal organization of the origin of RSC projections in PrS and PaS. Injections resulting in retrogradely labeled neurons in only distal parts of layer V of PrS and the transverse extent of PaS (yellow dots), proximal PrS at dorsal levels and progressively more distal parts of layer V of PrS and PaS at more ventral levels (purple dots), and in proximal parts of layer V of PrS (green dots) are indicated. Gray dots depict injections that did not display a clear patterned distribution of retrogradely labeled cells in PrS/PaS or did not contain retrogradely labeled neurons. Injections resulting in retrogradely labeled neurons in distal PrS and the whole PaS were located in A30, whereas A29 contained the injections resulting in retrogradely labeled neurons in proximal PrS. (d) Nissl stains of sections from animal 18387 (P11). Sections were used as background in E and F. Black contours depict location of high-power images in (e) and (f). (e) Representative examples of the distribution of retrogradely labeled neurons shown in three horizontal sections (e1–e3), taken at different dorsoventral levels after two injections in different animals of different ages. The injections were located in rostral A29 (magenta; 18742 P7) and centered in A30 (cyan; 18387 P11). Color-coded circles in (a) and (b) depict the location of each injection in RSC. High-power images of dorsal (left) and more ventral levels of SUB, PrS, and PaS (right) are shown. The injection centered in A30 (cyan) resulted in retrogradely labeled neurons in SUB, LV/VI of PrS and LII/III/V/VI of PaS. Retrogradely labeled neurons were present in dorsal levels (e1–2) of PrS and PaS and in ventral parts of PrS (e3). The very rostral injection in A29 (magenta) resulted in retrogradely labeled cells in SUB and in layer V/VI of PrS and PaS. Retrogradely labeled neurons were located in the dorsal part of PrS (e1–2). Scale bar: 500 μm. (f) Representative examples of the distribution of retrogradely labeled neurons. Sections are organized as in E. The injections were centered in A30 (yellow, 18381 P13) and centered in ventral A29 (green 18737 P15). The injection in A30 resulted in retrogradely labeled cells in layer V/VI of distal PrS and PaS, whereas the injection in A29 resulted in retrogradely labeled neurons in layer V/VI of proximal PrS. Both cases displayed retrogradely labeled neurons in SUB and neither displayed retrogradely labeled neurons in superficial layers of PaS. [Colour figure can be viewed at wileyonlinelibrary.com]

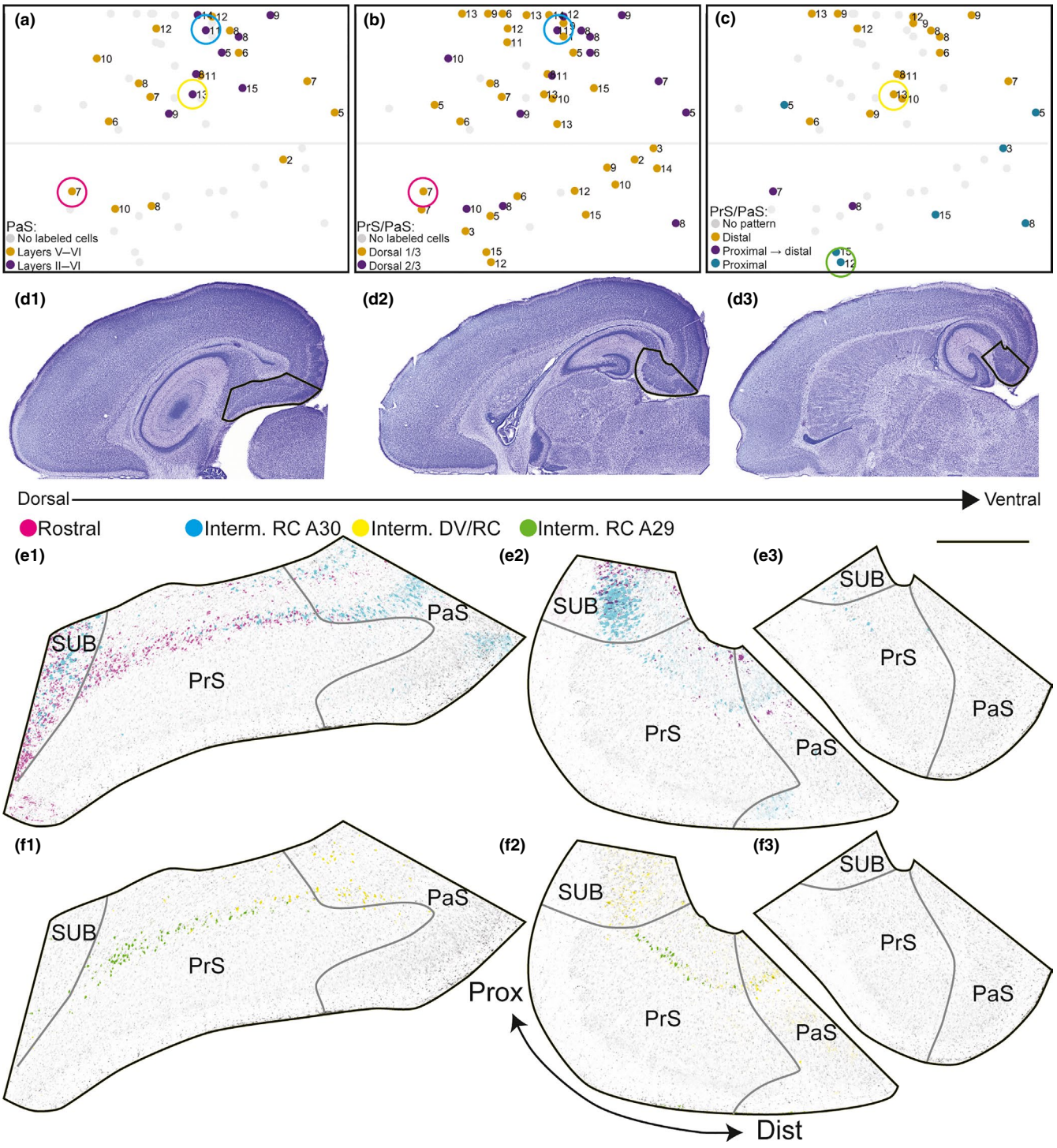

dorsal two-thirds of PrS. In contrast, an injection in the rostral extreme of A30 resulted in retrogradely labeled neurons in the dorsal extreme of PrS (magenta, Figure 5b,e).

We further observed in a minority of the experiments that retrogradely labeled neurons showed differential distributions along the proximodistal axis of PrS and PaS. In the cases which displayed such patterns, injections in A30 resulted in labeled neurons in distal PrS and the whole PaS (yellow, Figure 5c,f). In contrast, after injections in A29, retrogradely labeled neurons were confined to proximal parts of PrS (green, Figure 5c,f). In these cases, we did not observe retrogradely labeled cells in distal PrS and PaS. In two cases, we observed retrogradely labeled cells in both proximal PrS at dorsal levels and in more distal PrS and throughout the transverse extent of PaS at more ventral levels. The centers of these injections were located in rostral A30 and in the rostrocaudal middle of A29. A mixed topographical organization suggests that there are areas in RSC receiving inputs

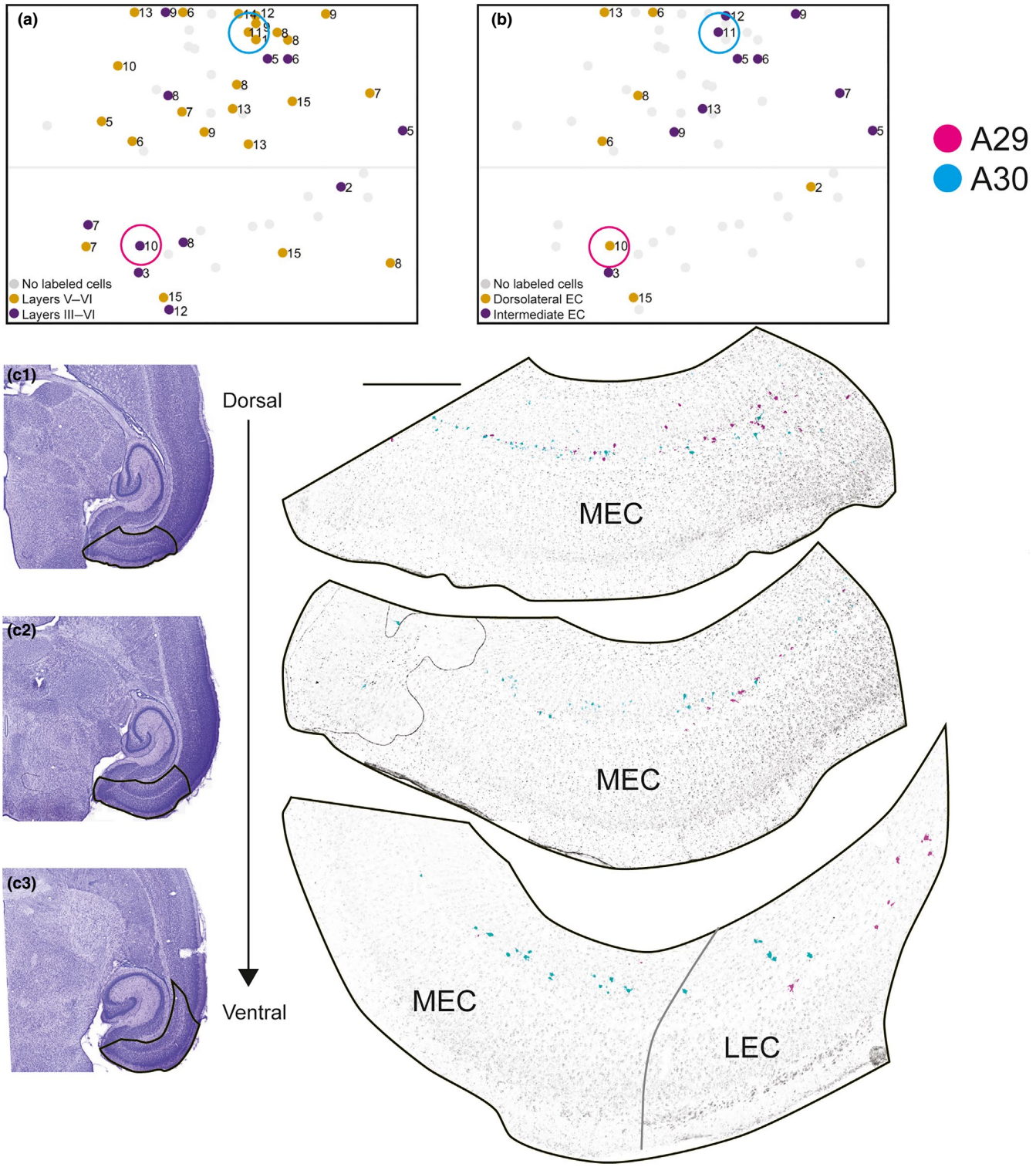

from both proximal and distal PrS. To our knowledge such a pattern has not been observed in the adult. However, the limited number of observed cases makes it difficult to draw clear conclusions. The dorsoventral and proximodistal organization of retrogradely labeled cells were present in both the youngest and older animals so we conclude that this topographical organization is independent of age.

3.6 | Labeling in EC

In 35 of the injections (63%), we observed retrogradely labeled neurons in MEC, whereas labeled neurons in lateral entorhinal cortex (LEC) were very sparse. The number of retrogradely labeled cells in MEC was lower than in SUB, PrS, and PaS. Similar to that seen in PrS and PaS, the

FIGURE 6 Labeled neurons in entorhinal cortex. (a) Normalized flatmap of RSC illustrating the superficial-to-deep organization of origin of RSC projections in EC. Injections were color-coded based on the distribution of the retrogradely labeled neurons: injections resulting in retrogradely labeled neurons in layers V and VI of entorhinal cortex (orange dots), and both layers V–VI and layer III of entorhinal cortex (purple dots). Gray dots depict injections resulting in no retrogradely labeled neurons in entorhinal cortex. (b) Normalized flatmap of RSC illustrating the mediolateral organization of origin in EC. Injections were color-coded based on the distribution of the retrogradely labeled neurons: injections resulting in retrogradely labeled neurons in dorsolateral EC (yellow dots) and intermediate dorsolateral-ventromedial EC (purple dots). Gray dots depict injections resulting in no clear dorsolateral-ventromedial organization of retrogradely labeled neurons in EC or injections with no retrogradely labeled neurons observed in EC. Injections resulting in retrogradely labeled cells in intermediate dorsolateral-ventromedial EC were located mainly in caudal A30, whereas caudal A30 received projections from dorsolateral EC. Color-coded circles in A, B depict the location of injections in RSC, shown in figure (c). (c) Representative examples of the distribution of retrogradely labeled neurons shown in three horizontal sections (c1–c3), taken at different dorsoventral levels after two FB injections in RSC. The distributions of the two cases were merged into one representation to illustrate the complex topography along the dorsomedial to ventrolateral axes of entorhinal cortex. The injections were located in A29 (magenta, 19473 P10) and A30 (cyan, 18387 P11). Circles in A and B depict location of each injection in RSC. High-power images (right) of dorsal (top) and more ventral levels of SUB (bottom) are shown. Black contours in adjacent Nissl-stained sections (left) depict location of high-power images. The injection in A30 resulted in retrogradely labeled cells in intermediate dorsolateral-ventromedial EC (cyan), whereas the injection in A29 result in retrogradely labeled cells in the dorsolateral EC. Scale bar: 500 μm. [Colour figure can be viewed at wileyonlinelibrary.com]

retrogradely labeled MEC and LEC neurons were mainly located in superficial parts of layer V with occasional labeling of neurons in layer VI directly adjacent to the angular bundle. In addition, we observed retrogradely labeled neurons in layer III of both MEC and LEC in 11 of the 35 injections (20% of all injections, Figure 6a). In these cases, we typically observed 1–5 retrogradely labeled neurons in layer III in each section.

In all cases showing retrogradely labeled neurons in MEC, labeled neurons in dorsal parts of MEC were more numerous compared with ventral parts of MEC. In addition, the distribution of retrogradely labeled neurons at ventral levels of MEC points to a topographical organization, where the mediolateral location of the neurons relates to the caudorostral position of the injection in RSC. In case of injections located in rostral A30 or A29, we observed retrogradely labeled neurons in lateral MEC (Figure 6b–c; magenta). At more ventral levels, some labeled neurons were also located in the part of LEC directly adjacent to MEC (Figure 6c3). Following injections in caudal RSC, in the present material only involving A30, we observed retrogradely labeled neurons in more medial parts of MEC (Figure 6c; cyan).

3.7 | Labeling in POR

In 27 of the injections (48%), we observed retrogradely labeled neurons in POR. Of these injections, 24 were located in A30, and only three were located in caudal A29 (Figure 7a). The retrogradely labeled neurons in POR were distributed across layers II–VI, and we observed retrogradely labeled neurons in both the posterior extreme of POR ($n = 18$, Figure 7c1) and in intermediate anteroposterior POR ($n = 9$, Figure 7c2). The injections resulting in retrogradely labeled cells in more intermediate anteroposterior parts of POR were mainly located in the caudal half of A30, whereas the injections resulting in retrogradely labeled neurons in only the posterior POR were located in both rostral and caudal A30. We never observed retrogradely labeled neurons in anterior parts of POR.

3.8 | Labeling in PER

In only two cases (4%), we observed retrogradely labeled cells in PER (Figure 7b). Typically, we observed 1–5 retrogradely labeled neurons in the most posterior part of PER directly adjacent to POR. These injections, which involved both A29 and A30, were from animals older than P10.

3.9 | Temporal development of HF-PHR projections to RSC

Next, we aimed to study the temporal development of HF-PHR projections to RSC. We did not observe retrogradely labeled neurons in any of the HF-PHR subfields following injections in rostral RSC in animals aged P1–3. On the other hand, after injections in the caudal RSC at the same ages, we observed several retrogradely labeled neurons in HF-PHR. After these injections, most neurons were observed in SUB and PrS, although a few neurons were present in CA1 and MEC and LEC (Figure 8). This suggests that projections to caudal RSC are present already at birth, whereas projections to more rostral parts of RSC started to develop in the second half of the first postnatal week. The labeled cells in SUB, PrS, and MEC were topographically organized similar to the older cases previously described (for instance compare magenta dots in Figure 8b vs. c). Even though we did not quantify the number of retrogradely labeled cells in each experiment, it was obvious that injections in very young animals resulted in fewer retrogradely labeled neurons than injections in older animals. In P1–2 animals, we generally observed up to 10 retrogradely labeled neurons in each section, whereas in older animals this number was substantially higher (Figure 8). This suggests that the overall density of HF-PHR projections

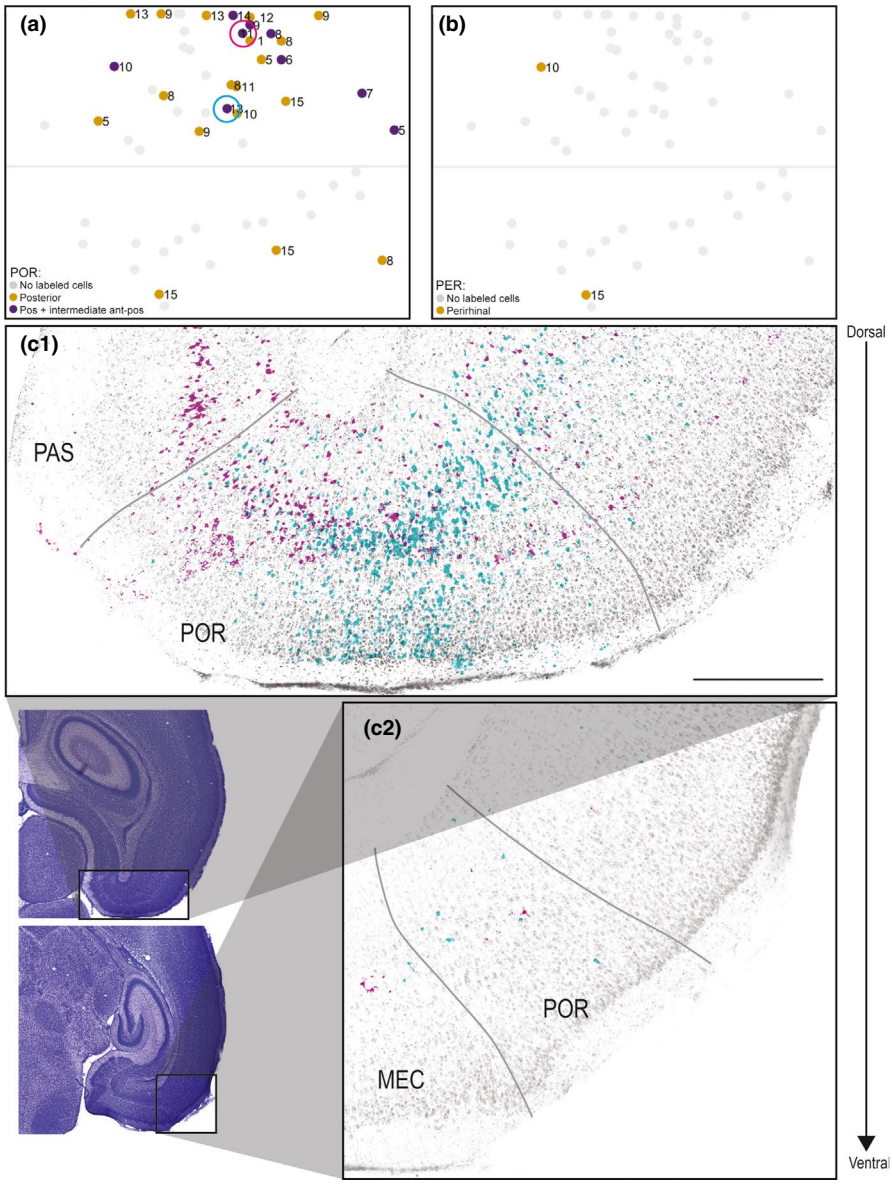

FIGURE 7 Labeled neurons in POR and PER. (a) Normalized flatmap of RSC illustrating the anteroposterior organization of origin of RSC projections in POR. Indicated are injections resulting in retrogradely labeled neurons in posterior POR (yellow dots) and intermediate anterioposterior POR (purple dots). Gray dots depict injections resulting in no retrogradely labeled neurons in POR. Most of the injections resulting in retrogradely labeled cells in POR were located in A30. Color-coded circles in A depict the location of injections in RSC, shown in figure (c). (b) Normalized flatmap of RSC illustrating the origin in PER of projections to RSC. Indicated are injections resulting in retrogradely labeled neurons in PER (yellow dots). Gray dots depict injections resulting in no retrogradely labeled neurons in PER. (c) Representative examples of the distribution of retrogradely labeled neurons shown in two horizontal sections, taken at different dorsoventral levels after two FB injections in A30 (cyan, 18381 P13 and magenta, 18387 P11). Representative examples of retrogradely labeled neurons were overlaid on a Nissl section from two posterior to anterior levels of POR (c1 and c2). Circles in A depict the locations of the two injections in RSC. Black contours in adjacent Nissl-stained sections depict location of high-power images. Both of the injections resulted in retrogradely labeled cells in deep and superficial layers of POR. In both examples, most of the retrogradely labeled neurons were located in posterior POR (c1), whereas at more anterior levels fewer labeled neurons were visible (c2). Scale bar: 500 μm. [Colour figure can be viewed at wileyonlinelibrary.com]

to RSC increases gradually during the postnatal period. Although we observed lower number of retrogradely labeled cells after injections in young animals, it was clear that the distributions of retrogradely labeled neurons after injections in animals aged P1–2 were similar to those resulting from similar injections in older animals (Figure 8). This observation suggests that the first axons arriving in RSC already have a mature topographic organization.

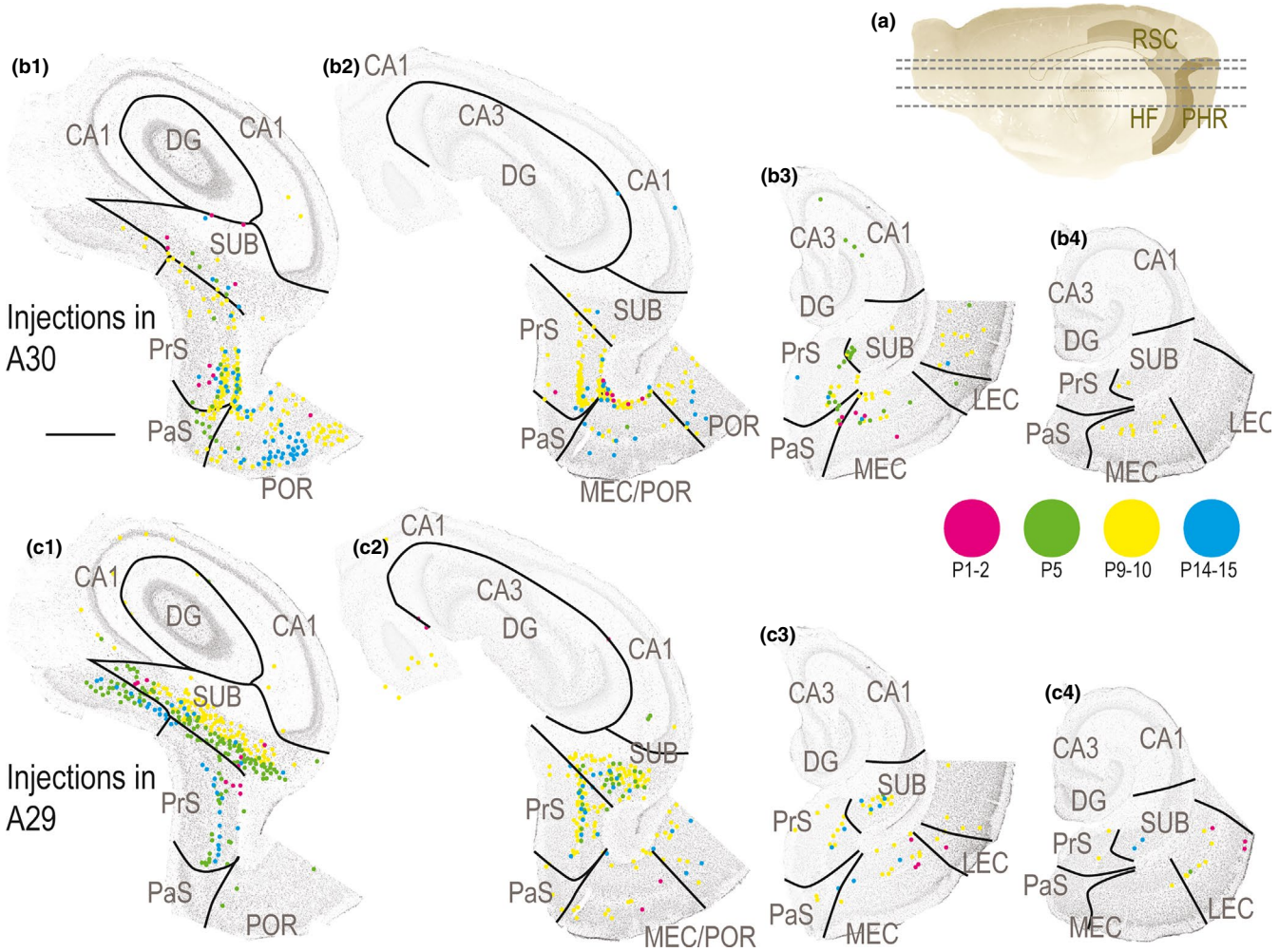

FIGURE 8 Development of HF-PHR projections to RSC. (a) Midsagittal view of the rat right hemisphere. Gray lines depict dorsoventral levels of sections in (b) and (c). (b) Retrogradely labeled cells in HF-PHR after injections in A30. Each dot represents one retrogradely labeled cell and is plotted on Nissl-stained sections from four dorsal (left) to ventral levels of HF-PHR (right). Magenta dots represent labeled neurons in a P1 animal (19232 DiI), green dots in a P5 animal (19258 DiI), yellow dots in a P9 animal (18730 FB), and cyan dots in case of a P14 animal (18819 DiI). At all ages, the retrogradely labeled neurons were mainly located in distal SUB, distal PrS, and medial MEC. At the youngest ages (magenta), only a few labeled neurons were seen, whereas in the older ages, a higher number of labeled cells was present. Scale bar: 1,000 μm. (c) Retrogradely labeled cells in HF-PHR after injections in A29. Panels are organized similar to B. Magenta dots represent labeled neurons in a P2 animal (19298 FB), green dots in a P5 animal (19257 FB), yellow dots in a P10 animal (19473 FB), and cyan dots in case of a P15 animal (19240 FB). At all ages, the retrogradely labeled neurons were mainly located in more proximal parts of SUB compared to after A30 injections, proximal PrS and lateral MEC. At the youngest ages (magenta), only a few labeled neurons were seen, whereas in the older ages, a higher number of labeled cells were present. [Colour figure can be viewed at wileyonlinelibrary.com]

3.10 | Topographical organization of developing projections

A subsequent series of anterograde tracing experiments addressed the question whether the developmentally stable topographical distribution of originating neurons in hippocampus and parahippocampus was reflected by a preserved topographical organization of their axons in RSC. We analyzed results from anterograde injections in three of the main input areas, SUB, MEC, and PrS. After anterograde injections in the distal half of SUB at P14 (Figure 9a), labeled axons were present mainly in RSC area 30, in layer I, and layer IV, although a few labeled fibers where present in layer V and VI. A similar projecting pattern was observed in all ages assessed. As an example, an injection at the border between dorsal SUB and dorsal PrS in a P4 animal confirmed that axons were present in RSC already during the first postnatal week (Figure 9b). In this case, labeled fibers were mainly present in caudal A30 and A29, whereas a lower number of fibers were present in rostral parts of A29 and A30. Similarly placed distal injections, but involving more ventral levels of SUB, showed similar results. We also analyzed six injections in proximal SUB (age of injected animal ranging from P1 to P17). We did not identify any labeled axons in RSC in these latter experiments.

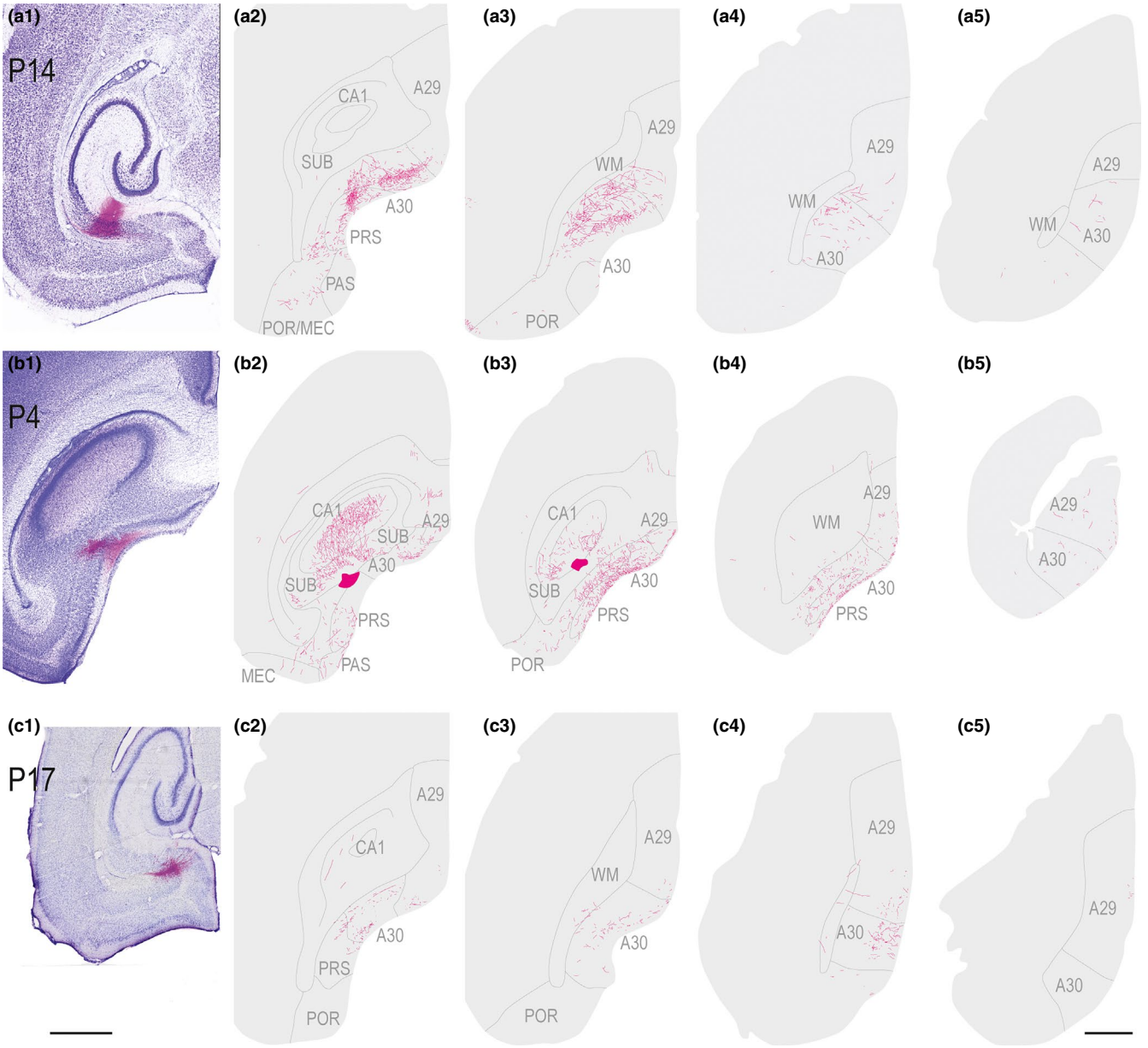

FIGURE 9 Anterograde injections in subiculum and presubiculum. Left (1): Images of horizontal Nissl-stained sections overlaid with an adjacent section containing the center of the fluorescent tracer injection. Scale bar; 1,000 μm. Right (2–4): The projections represented in a dorsoventral series of drawings of horizontal sections through RSC. Scale bar: 1,000 μm. (a) A BDA injection in a P14 animal located in distal half of SUB at intermediate dorsoventral levels of SUB. Labeled fibers were present mainly in layer IV and V–VI in A30 and caudal A29. (b) A BDA injection in a P4 animal located at the border between dorsal PrS and dorsal SUB. Labeled fibers were present mainly in layer I and IV of caudal and rostral A30 and A29. (c) A BDA injection in a P17 animal located in deep layers of PrS at intermediate dorsoventral levels. Labeled fibers were present in layer II and V of RSC. [Colour figure can be viewed at wileyonlinelibrary.com]

After an injection in deep layers of the intermediate dorsoventral PrS, labeled fibers were located mainly in layer IV of RSC although layer I contained some labeled fibers as well (Figure 9c). These fibers were mainly located in caudal A30, whereas a few fibers were located in caudodorsal A29.

We also assessed 11 anterograde injections located in superficial and/or deep layers of dorsal-to-intermediate MEC (age of injected animals ranging from P3 to P15). Five of these injections (age = P5, P8, P10, and P12) were localized in dorsolateral MEC and resulted in axon labeling in caudal RSC (Figure 10). Labeled fibers were mainly found in all layers of A29 close to the border between RSC and PrS/PaS/SUB. A few fibers were also seen in deep layers of the caudal pole of RSC near the border to visual cortex. In none of the animals did we observe labeled fibers in rostral parts of rostral A29 or rostral A30. The remaining six injections were localized in the intermediate dorsoventral MEC. In these animals, we did not observe any labeled fibers in RSC. A few fibers in the cingular

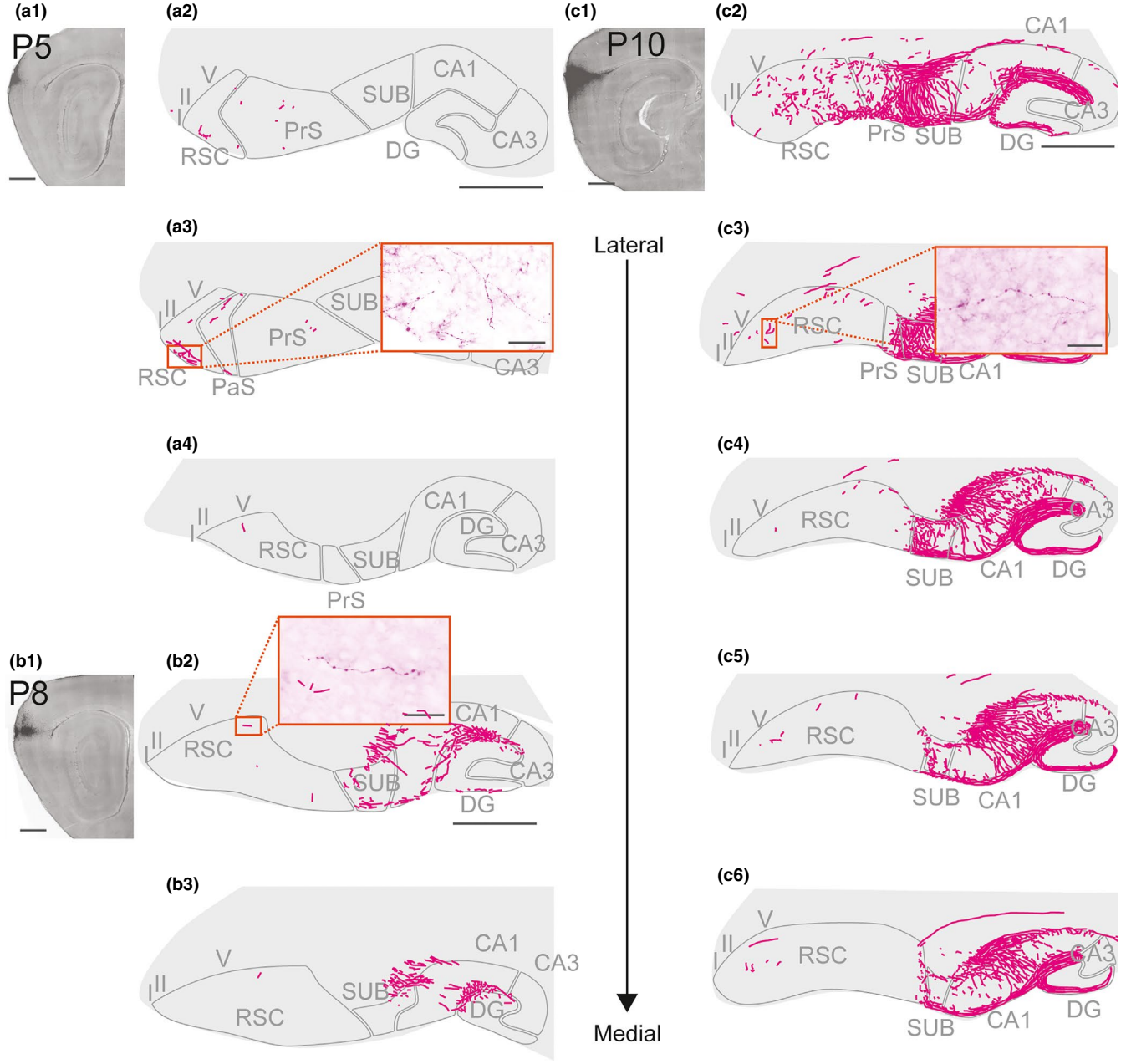

FIGURE 10 Anterograde injections in MEC. Three representative experiments with anterograde injections in dorsal MEC. Images of injections (left hand upper panels) were taken with a fluorescent microscope. The projections after the injection were traced and represented in a lateral (top) to medial (bottom) series of drawings of sagittal sections through RSC, hippocampus, and parahippocampus. (a) A BDA injection in a P5 animal located in dorsal MEC. A few labeled fibers were present in layer I of RSC. (a1) and (a2); Scale bar: 1,000 µm. A5; Scale bar: 50 µm. (b) A BDA injection in a P8 animal located in dorsal MEC. A few labeled fibers were present in layer I and V of RSC. A dense projection is seen in HC. (b1) and (b2); Scale bar: 1,000. B4; Scale bar: 25 µm. (c) A BDA injection in a P10 animal located in dorsal MEC. Labeled fibers were present in layer I and V of RSC. A dense projection is seen in HC. (c1) and (c2); Scale bar: 1,000 µm. C7; Scale bar: 50 µm. [Colour figure can be viewed at wileyonlinelibrary.com]

bundle were observed in two of these cases (not illustrated). The failure to observe labeled axons in RSC was not caused by failure of anterograde transport of the tracer as we observed densely labeled axonal plexuses in DG, CA1-3, and SUB. We therefore conclude that the axonal distribution of hippocampal and parahippocampal projections to RSC displays a similar topographical organization in all ages present in our material.

4 | DISCUSSION

Most of our data obtained in postnatal rats are in line with previous studies in the adult rat, showing that the distal half of SUB is the main origin of HF-PHR outputs terminating in RSC (Kim & Spruston, 2012; Kinnavane, Vann,

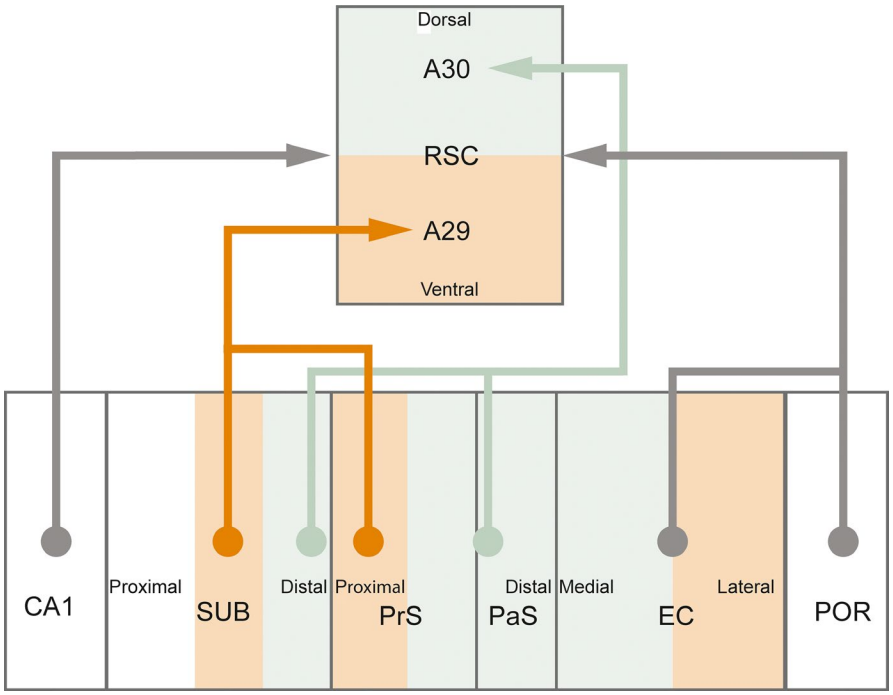

FIGURE 11 Summary of projections from hippocampus and parahippocampus to retrosplenial cortex. Retrosplenial cortex (RSC) receives inputs from CA1, subiculum (SUB), presubiculum (PrS), parasubiculum (PaS), entorhinal cortex (EC), and postrhinal cortex (POR). These projections are topographically organized such that A30 receives inputs from distal SUB, distal PrS, and PAS, whereas A29 receives inputs from more proximal parts of SUB and proximal PrS. Next, rostral parts of A30 receives inputs only from dorsal parts of SUB, PrS, PaS, EC, and POR, whereas caudal A30 receives inputs also from more ventral parts of these structures (not illustrated in figure). [Colour figure can be viewed at wileyonlinelibrary.com]

Nelson, O'Mara, & Aggleton, 2018; Witter, Ostendorf, & Groenewegen, 1990). Additional projections arise from POR, PrS, PaS, and MEC (Figure 11¸ Honda et al., 2011; Ding, 2013). Our data further confirm that the majority of the latter projections arise in the superficial parts of layer V (van Groen & Wyss, 2003; Honda et al., 2011; Insausti, Herrero, & Witter, 1997; Surmeli et al., 2016; Vogt & Miller, 1983), with a minor origin in deep parts of layer VI and superficial layers. Additional very minor projections arise from LEC, PER, and CA1. The latter probably includes a previously reported projection of GABAergic neurons to RSC (Miyashita & Rockland, 2007).

In accordance with earlier published data in both adult rats and monkeys, we show that also in the rat pup, the HF-PHR projections to RSC are topographically organized along the dorsoventral axis of HF-PHR. Projections from SUB and PrS are organized such that caudodorsal RSC receives projections from the entire dorsoventral SUB and PrS, whereas rostral and ventral RSC receives afferents only from neurons in dorsal SUB and dorsal PrS, both in pups (present study), as in adults (Aggleton, Wright, Vann, & Saunders, 2012; van Groen & Wyss, 1990, 2003; Wyss & Van Groen, 1992). Our results add to these findings that the projections from PaS are similarly organized, and we therefore expect this to be true in the adult.

We further report that the projections originating in SUB, PrS, and PaS are topographically organized along the transverse plane of HF-PHR (Figure 11). Similar to what has been reported in a recent paper in adult animals, we observed that in pups, distal SUB projects to dorsal RSC (A30), whereas more proximal parts of SUB project to ventral RSC (A29; Honda & Ishizuka, 2015). Our findings add to these results, showing that distal PrS and PaS preferentially project to A30, whereas more proximal PrS (but not PaS) preferentially projects to A29. The transverse organization of SUB projections to RSC is interesting as proximal SUB neurons are reported to be less spatially modulated than distal ones, suggesting a functional gradient along the proximodistal axis of SUB (Sharp & Green, 1994). In addition, distal neurons in SUB project to areas which are known to be important in processing of spatial information such as MEC, PrS, POR, and the anterior complex of the thalamus, whereas more proximal parts of SUB project to areas known be involved in complex cortical integration such as infralimbic and PER (Witter et al., 1990). The anatomical organization of SUB projections to RSC and the functional gradient within SUB thus suggest a functional difference between A30 and A29. This is in line with previous behavioral studies in which the effect of selective lesions of the two areas of RSC have been assessed (van Groen, Kadish, & Wyss, 2004; Pothuizen, Davies, Aggleton, & Vann, 2010; Pothuizen, Davies, Albasser, Aggleton, & Vann, 2009; Vann & Aggleton, 2005).

Based on both the retrograde and anterograde experiments, we conclude that in pups, like in adults, there is a sparse projection from MEC to RSC. This projection is organized such that rostral parts of A30 receive input from dorsal MEC, whereas caudal parts of A30 receive input from both dorsal and intermediate dorsoventral levels of MEC. We observed an additional gradient in that caudal A30 receives input from neurons located in more medial parts of MEC than those that project to rostral A30. A similar organization of the projections to A29 was not clear in our material. To our

knowledge, the topographical organization of MEC inputs to A30 has not been reported previously. This organization is partly mirrored by the reciprocal projection from RSC to MEC in pups, as rostral A29 and A30 project to dorsal parts of EC, whereas caudal A29 and A30 project to more ventral parts of MEC (Sugar & Witter, 2016).

Our temporal analysis shows that all of the individual HF-PHR projections to caudal RSC are present at P1, although shortly after birth the projections are still weakly developed. During the first postnatal week, the substantial increase in the number of retrogradely labeled neurons indicates a rapid development, such that the projection reaches adult-like densities between P5 and P10, which is in line with the reported anterograde tracing observations. In contrast, we suggest that projections to rostral RSC develop a few days later than the projections to caudal RSC, as we did not observe retrogradely labeled neurons in HF-PHR in animals younger than P3 with injections in rostral RSC. We therefore conclude that HF-PHR projections to RSC are present very early during postnatal development and that the first arriving axons already adhere to the topographic and laminar patterning seen in the adult. This notion is similar to what has been reported in other developing circuits within HF-PHR and also to what we reported for the reciprocal projection from RSC to HF-PHR (Canto et al., 2011; O'Reilly et al., 2013, 2014; Sugar & Witter, 2016). All together, these findings suggest that long-range inputs and outputs with RSC and intrinsic connections of the HF-PHR system display adult-like features long before eye-opening and before the animal starts active exploration of the environment by approximately P15.

ACKNOWLEDGEMENTS

This work was supported by the Kavli Foundation and the Research Council of Norway, the Centre of Excellence scheme (Centre for Neural Computation, grant number 223262), the National Infrastructure (NORBRAIN1, grant number 197467), and a research grant (grant number 227769). We thank Bruno Monterotti and Paulo Giraõ for technical assistance with experiments. We also thank Kally O'Reilly, Annelene Gulden Dahl, and Maria José Lagartos Donate for providing access to the anterograde tracing data included in the paper.

CONFLICT OF INTEREST

The authors report no competing interests.

DATA ACCESSIBILITY

Original data will be available upon request. Request should be addressed to Menno P. Witter (menno.witter@ntnu.no).

AUTHOR CONTRIBUTIONS

All authors designed research. K.G.H. and J.S. conducted experiments and analyzed data. All authors wrote the manuscript.

ORCID


Menno P. Witter https://orcid.org/0000-0003-0285-1637

REFERENCES

Aggleton, J. P., Wright, N. F., Vann, S. D., & Saunders, R. C. (2012). Medial temporal lobe projections to the retrosplenial cortex of the macaque monkey. *Hippocampus*, *22*, 1883–1900. https://doi.org/10.1002/hipo.22024

Agster, K. L., & Burwell, R. D. (2009). Cortical efferents of the perirhinal, postrhinal, and entorhinal cortices of the rat. *Hippocampus*, *19*, 1159–1186. https://doi.org/10.1002/hipo.20578

Alexander, A. S., & Nitz, D. A. (2015). Retrosplenial cortex maps the conjunction of internal and external spaces. *Nature Neuroscience*, *18*, 1143–1151. https://doi.org/10.1038/nn.4058

Berger, B., Alvarez, C., & Pelaprat, D. (1997). Retrosplenial/presubicular continuum in primates: A developmental approach in fetal macaques using neurotensin and parvalbumin as markers. *Developmental Brain Research*, *101*, 207–224. https://doi.org/10.1016/S0165-3806(97)00067-9

Bjerknes, T. L., Langston, R. F., Kruge, I. U., Moser, E. I., & Moser, M. B. (2015). Coherence among head direction cells before eye opening in rat pups. *Current Biology*, *25*, 103–108. https://doi.org/10.1016/j.cub.2014.11.009

Boccara, C. N., Sargolini, F., Thoresen, V. H., Solstad, T., Witter, M. P., Moser, E. I., & Moser, M. B. (2010). Grid cells in pre- and parasubiculum. *Nature Neuroscience*, *13*, 987–994. https://doi.org/10.1038/nn.2602

Bonnevie, T., Dunn, B., Fyhn, M., Hafting, T., Derdikman, D., Kubie, J. L., … Moser, M. B. (2013). Grid cells require excitatory drive from the hippocampus. *Nature Neuroscience*, *16*, 309–317. https://doi.org/10.1038/nn.3311

Canto, C. B., Koganezawa, N., & Witter, M. P. (2011) Development of Functional Projections from Pre- and Parasubiculum to Medial Entorhinal Cortex in the Rat. Doctoral theses: Layer Specific Integrative Properties of Entorhinal Principal Neurons. Kavli Institute for Systems Neuroscience and Centre for the Biology of Memory, Norwegian University of Science and Technology, Trondheim, Norway, pp. 181–214.

Cappaert, N. L. M., Van Strien, N. M., & Witter, M. P. (2015). Chapter 20 - Hippocampal Formation. In G. Paxinos (Ed.), *The rat nervous system*, 4th ed. (pp. 511–573). San Diego, CA: Academic Press. https://doi.org/10.1016/B978-0-12-374245-2.00020-6

Cho, J., & Sharp, P. E. (2001). Head direction, place, and movement correlates for cells in the rat retrosplenial cortex. *Behavioral Neuroscience*, *115*, 3–25. https://doi.org/10.1037/0735-7044.115.1.3

Ding, S. L. (2013). Comparative anatomy of the prosubiculum, subiculum, presubiculum, postsubiculum, and parasubiculum in human, monkey, and rodent. *Journal of Comparative Neurology*, *521*, 4145–4162. https://doi.org/10.1002/cne.23416

Donato, F., Jacobsen, R. I., Moser, M. B., & Moser, E. I. (2017). Stellate cells drive maturation of the entorhinal-hippocampal circuit. *Science*, *355*, eaai8178. https://doi.org/10.1126/science.aai8178

Finch, D. M., Derian, E. L., & Babb, T. L. (1984). Excitatory projection of the rat subicular complex to the cingulate cortex and synaptic integration with thalamic afferents. *Brain Research*, *301*, 25–37. https://doi.org/10.1016/0006-8993(84)90399-8

Fyhn, M., Molden, S., Witter, M. P., Moser, E. I., & Moser, M. B. (2004). Spatial representation in the entorhinal cortex. *Science*, *305*, 1258–1264. https://doi.org/10.1126/science.1099901

van Groen, T., Kadish, I., & Wyss, J. M. (2004). Retrosplenial cortex lesions of area Rgb (but not of area Rga) impair spatial learning and memory in the rat. *Behavioral Brain Research*, *154*, 483–491. https://doi.org/10.1016/j.bbr.2004.03.016

van Groen, T., & Wyss, J. M. (1990). Connections of the retrosplenial granular a cortex in the rat. *Journal of Comparative Neurology*, *300*, 593–606. https://doi.org/10.1002/(ISSN)1096-9861

van Groen, T., & Wyss, J. M. (1992). Connections of the retrosplenial dysgranular cortex in the rat. *Journal of Comparative Neurology*, *315*, 200–216. https://doi.org/10.1002/(ISSN)1096-9861

van Groen, T., & Wyss, J. M. (2003). Connections of the retrosplenial granular b cortex in the rat. *Journal of Comparative Neurology*, *463*, 249–263. https://doi.org/10.1002/(ISSN)1096-9861

Honda, Y., Furuta, T., Kaneko, T., Shibata, H., & Sasaki, H. (2011). Patterns of axonal collateralization of single layer V cortical projection neurons in the rat presubiculum. *Journal of Comparative Neurology*, *519*, 1395–1412. https://doi.org/10.1002/cne.22578

Honda, Y., & Ishizuka, N. (2015). Topographic distribution of cortical projection cells in the rat subiculum. *Neuroscience Research*, *92*, 1–20. https://doi.org/10.1016/j.neures.2014.11.011

Iaria, G., Bogod, N., Fox, C. J., & Barton, J. J. (2009). Developmental topographical disorientation: Case one. *Neuropsychologia*, *47*, 30–40. https://doi.org/10.1016/j.neuropsychologia.2008.08.021

Insausti, R., Herrero, M. T., & Witter, M. P. (1997). Entorhinal cortex of the rat: Cytoarchitectonic subdivisions and the origin and distribution of cortical efferents. *Hippocampus*, *7*, 146–183.

Jarrard, L. E. (1978). Selective hippocampal lesions: Differential effects on performance by rats of a spatial task with preoperative versus postoperative training. *Journal of Comparative and Physiological Psychology*, *92*, 1119–1127. https://doi.org/10.1037/h0077516

Jones, B. F., Groenewegen, H. J., & Witter, M. P. (2005). Intrinsic connections of the cingulate cortex in the rat suggest the existence of multiple functionally segregated networks. *Neuroscience*, *133*, 193–207. https://doi.org/10.1016/j.neuroscience.2005.01.063

Kim, Y., & Spruston, N. (2012). Target-specific output patterns are predicted by the distribution of regular-spiking and bursting pyramidal neurons in the subiculum. *Hippocampus*, *22*, 693–706. https://doi.org/10.1002/hipo.20931

Kinnavane, L., Vann, S. D., Nelson, A. J. D., O'Mara, S. M., & Aggleton, J. P. (2018). Collateral projections innervate the mammillary bodies and retrosplenial cortex: A new category of hippocampal cells. *eNeuro*, *5*, ENEURO.0383-17.2018. https://doi.org/10.1523/ENEURO.0383-17.2018

Kropff, E., Carmichael, J. E., Moser, M. B., & Moser, E. I. (2015). Speed cells in the medial entorhinal cortex. *Nature*, *523*, 419–424. https://doi.org/10.1038/nature14622

Langston, R. F., Ainge, J. A., Couey, J. J., Canto, C. B., Bjerknes, T. L., Witter, M. P., … Moser, M. B. (2010). Development of the spatial representation system in the rat. *Science*, *328*, 1576–1580. https://doi.org/10.1126/science.1188210

Maguire, E. A. (2001). The retrosplenial contribution to human navigation: A review of lesion and neuroimaging findings. *Scandinavian Journal of Psychology*, *42*, 225–238. https://doi.org/10.1111/1467-9450.00233

Maguire, E. A., Nannery, R., & Spiers, H. J. (2006). Navigation around London by a taxi driver with bilateral hippocampal lesions. *Brain*, *129*, 2894–2907. https://doi.org/10.1093/brain/awl286

Mao, D., Kandler, S., McNaughton, B. L., & Bonin, V. (2017). Sparse orthogonal population representation of spatial context in the retrosplenial cortex. *Nature Communications*, *8*, 243. https://doi.org/10.1038/s41467-017-00180-9

Miyashita, T., & Rockland, K. S. (2007). GABAergic projections from the hippocampus to the retrosplenial cortex in the rat. *European Journal of Neuroscience*, *26*, 1193–1204. https://doi.org/10.1111/j.1460-9568.2007.05745.x

Muessig, L., Hauser, J., Wills, T. J., & Cacucci, F. (2015). A developmental switch in place cell accuracy coincides with grid cell maturation. *Neuron*, *86*, 1167–1173. https://doi.org/10.1016/j.neuron.2015.05.011

O'Keefe, J., & Dostrovsky, J. (1971). The hippocampus as a spatial map. Preliminary evidence from unit activity in the freely-moving rat. *Brain Research*, *34*, 171–175. https://doi.org/10.1016/0006-8993(71)90358-1

O'Reilly, K. C., Flatberg, A., Islam, S., Olsen, L. C., Kruge, I. U., & Witter, M. P. (2014). Identification of dorsal-ventral hippocampal differentiation in neonatal rats. *Brain Structure and Function*, *220*(5), 2873–2893.

O'Reilly, K. C., Gulden Dahl, A., Ulsaker Kruge, I., & Witter, M. P. (2013). Subicular-parahippocampal projections revisited: Development of a complex topography in the rat. *Journal of Comparative Neurology*, *521*, 4284–4299. https://doi.org/10.1002/cne.23417

Papp, E. A., Leergaard, T. B., Calabrese, E., Johnson, G. A., & Bjaalie, J. G. (2014). Waxholm Space atlas of the Sprague Dawley rat brain. *NeuroImage*, *97*, 374–386. https://doi.org/10.1016/j.neuroimage.2014.04.001

Papp, E. A., Leergaard, T. B., Calabrese, E., Johnson, G. A., & Bjaalie, J. G. (2015). Addendum to "Waxholm Space atlas of the Sprague Dawley rat brain" [NeuroImage 97 (2014) 374-386]. *NeuroImage*, *105*, 561–562. https://doi.org/10.1016/j.neuroimage.2014.10.017

Pothuizen, H. H., Davies, M., Aggleton, J. P., & Vann, S. D. (2010). Effects of selective granular retrosplenial cortex lesions on spatial working memory in rats. *Behavioral Brain Research*, *208*, 566–575. https://doi.org/10.1016/j.bbr.2010.01.001

Pothuizen, H. H., Davies, M., Albasser, M. M., Aggleton, J. P., & Vann, S. D. (2009). Granular and dysgranular retrosplenial cortices provide qualitatively different contributions to spatial working memory: Evidence from immediate-early gene imaging in rats. *European Journal of Neuroscience*, *30*, 877–888. https://doi.org/10.1111/j.1460-9568.2009.06881.x

Ranganath, C., & Ritchey, M. (2012). Two cortical systems for memory-guided behaviour. *Nature Reviews Neuroscience*, *13*, 713–726. https://doi.org/10.1038/nrn3338

Renno-Costa, C., & Tort, A. B. L. (2017). Place and grid cells in a loop: Implications for memory function and spatial coding. *Journal of Neuroscience*, *37*, 8062–8076. https://doi.org/10.1523/JNEUROSCI.3490-16.2017

Sharp, P. E., & Green, C. (1994). Spatial correlates of firing patterns of single cells in the subiculum of the freely moving rat. *Journal of Neuroscience*, *14*, 2339–2356. https://doi.org/10.1523/JNEUROSCI.14-04-02339.1994

Solstad, T., Boccara, C. N., Kropff, E., Moser, M. B., & Moser, E. I. (2008). Representation of geometric borders in the entorhinal cortex. *Science*, *322*, 1865–1868. https://doi.org/10.1126/science.1166466

Solstad, T., Moser, E. I., & Einevoll, G. T. (2006). From grid cells to place cells: A mathematical model. *Hippocampus*, *16*, 1026–1031. https://doi.org/10.1002/hipo.20244

Sugar, J., & Witter, M. P. (2016). Postnatal development of retrosplenial projections to the parahippocampal region of the rat. *Elife*, *5*.

Surmeli, G., Marcu, D. C., McClure, C., Garden, D. L. F., Pastoll, H., & Nolan, M. F. (2016). Molecularly defined circuitry reveals input-output segregation in deep layers of the medial entorhinal cortex. *Neuron*, *92*, 929. https://doi.org/10.1016/j.neuron.2016.11.011

Sutherland, R. J., Whishaw, I. Q., & Kolb, B. (1988). Contributions of cingulate cortex to two forms of spatial learning and memory. *Journal of Neuroscience*, *8*, 1863–1872. https://doi.org/10.1523/JNEUROSCI.08-06-01863.1988

Taube, J. S., Muller, R. U., & Ranck, J. B. Jr (1990). Head-direction cells recorded from the postsubiculum in freely moving rats. I. Description and quantitative analysis. *Journal of Neuroscience*, *10*, 420–435. https://doi.org/10.1523/JNEUROSCI.10-02-00420.1990

Vann, S. D., & Aggleton, J. P. (2005). Selective dysgranular retrosplenial cortex lesions in rats disrupt allocentric performance of the radial-arm maze task. *Behavioral Neuroscience*, *119*, 1682–1686. https://doi.org/10.1037/0735-7044.119.6.1682

Vann, S. D., Aggleton, J. P., & Maguire, E. A. (2009). What does the retrosplenial cortex do?. *Nature Reviews Neuroscience*, *10*, 792–802. https://doi.org/10.1038/nrn2733

Vogt, B. A., & Miller, M. W. (1983). Cortical connections between rat cingulate cortex and visual, motor, and postsubicular cortices. *Journal of Comparative Neurology*, *216*, 192–210. https://doi.org/10.1002/(ISSN)1096-9861

Wills, T. J., Cacucci, F., Burgess, N., & O'Keefe, J. (2010). Development of the hippocampal cognitive map in preweanling rats. *Science*, *328*, 1573–1576. https://doi.org/10.1126/science.1188224

Witter, M. P., Ostendorf, R. H., & Groenewegen, H. J. (1990). Heterogeneity in the dorsal subiculum of the rat. Distinct neuronal zones project to different cortical and subcortical targets. *European Journal of Neuroscience*, *2*, 718–725. https://doi.org/10.1111/j.1460-9568.1990.tb00462.x

Wyss, J. M., & Van Groen, T. (1992). Connections between the retrosplenial cortex and the hippocampal formation in the rat: A review. *Hippocampus*, *2*, 1–11.

How to cite this article: Haugland KG, Sugar J, Witter MP. Development and topographical organization of projections from the hippocampus and parahippocampus to the retrosplenial cortex. *Eur J Neurosci*. 2019;50:1799–1819. https://doi.org/10.1111/ejn.14395

Paper 2

Haugland, K.G., Olberg, A., Lande, A., Kjelstrup K.B., Brun, V.H.

Hippocampal growth hormone modulates relational memory and the dendritic spine density in CA1

Learning and Memory, January 2020, doi: 10.1101/lm.050229.119.

Research

Hippocampal growth hormone modulates relational memory and the dendritic spine density in CA1

Kamilla G. Haugland,[1] Anniken Olberg,[1] Andreas Lande,[1] Kirsten B. Kjelstrup,[1,2] and Vegard H. Brun[1,2]

[1]*Department of Clinical Medicine, University in Tromsø—The Arctic University of Norway, 9019 Tromsø, Norway;* [2]*University Hospital of North Norway, 9019 Tromsø, Norway*

Growth hormone (GH) deficiency is associated with cognitive decline which occur both in normal aging and in endocrine disorders. Several brain areas express receptors for GH although their functional role is unclear. To determine how GH affects the capacity for learning and memory by specific actions in one of the key areas, the hippocampus, we injected recombinant adeno-associated viruses (rAAVs) in male rats to express green fluorescent protein (GFP) combined with either GH, antagonizing GH (aGH), or no hormone, in the dorsal CA1. We found that aGH disrupted memory in the Morris water maze task, and that aGH treated animals needed more training to relearn a novel goal location. In a one-trial spontaneous location recognition test, the GH treated rats had better memory performance for object locations than the two other groups. Histological examinations revealed that GH increased the dendritic spine density on apical dendrites of CA1, while aGH reduced the spine density. GH increased the relative amount of immature spines, while aGH decreased the same amount. Our results imply that GH is a neuromodulator with strong influence over hippocampal plasticity and relational memory by mechanisms involving modulation of dendritic spines. The findings are significant to the increasing aging population and GH deficiency patients.

[Supplemental material is available for this article.]

The hippocampal network is essential for the acquisition and organization of relational memory (Eichenbaum 2017). The dense *N*-methyl-D-aspartate (NMDA) receptor distribution on hippocampal synapses allows their strengths to be quickly altered, making the network ideal for memory formation (Moser et al. 1994; Shimizu et al. 2000; Brun et al. 2001; Nakazawa et al. 2004). Numerous neuromodulators influence the plasticity of the hippocampus and modify the neural circuits (Cobb and Lawrence 2010). While research on synaptic plasticity has focused on common neuromodualtors like acetylcholine, noradrenaline, serotonin, and dopamine (Palacios-Filardo and Mellor 2018), the potential influence of growth hormone (GH) is less explored.

Growth hormone is commonly known as a peptide hormone secreted by the pituitary into the bloodstream to regulate somatic growth, but can also function as a neuromodulator in the central nervous system (Nyberg 2000; Åberg et al. 2006). Receptors for GH are robustly expressed throughout the central nervous system, including the hippocampus (Burton et al. 1992; Lobie et al. 1993, 2000; Nyberg 2000). Although systemic GH can cross the blood–brain barrier and enter the brain (Pan et al. 2005), GH is also produced locally in the hippocampus (Donahue et al. 2006), suggesting a self-regulating function. One of the first indications of an autonomous GH regulation in the hippocampus came from observations with the GH-deficient Ames dwarf mice. With impaired GH secretion from the anterior pituitary, the Ames dwarf mice retain compensatory higher levels of GH levels in the hippocampus, making their memory significantly improved (Sun et al. 2005). Furthermore, there is evidence that GH can affect memory systems through hippocampal NMDA and α-amino-3-hydroxy-5-methyl-4-isoxazole propionic acid (AMPA) receptor signaling (Le Greves et al. 2002; Ramis et al. 2013; Studzinski et al. 2015). These receptors are key components of long-term potentiation (LTP), which in turn can influence dendritic spine density (Matsuzaki 2007). However, the evidence that directly relates the behavioral outcome of GH to the possible underlying morphological changes is still missing.

Although several reports argue for a role of GH in learning and memory (Nyberg and Hallberg 2013; Ashpole et al. 2015), few have tried to decipher the involved neurobiological mechanisms. There are studies showing cognitive improvements after GH therapy in patients diagnosed with GH deficiency (Deijen et al. 1998; Sathiavageeswaran et al. 2007; Nieves-Martinez et al. 2010). In animals, systemic administration of GH or the GH secretagogue ghrelin improves spatial memory (Schneider-Rivas et al. 1995; Diano et al. 2006; Grönbladh et al. 2013), while spontaneous dwarf rats with a deficient version of the GH-gene show impaired memory performance in the Morris water maze task (Li et al. 2011). Conflicting reports describe improved spatial memory after GH receptor knockout (Basu et al. 2017) and ghrelin receptor knockout (Albarran-Zeckler et al. 2012), as well as impaired memory after systemic ghrelin administration (Zhao et al. 2014). An explanation for these various results after GH manipulation could be that *systemic* GH has diverse effects in different kinds of tissues

Corresponding author: vegard.h.brun@uit.no
Article is online at http://www.learnmem.org/cgi/doi/10.1101/lm.050229.119.

(Sun and Bartke 2014). Many reports make claims about cognitive effects based on systemic GH manipulations, but the observed behavior could result from peripheral stimulation, including alterations in muscle strength, locomotor activity or other abilities. Consequently, to reveal the function of GH specifically in the hippocampus, we performed targeted manipulations of GH in the cornu ammonis (CA)1 in vivo to see if this was enough to produce both behavioral and morphological changes.

Results

To investigate the role of GH as a neuromodulator in learning and memory, we injected recombinant adeno-associated viruses (rAAVs) in the dorsal hippocampus to express GH, antagonizing GH (aGH) or green fluorescent protein (GFP) only (control). The antagonizing GH was a muted GH with the exchange of a single amino acid in the GH-gene (Chen et al. 1990, 1991). All the rAAVs contained sequences for GFP for visual verification of the transfections. The viral constructions were similar for the GH modulated groups, AAV-CMV-GH-IRES-GFP or AAV-CMV-aGH-IRES-GFP, respectively. The control groups were either unoperated or transfected with rAAV expressing GFP only (AAV-CMV-IRES-GFP). The animals that received virus were allowed 3 wk of viral incubation time before the memory performance was tested in hippocampal-dependent memory tasks (Fig. 1A).

Injections sites and transfected neurons in the dorsal hippocampus

Injections were made bilaterally at four antero-posterior sites with different proximal-distal coordinates, to cover large parts of the dorsal hippocampal CA1 (Fig. 1B). The viral load was calibrated to avoid excitotoxic lesions and epilepsy, which occurred in pilot experiments in some animals receiving substantially higher viral loads, in particular with the GH virus. In the presented data, we observed no convulsive seizures and found no signs of lesions in Nissl stained brain sections other than the expected minor mechanic lesions from the surgery in all groups. All animals had successful viral transfection in the hippocampus verified by the presence of GFP expression (Fig. 1C; $n=8$ for GH, $n=8$ for aGH, $n=13$ for control), although the amount of GFP expression varied. Transfected neurons with GFP expression were mainly observed in CA1 pyramidal neurons, but also some CA3 pyramidal neurons and dentate gyrus (DG) granule cells were transfected. In addition, GFP was also seen in some nonpyramidal cells, especially in stratum radiatum in close proximity to injections in CA1 (Supplemental Fig. 1).

Growth hormone increases activation of p-Stat5

The GH peptide has properties to bind and activate the GH receptor in the hippocampus (Burton et al. 1992). The function of the GH receptor can be modulated by changing the availability and structure of the GH ligand (Birzniece et al. 2009), which is reflected by the receptor activation. By calculating the amount of phosphorylated Signal transducer and activator of transcription 5 (p-Stat5), changes in GH-induced receptor activation are observable (Furigo et al. 2017). To validate that our viral treatments affected GH receptor activation, we used immunohistochemistry for p-Stat5 combined with 4′,6-Diamidino-2-Phenylindol (DAPI) as a nuclear staining (Fig. 2A–F). This allowed comparison of the amount of p-Stat5 cells in the injection area of the hippocampus. Viral treatment significantly elevated the amount of p-Stat5 staining in the GH group (Fig. 2B,E, one-way ANOVA $F_{(2,36)}=6.34$, $P=0.004$, post-hoc Bonferroni t-test $t_{(36)}=2.59$, $P=0.013$). However, the amount of p-Stat5 positive cells in the aGH group was not significantly lower than in controls ($t_{(36)}=0.70$, $P=0.48$). Increasing the viral load fivefold in pilot experiments similarly failed to suppress p-Stat5 counts significantly below control animals, suggesting a floor effect (Supplemental Fig. 3).

Growth hormone increases dendritic spine density in CA1 stratum radiatum

As systemic ghrelin administration has been shown to increase the spine density in the hippocampus (Diano et al. 2006), and GH

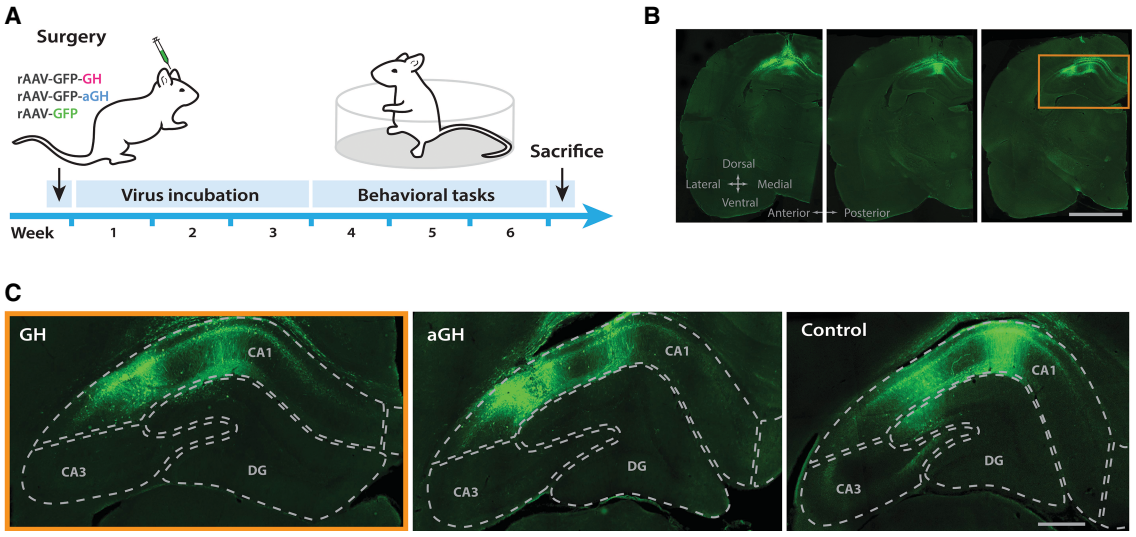

Figure 1. Experimental time line and illustration of viral transfection. (*A*) Rats received recombinant adeno-associated virus (rAVV) injections with either growth hormone (GH), antagonizing GH (aGH), or green fluorescent protein (GFP) only (control). After three weeks of virus incubation, behavioral assessments began. (*B*) Injection sites in dorsal hippocampus are shown by GFP labeling in a representative animal (GH) in coronal sections of the right hemisphere at different anteroposterior levels. Scale bar 200 µm. (*C*) Representative distribution of GFP labeled cells in the hippocampus of a GH, aGH, and control animal. The GFP labeling showed transfected cells in CA1, but also some in CA3 and DG. *Left* panel in *C* is a close-up from the most posterior section in *B* (orange frame). Scale bar 50 µm.

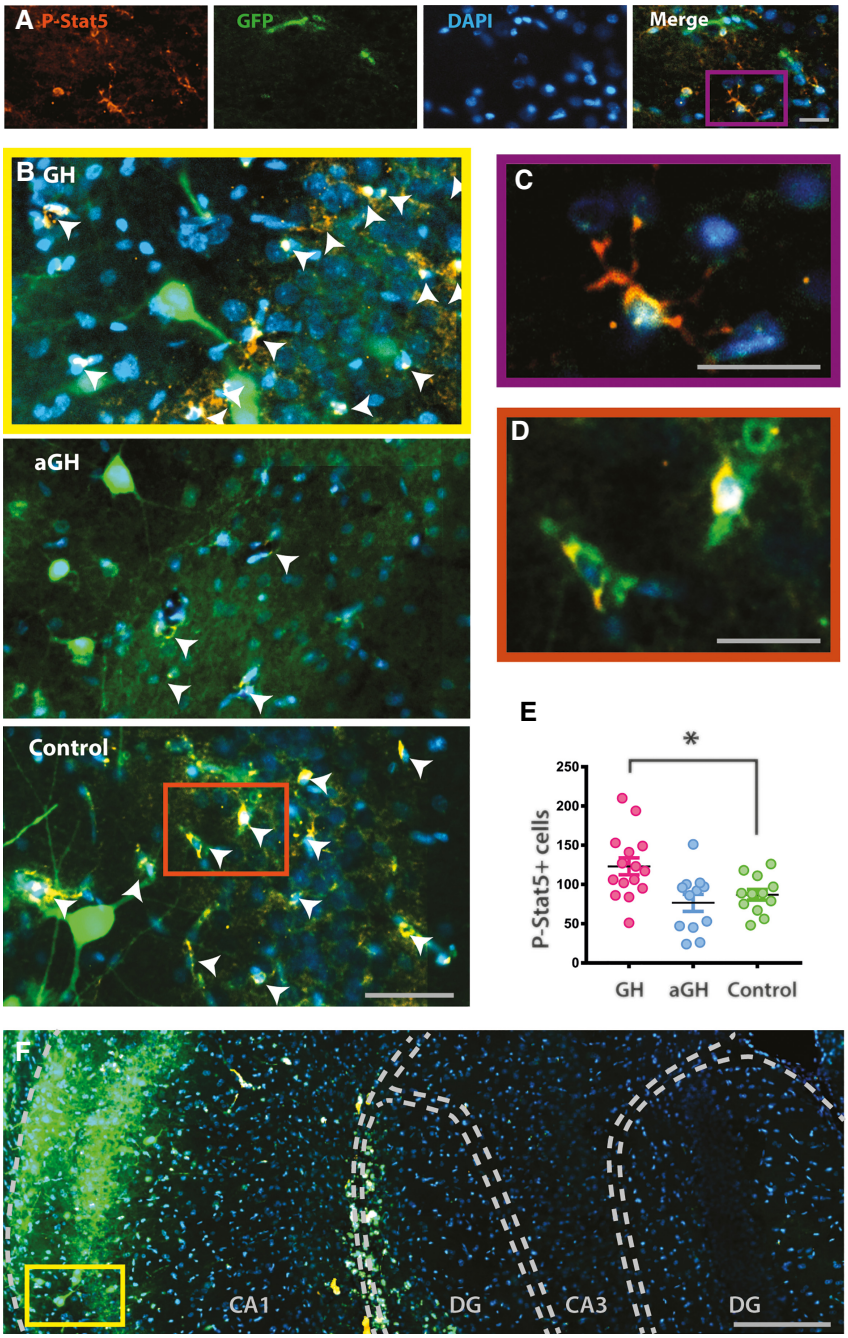

Figure 2. Growth hormone (GH) receptor activation quantified by p-Stat5 in the hippocampus. (*A*) Examples of p-Stat5 signal (red), green fluorescent protein (GFP; green), DAPI (blue), and merged in a control animal. Scale bar 20 µm. (*B*) Representative sections from a GH treated animal (close-up from illustration in F, yellow frame), aGH treated animal, and control animal, with p-Stat5, GFP, and DAPI. Scale bar 50 µm. (C) Illustration of a p-Stat5 positive DAPI cell, close-up from the merged illustration in *A* (purple frame). Scale bar 20 µm. (*D*) Illustration of two p-Stat5 positive, GFP positive DAPI cells (merged green and red becomes yellow), close-up from the example control animal in *B* (orange frame). Scale bar 20 µm. (*E*) The amount of p-Stat5 in the GH, aGH, and control group: GH significantly increased the number of p-Stat5 positive DAPI cells (ANOVA $F_{(2,36)} = 6.33$, $P = 0.004$, *t*-test $P = 0.013$), but p-Stat5 in the aGH group was not significantly lower than in controls. (*F*) Cross section overview of hippocampus from the GH treated animal in B, showing p-Stat5, GFP, and DAPI. GFP labeling is seen most dense in injection area CA1. Scale bar 200 µm.

application on CA1 hippocampal slices increases excitatory synaptic transmission (Molina et al. 2012), we wanted to see if the local GH manipulation in our rats affected the spine density. Spines on apical dendrites from pyramidal cells in CA1 were visualized by the GFP expression (Fig. 3A,B), and only spines on apical dendrites in the stratum radiatum were included in our analysis ($n = 22$ putative pyramidal cells in four aGH treated animals, $n = 8$ in three control animals, and $n = 15$ in three GH treated animals). Average spine density was calculated for each putative neuron before a Jonckheere–Terpstra test for ordered alternatives showed significant groups differences in the expected order (Fig. 3C), with the lowest spine density (0.85 ± 0.04 spines/µm) in the aGH group, 1.00 ± 0.04 spines/µm in controls and highest spine density (1.26 ± 0.07 spines/µm) in the GH group ($T_{JT} = 530$, $P < 0.001$). The same group order was also significant when we did the statistical analysis at animal level (aGH 0.89 ± 0.06, control 1.09 ± 0.04, and GH 1.29 ± 0.10; $T_{JT} = 32$, $P < 0.005$). Pairwise group comparisons at neuron level revealed that the GH treatment increased spine density compared to the control (Mann–Whitney *U*-test, $Z = 2.58$, $P < 0.05$) and that aGH lowered the spine density compared to the control ($Z = 1.92$, $P < 0.05$).

Spine shapes varies over a continuum of morphologies, and can be categorized as filopodia, immature or mature spines. If GH has a function in maintaining learning capacity, it could specifically increase filopodia or immature spines which are associated with plasticity and learning capacity (Berry and Nedivi 2017; Ozcan 2017). We therefore categorized the counted spines blindly into filopodia-like, immature or mature and analyzed them at a neuron level ($n = 15$ GH, $n = 22$ aGH, $n = 8$ control). We found that the percentage of immature spines was increased in the GH group as compared to controls (Fig. 3D, one-way ANOVA $F_{(2,42)} = 23.7$, $P < 0.001$, post-hoc contrast $t_{(42)} = 6.36$, $P = 0.036$), and decreased in the aGH group ($t_{(42)} = 11.4$, $P < 0.001$). An opposite effect was observed for mature spines, GH treatment decreased the relative amount of mature spines (one-way ANOVA $F_{(2,42)} = 21.3$, $P < 0.001$, $t_{(42)} = 11.84$), $P = 0.003$), while aGH treatment increased the relative amount of mature spines ($t_{(42)} = 8.12$, $P = 0.019$) as compared to controls. The relative amount of filopodia-like spines was similar in all three groups (one-way ANOVA $F_{(2,42)} = 0.79$, $P = 0.46$).

Hippocampal growth hormone receptor antagonism disrupts memory

To determine if hippocampal GH modulation affects hippocampal-dependent long-term memory processes, we trained the rats in the water maze over five subsequent days. The rats learned to

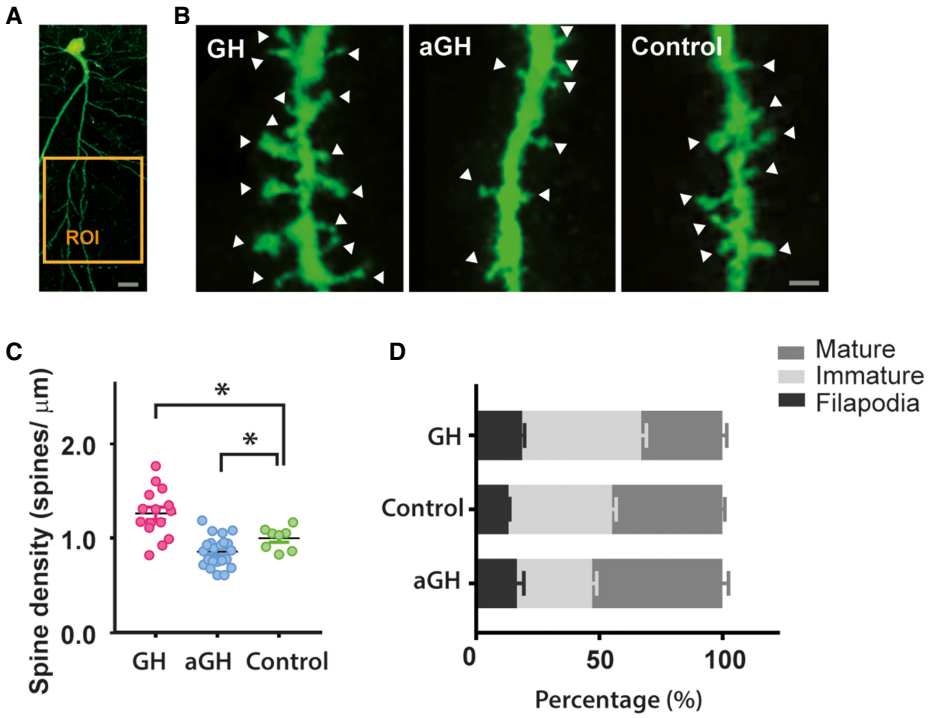

Figure 3. Growth hormone (GH) increases the density of dendritic spines in CA1, while antagonizing GH (aGH) reduced the spine density. (*A*) Example of green fluorescent protein (GFP) labeled pyramidal cell in CA1. Spines 100–200 µm from the soma (region of interest [ROI]; orange frame) on apical dendrites were used in the analysis when the entire neuron was traceable. Scale bar 20 µm. (*B*) Representable segments of dendrites with spines in the GH, aGH, and control group, respectively. Scale bar 1 µm. (*C*) Average spine density for individual spine segments (each dot) was highest in GH treated animals, while aGH had lower spine density than the other group ($n=15$ in three GH treated animals, $n=22$ spine counted regions in four aGH animals, and $n=8$ in three control animals; Jonckheere–Terpstra test, JT = 32, $P=0.003$). (*D*) The distribution of spine morphologies (filipodia, immature or mature) shown in percentages. GH animals had more immature spines than controls (one-way ANOVA $F_{(2,42)}=23.7$, $P<0.001$, *t*-test, $P=0.036$) while aGH had less immature spines than controls (*t*-test, $P<0.001$). On the other hand, aGH increased the percentage of mature spines (one-way ANOVA $F_{(2,42)}=23.7$, $P<0.001$, *t*-test, $P=0.019$) while mature spines were decreased after GH treatment (*t*-test, $P=0.003$).

find a submerged platform 1 cm under opaque water using distal landmarks in the room. The first trial of each day started as a probe trial with the platform inaccessible for 60 sec to reveal a potential search bias. To reduce the number of animals needed in the experiments, our control group included data from seven animals from pilot experiments that used the same GFP-expressing AAV virus in fivefold higher dose than used for all other animals. The high titer control group ($n=7$) did not differ from the normal titer control animals ($n=6$) on any of the water maze probe tests (two-way ANOVA showed no Group × Zone interaction on day 6, 12, 13, or 14, *P* value range 0.20–0.87).

We found successful learning curves for all the three groups during the 5 d of training (Fig. 4A, repeated measures ANOVA $F_{(4,104)}=40.97$, $P<0.001$), but no group difference (ANOVA Day × Group interaction $F_{(8,104)}=1.76$, $P=0.09$). As even hippocampus lesioned rats can learn this task after repeated training, we also looked for early effects of the treatment. A subanalysis of the first day of water maze training showed that the slightly shorter escape latencies of the GH group were not significantly different from the other groups (Fig. 4A, one-way ANOVA of Day 1 Latencies $F_{(2,26)}=1.42$, $P=0.26$). After the 5 d of training, memory for the target platform location was tested on a probe test with the platform unavailable. There was a significant Zone × Group interaction (Fig. 4B; two-way ANOVA ($F_{(6,78)}=3.59$, $P=0.003$). One-way ANOVA of time in the platform zone showed a significant group difference ($F_{(2,26)}=4.61$, $P<0.019$). Subsequent orthogonal comparisons showed that GH and control groups performed at the same level ($t_{(26)}=0.34$, n.s.), and that the aGH group spent less time in the platform zone compared to the other two groups ($t_{(26)}=2.95$, $P=0.004$). Examples of typical swim paths are shown in Figure 4C.

To reveal a possible benefit of GH treatment, we hypothesized that changing the goal location for these rats, which already knew the procedural parts of the task, could uncover group differences in flexible relational learning. After a 6-d break, we changed the platform location to the opposite quadrant in the water maze and trained the same animals for two more days, 4 × 4 trials (Fig. 4D). At the start of reversal training, all groups had a similar bias toward the old platform location, (Fig. 4E, ANOVA Group × Zone interaction $F_{(6,78)}=0.48$, n.s.). However, after 1 d of reversal training only the control rats and the GH treated rats spent more time in the platform zone than the aGH rats on the 60 sec probe test (Fig. 4F, two-way ANOVA Zone × Group interaction $F_{(6,78)}=2.54$, $P<0.05$; one-way ANOVA of time in target zone $F_{(2,26)}=3.64$, $P<0.05$, subsequent orthogonal comparisons showed no difference between GH and control ($t_{(26)}=0.5$), n.s.), but aGH searched significantly less in the new platform zone than the other two groups ($t_{(26)}=2.69$, $P<0.01$). Interestingly, the aGH rats tended to search for the old platform location on the first test (day 13; note the color plot in Fig. 4F), although a Day × Group interaction on escape latencies was not observed (Fig. 4D, repeated measures ANOVA $F_{(2,25)}=1.30$, n.s.). After the second day of reversal training, on the final probe test on day 14, all the groups showed that they had learned the task (Fig. 4G, significant effect of Zone $F_{(3,75)}=22.98$, $P<0.001$, but no Zone × Group interaction, $F_{(3,75)}=1.25$, $P>0.25$). Interestingly, the GH group now tended to dwell at both the new and the old platform locations (color plot in Fig. 4G). This behavior

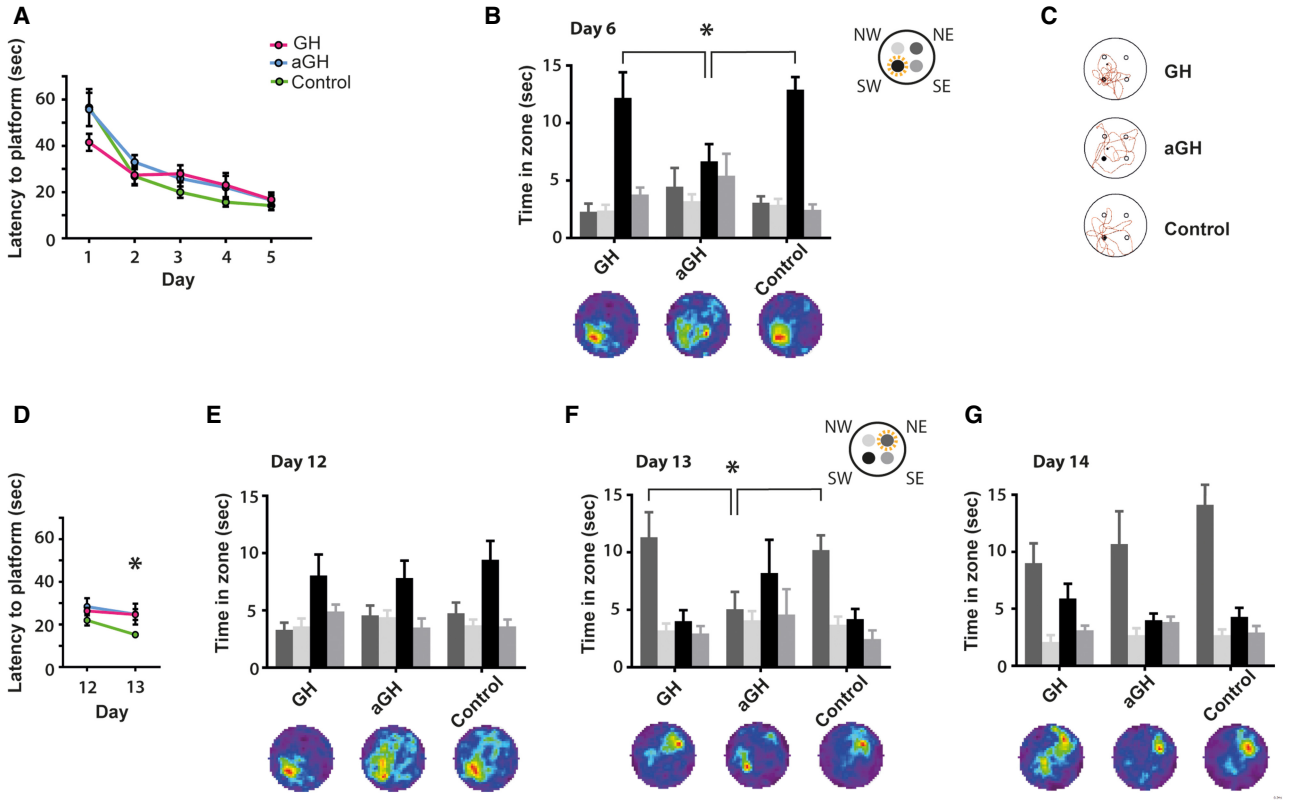

Figure 4. Antagonizing growth hormone (aGH) in the dorsal hippocampus impairs memory in the water maze. (*A*) Latencies on initial training on day 1–5 to the target zone southwest (SW). $n = 8$ GH, $n = 8$ aGH, $n = 13$ controls. (*B*) Search patterns during the 60 sec probe trial on day 6: The histogram of time spent in four 50 cm diameter zones shows that the aGH treated animals spent less time in the platform zone than the GH treated and control animals (post-hoc orthogonal comparisons of aGH versus the two other groups, $t_{(26)} = 2.95$, $P < 0.004$). The *upper right* figure illustrates the zones; the target zone SW (yellow dotted circle), southeast (SE), northeast (NE), and northwest (NW). The occupancy maps below illustrate the average search pattern for each group. Red in the occupancy maps indicates the most time spent in that location, while dark blue indicates the least time spent in that part of the water maze. (*C*) Representative individual swim paths on probe test day 6 for the GH, aGH, and control group, respectively. (*D*) Latencies during reversal training, same animals as in *A*. (*E*) Search pattern for probe trial on day 12, at initiation of reversal training. All groups remembered the platform location SW equally (two-way ANOVA effect of Zone × Group $F_{(6,78)} = 0.48$, $P = 0.82$). Occupancy maps below illustrate that all groups spent the most time in the SW zone. (*F*) Probe trial on day 13, the GH and control animals spent more time near the new NE goal location than aGH (post-hoc orthogonal comparisons of aGH vs the two other groups $t_{(26)} = 2.69$, $P = 0.006$). The aGH group tended to search for the old platform location. The *upper right* figure illustrates the platform zones with the new target zone NE (yellow dotted circle). Occupancy maps below illustrates that GH and control animals spent the most time in NE zone, while aGH animals spent the most time in the SW zone. (*G*) After 2 d of training, on day 14, all groups searched for the novel platform location (two-way ANOVA $F_{(3,75)} = 22.98$; $P < 0.001$, but no Zone × Group interaction $P > 0.25$). Occupancy maps below illustrate that all the groups spent the most time in the NE zone, although the GH animals also spent time searching for the old goal location (SW).

could express that GH treated rats are fast switchers of strategy when the platform position is made unavailable.

The GH transfections did not seem to cause any unspecific somatic or locomotor effects, unlike systemic GH administration (Sun and Bartke 2014). In particular, we observed no differences in weight gain (ANOVA $F_{(2,34)} = 0.67$, n.s.), swimming speed (ANOVA $F_{(5,120)} = 1.07$, n.s.), or path length (ANOVA $F_{(5,120)} = 0.43$, n.s.; Supplemental Fig. 2). To verify that our results in the water maze were due to spatial memory deficits, and not motor or balance impairments interfering with the rats' ability to climb onto the platform, all the animals completed a balance beam test with no observed impairments (none fell off in either group during the 60 sec test).

Growth hormone enhances spontaneous location recognition

If GH is beneficial to hippocampal function, multiple-trial water maze learning may be too complex to reveal the effects, as procedural and relational learning happens in parallel. We therefore exposed the rats to several versions of a memory task that only require a single learning trial, the spontaneous location recognition (SLR) task. In the simplest version we made of this task (Fig. 5A), the animals were first presented with two identical objects in two pseudorandomized corners of a familiar box. After a 3 h delay, two identical copies were accessible, one in the old corner (familiar location), whereas the other was placed in a new corner (novel location). Rats naturally tend to explore the displaced object more. In the test phase, all the groups of animals spent more time exploring the novel object location (Fig. 5B upper panel; 29.4 ± 2.5 sec, 32.0 ± 4.5 sec, and 32.9 ± 3.6 sec in the GH, aGH, and control group), compared to the familiar location (20.4 ± 1.8 sec, 18.7 ± 3.9 sec, and 22.4 ± 1.5 sec, respectively; paired *t*-tests, $t_{(7)} = 3.78$; $t_{(7)} = 3.41$; $t_{(11)} = 2.50$; $P < 0.05$ for all). To ensure no bias in our data, all four corners of the arena were used in a pseudorandomized order (Fig. 6A–C). Object exploration was independent of the corners used during the sample phase, indicating no bias to a certain corner in the box (Fig. 6C; one-way ANOVA of object exploration in all four corners on the first sample trial, before 3 h delay $F_{(3,54)} = 0.64$ n.s.). Neither did we see a bias toward corner on the second

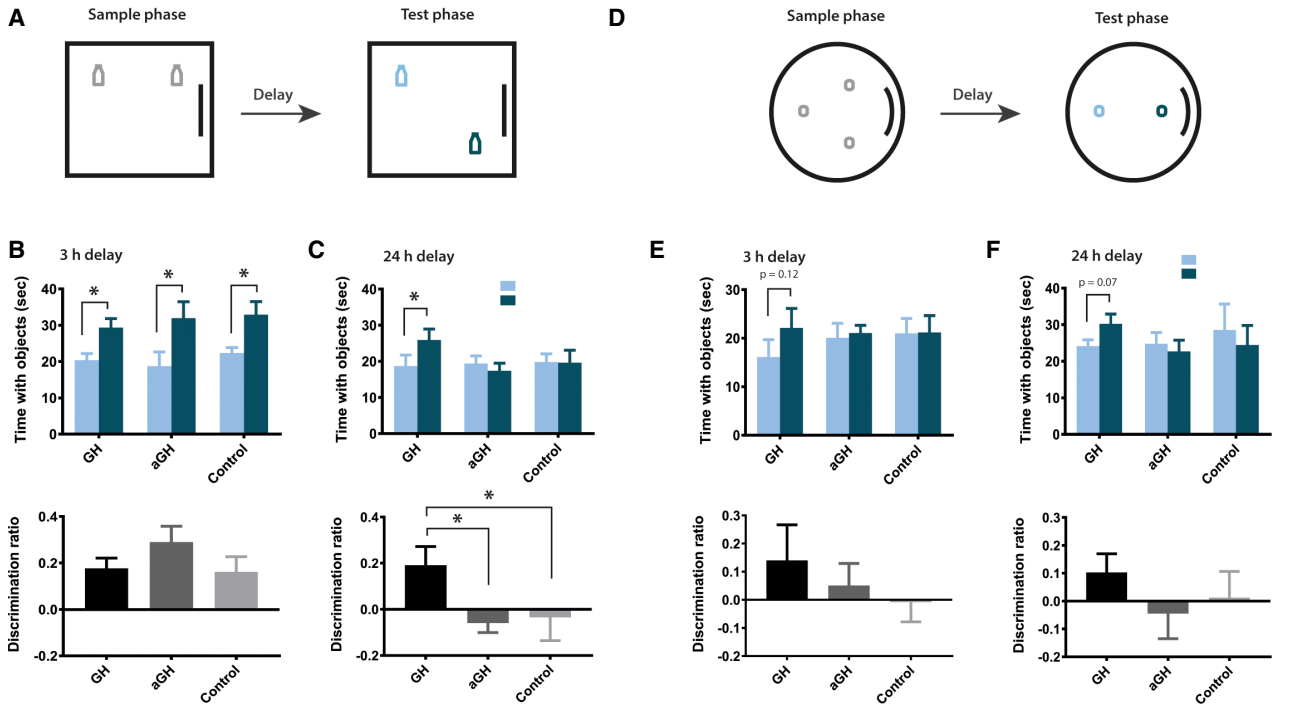

Figure 5. Growth hormone (GH) increases the preference for novel locations. (*A–C*) Easy version of the spontaneous location recognition (SLR) task using a square box with objects placed in the corners. New objects and pseudorandomized corners were used for each trial. (*B*) (*Upper* panel) After a 3-h delay, all groups spent significantly more time with the displaced object compared to the object in the familiar location (*upper* panel, paired *t*-tests, $P<0.05$). (*Lower* panel) Comparison of discrimination ratio revealed no group differences (ANOVA $F_{(2,25)}=1.16$, n.s., $n=8$ GH, $n=8$ antagonizing GH (aGH), $n=13$ controls). (*C*) (*Upper* panel) Using a 24-h delay, only the GH treated animals explored the novel location significantly more than the familiar location ($t_{(7)}=2.56$, $P<0.05$.). (*Lower* panel) The GH rats also had a significantly higher discrimination ratio than the other two groups (ANOVA $F_{(2,26)}=3.36$, $P=0.05$, post-hoc contrasts $t_{(26)}=2.59$, $P=0.016$, as compared to controls and animals treated with aGH. (*D–F*) Second variation of the SLR task, using a circular arena with three objects in the sample phase. After the delay, the location of two objects were merged into one novel location. (*E,F*) (*Upper* panels) Only the GH group tended to explore the novel object location more, but not significantly (3 h delay condition: paired *t*-test, $t_{(7)}=0.12$, 24 h delay condition: *t*-test $t_{(7)}=0.07$). (*Lower* panels) ANOVA of the discrimination ratio showed no significant group differences ($P>0.5$).

sample trial, with the 24 h delay (ANOVA $F_{(3,54)}=1.18$, n.s.). Also, to rule out bias in the exploration data, we compared the exploration of the object location that would later remain in constant position, compared with the object location that would later be displaced. During the sample phase, there was no difference between these object locations (Fig. 6D–F; two-way ANOVAs n.s.).

For comparison between groups, we expressed the preference for novel/familiar location as a discrimination ratio from −1 to 1 (see Materials and Methods), which showed no effect of group in this easiest version of the SLR task (Fig. 5B lower panel; one-way ANOVA $F_{(2,25)}=1.16$, n.s.). The discrimination ratio was also used to check that unoperated controls ($n=6$) and AAV controls ($n=7$) did not differ on any of the SLR tasks (*t*-tests, all *P* values >0.5) before the control groups were merged for all further statistics.

Next, we increased task difficulty by extending the delay between sample and test to 24 h. In the test phase, only the GH treated animals preferred to explore the object placed in the novel location (Fig. 5C upper panel; 25.9 ± 3.1 sec with novel, 18.7 ± 3.6 sec with familiar location; ($t_{(7)}=2.56$, $P<0.05$). The aGH and control groups spent equal amounts of time exploring the objects in both the novel and familiar locations (aGH: $t_{(7)}=1.23$, n.s., control $t_{(12)}=0.01$, n.s.). One-way ANOVA of the discrimination ratio (Fig. 5C lower panel; $F_{(2,26)}=3.36$, $P=0.05$) revealed a significant effect of group (discrimination ratio = 0.19 for GH, 0.06 for aGH, and −0.03 for control). Subsequent orthogonal comparisons showed that the aGH and control group did not differ ($t_{(26)}=0.12$, n.s.), while the GH group performed above the other two groups ($t_{(26)}=2.59$, $P<0.05$).

In the last version of the SLR task, task difficulty was further increased by letting the rats explore three identical object in a circular familiar environment (Fig. 5D). In the test phase, two of the locations were merged to one novel location, so that only two identical copies of the objects were used. One object location remained constant (familiar location). As before, all the groups explored the objects equally in the sample phase (Fig. 6G–I, two-way ANOVAs n. s.). After a 3-h delay, only the GH rats tended to explore the novel object location more than the familiar location, but the effect was not statistically significant (Fig. 5E upper panel, one-tailed paired *t*-tests, GH $t_{(7)}=1.27$, $P=0.12$; aGH $t_{(7)}=0.30$, $P=0.38$; controls $t_{(12)}=0.04$, $P=0.48$). The discrimination ratio was not different between the groups (Fig. 5E lower panel, one-way ANOVA $F_{(2,26)}=0.70$, n.s.). Last, we used a task setup with 24 h delay and a smaller distance between locations B and C (that would be merged). The GH group again showed a tendency to explore the novel object location more than the familiar object location, although the result did not reach statistical significance (Fig. 5F upper panel, one-tailed paired *t*-tests, GH group $t_{(7)}=1.69$, $P=0.07$; aGH $t_{(7)}=0.20$, $P=0.42$; controls $t_{(5)}=0.16$, $P=0.44$). The discrimination ratio was not different between groups (Fig. 5F lower panel, one-way ANOVA $F_{(2,19)}=0.43$, n.s.).

Discussion

We have shown that relational memory is influenced by local levels of GH in the dorsal hippocampus. Antagonizing the GH

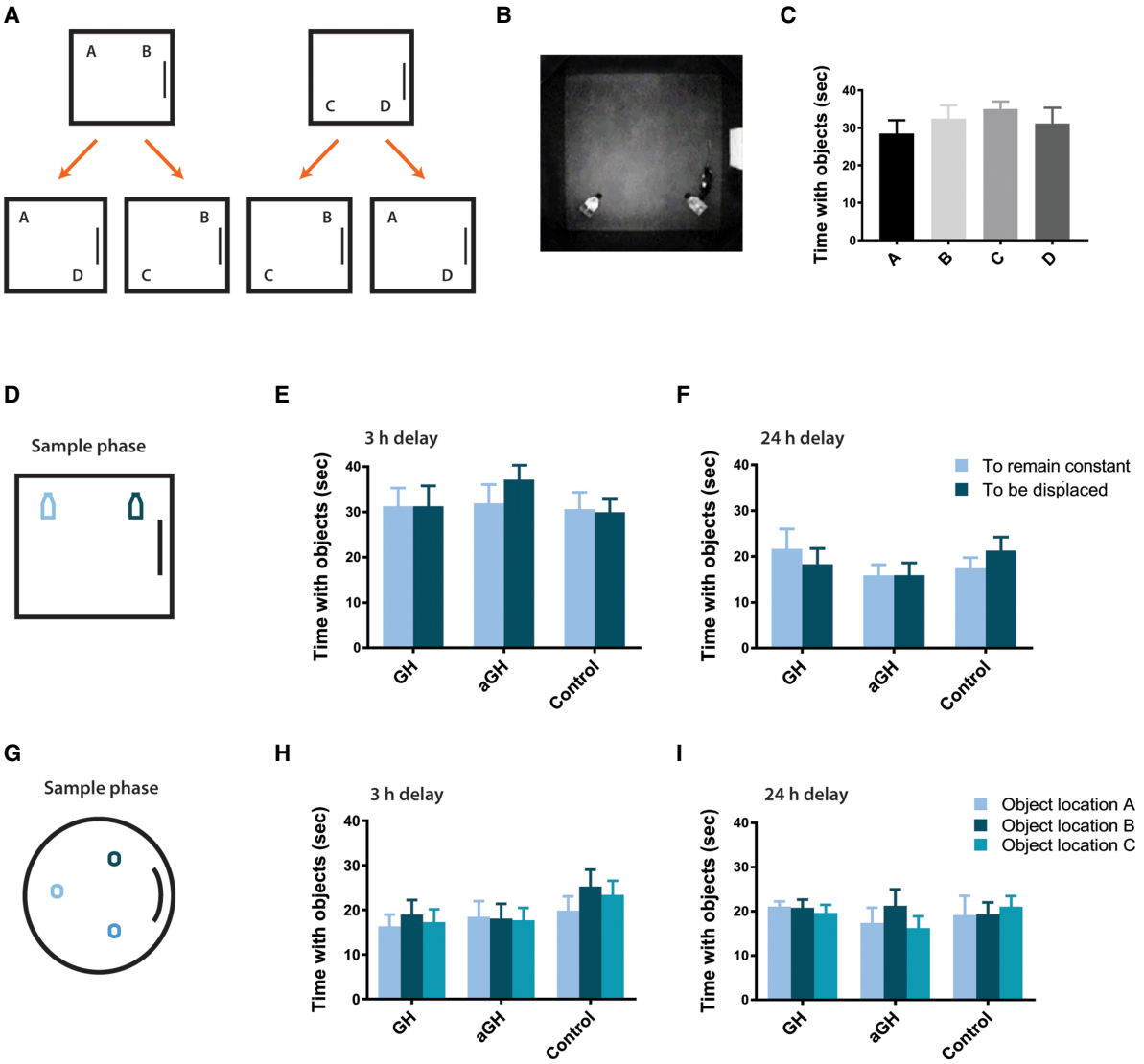

Figure 6. Exploration times with objects during the sample phase in the spontaneous recognition of location (SLR) tasks show no differences between the groups. (*A*) Randomized design for the SLR task with square box: During the sample phase (panel above), objects were placed in corners *A* and *B* or *C* and *D*. During later testing, one object was displaced as indicated by orange arrows (panel below). (*B*) Example frame from video camera when a rat explored an object in corner D during the sample phase. (*C*) Object exploration time for each corner during the sample phase showed no bias for corner. (*D*) Example of sample phase for the square arena. One object location (light blue) is to remain constant, and one object location (dark blue) is to be displaced upon later testing. The objects were identical. (*E*,*F*) Object exploration times for the object locations to remain in constant position (familiar) versus the object locations to be displaced, during the first 3 min of the sample phase. Two-way ANOVAs showed no effect of object location $F_{(1,26)} = 0.04$, n.s. and no Group × Location interaction $F_{(2,26)} = 0.68$, n.s.), before the 3 h delay (*E*) or before the 24 h delay (*F*; two-way ANOVAs effect of object location $F_{(1,26)} = 0.06$, n.s. and Group × Location interaction $F_{(2,26)} = 1.84$, n.s.). (*G*) Sample phase for the circular arena. One object location is to remain constant (*A*, light blue), while the two other object locations (*B*, dark blue and *C*, blue) are to be displaced upon later testing. All the objects were identical. (*H*,*I*) Object exploring times for the three objects *A*, *B*, and *C* during the three first minutes of the sample phase in the circular arena. Two-way ANOVAs showed no effect of object location $F_{(2,52)} = 0.60$, n.s. and no Group × Location interaction $F_{(4,52)} = 0.32$, n.s.), before the 3 h delay (*H*) or before the 24 h delay (*I*; two-way ANOVAs effect of object location $F_{(2,38)} = 0.57$, n.s. and Group × Location interaction $F_{(4,38)} = 1.05$, n.s.).

receptor resulted in poorer memory performance in the water maze, a lower density of CA1 dendritic spines, and a lower percentage of immature spines. On the other hand, elevation of hippocampal GH levels was associated with higher density of dendritic spines, more immature spines, and enhanced memory in a single-trial SLR task under one of the test conditions. Our results suggest that GH is a neuromodulator that enhances learning capacity by affecting the dendritic spines (von Bohlen Und Halbach 2009). Several studies have reported cognitive impairments in cases of systemic GH deficiency, and cognitive improvement after systemic GH replacement (Åberg 2010; Nyberg and Hallberg 2013; Ashpole et al. 2015). Our study provides important evidence for a common underlying assumption in these studies; namely that the effect on cognition, and in particular on memory, is mediated by the hippocampus. Extra-hippocampal mechanisms exist, for example in the amygdala (Meyer et al. 2014) and the prefrontal cortex (Enhamre et al. 2012), and the relative importance of GH in each brain region is still elusive.

Effects of the viral treatments

To verify the efficacy of the treatments used in this study, we analyzed the downstream phosphorylation of Stat5 (Fig. 2), which is a common method for measuring GH receptor activation (Furigo et al. 2017). The method successfully showed the expected increase in receptor activation in the GH group. However, the aGH group only showed a trend toward lower p-Stat5 count, not statistically significant from control rats. The measured outcome in spine density and behavior nevertheless indicated that the virus worked as intended, and we have considered several possible explanations for the lack of statistically significant change in p-Stat5 count. First, a floor effect is likely. It is well known that p-Stat5 as indicator of GH receptor activation is hard to observe without a significant GH injection/stimulation immediately before sacrifice and staining. A chronic blockade of GH receptors by the mutated GH would therefore not necessarily lower the overall receptor activation in the hippocampus, but rather prevent proper activation of the receptor during critical periods of learning. This is also consistent with results from pilot experiments in our laboratory using a fivefold higher virus dose (Supplemental Fig. 3). Second, the several weeks of overexpression of GH and aGH could have initiated downstream compensatory mechanisms or caused other parts of the network to change. Although we believe that the transfected cells in the injected area CA1 were principally responsible for the changes observed in this study, we know that AAV transfections easily spread to the DG. We therefore cannot claim that our effect was restricted to the CA1 only, as we also report GFP labeled neurons in CA3 and DG. In addition, GH is found to have both autocrine and paracrine effects (Gisabella et al. 2016), which means that GH could influence neighboring cells or other parts of the hippocampus as well as the transfected cells. Other genetic tools may allow experiments that decipher the relative contribution of GH in each hippocampal subarea. The fact that we still see behavioral and morphological effects after several weeks of chronic GH manipulation in only a part of the dorsal hippocampus suggests that the role of GH is important and could even be underestimated by the presented results. A larger transfection was avoided because of the risk of epilepsy and excitotoxic cell damage.

What are the mechanisms involved in hippocampal GH modulation?

To our knowledge, our report is the first to show that a direct GH manipulation in the hippocampus correlates with both behavioral and morphological changes. We found that GH enhances spine density while aGH reduces the spine density, but also report that aGH reduces the amount immature spines, important for learning and synaptic plasticity (Berry and Nedivi 2017). On the other hand, the GH rats had a lower percentage of mature spines and more immature spines, which indicate that the network plasticity is high. Spine formation is a morphological substrate for LTP, which is suggested to be the cellular mechanism behind learning and memory (Matsuzaki 2007). Previous studies have described the effects on spine density after the systemic elevation of ghrelin (Diano et al. 2006) and IGF2 in APP mice (Pascual-Lucas et al. 2014).

We cannot conclude that spine density is the only mechanism involved to alter learning and memory when GH levels are manipulated. For example, there is evidence implying the *N*-methyl-D-aspartate (NMDA) receptor, crucial for both water maze and object recognition tasks (Nakazawa et al. 2004; Warburton et al. 2013). Electrophysiological studies in vitro show that GH directly modulates glutamatergic synaptic transmission in the CA1 subfield of the hippocampus. Acute GH application in CA1 brain slices enhances both isolated NMDA and AMPA receptor field excitatory postsynaptic potentials (fEPSPs) in young and old rats (Mahmoud and Grover 2006; Molina et al. 2012, 2013). GH affects synaptic transmission in the absence of presynaptic changes, indicating postsynaptic changes responsible for the detected fEPSPs (Molina et al. 2012). Exogenous GH increases the expression of NMDA receptor subunit NR2B in young adult rats, thus changing the NR2A/NR2B ratio (Le Greves et al. 2002). Changing the ratio of these subunits alters the Ca^{2+} regulation, which can enhance LTP and synaptic plasticity (Nyberg and Hallberg 2013). Future studies should focus on the longitudinal dynamics of the GH-dependent changes, as in vivo imaging of spine dynamics indicate that increases in spine density are followed by a phase of elimination (Xu et al. 2009).

The relative contribution of the other components in the GH-axis, like ghrelin and/or the insulin-like growth factor (IGF)1 and 2, is also not well understood. IGF1 enhances adult neurogenesis by increasing the number of progenitor cells in the subgranular layer of DG (Åberg 2010), while IGF2 administration in the hippocampus improves memory consolidation (Chen et al. 2011), and reverses synaptic deficits in mice modeling Alzheimer's disease. Local IGF2 in the hippocampus has also been shown to promote spine formation (Pascual-Lucas et al. 2014). On the other hand, GH may improve hippocampal memory independently on IGF1 and IGF2, as patch-clamp studies indicate that GH directly enhances neural plasticity by increasing excitatory transmission in CA1 (Molina et al. 2012). To fully understand the impact GH in the hippocampus, further experiments are required to investigate effects of GH in the entire hippocampus, as well as the importance of the downstream processes.

Does growth hormone therapy require a deficiency to work?

The GH group performed better than controls only in one task setting, the 24 h delay square box SLR task. To enhance the performance above that of healthy control animals, some kind of residual potential in the organism may be necessary. This could happen in laboratory animals living under unstimulating or stressful conditions. However, as our rats were housed in an enriched environment and handled extensively before training, the residual potential for increasing the memory capacity by GH could be minimal. This may explain why the impact of GH in our study was not larger. This interpretation is in line with papers describing the rescue effects after GH treatment under conditions of distress or disease. For example, systemic GH treatment has been shown to restore normal cognitive function after sleep deprivation (Kim et al. 2010). Recombinant human GH in hypophysectomized male Sprague Dawley rats is reported to improve spatial memory of the hormone-ablated rats (Le Greves et al. 2006), which in a similar study was dose-dependent (Kwak et al. 2009). Rescue of the hippocampal GH levels is probably a key mechanism in these studies, as GH gene therapy in the hippocampus, an approach similar to ours, was shown to restore hippocampal memory function to normal levels after stress (Vander Weele et al. 2013). In humans, GH treatments in children with GH deficiency, or in older adults, have resulted in some cognitive improvement (Maruff and Falleti 2005; Baker et al. 2012). Another possible explanation why the GH group did not perform above controls in the water maze, is that the intensive training makes the task more sensitive to memory persistence than to memory acquisition.

Clinical significance of growth hormone in the aging brain

For memory to serve as a useful guide in decision-making, we need a combination of memory that maintains stable information (persistence) combined with the ability to forget and replace information (transience) (Richards and Frankland 2017). This perspective is useful when interpreting our data, rather than a classical

acquisition–retrieval perspective, and relates the data to everyday life. The aGH group showed a deficit in memory persistence on day 6, although at later testing they performed at the same level as controls. Perhaps their deficit was mainly in memory transience, the flexibility that allows rapid adaptation to new information, as they needed longer to relearn a novel goal location. This view fits with the notion that the GH group tended to search for both goal locations on the very last water maze probe trial, and also showed the greatest ability in the SLR tasks. The SLR tasks were performed with novel objects in the same room on subsequent days, challenging their pattern separation abilities as well as memory transience.

It is tempting to speculate that GH deficiency in the aging brain could be associated with a lower capacity for memory transience and a resistance to remodulate already acquired memories. Cementing behavior in adulthood could in general be an advantageous mechanism, preventing the common successful behavior to be overwritten by insignificant experience. Beneficial cognitive effects of GH treatment have been documented for aged animals and humans in several studies (Bartke 2008; Baker et al. 2012; Sonntag et al. 2012). GH is considered to be a replacement therapy, as adult GH levels drop dramatically in aging along with GH binding sites (Lai et al. 1993; Lobie et al. 1993), and GH is barely detectable after age 60 in some humans (Toogood and Shalet 1998). As systemic treatments may have severe side effects, especially in oncogenesis, a targeted approach to restore GH levels in the brain should be researched. Understanding the impact of GH in memory and learning may not only benefit GH deficient patients, but also all individuals that experience cognitive decline during normal aging.

Materials and Methods

Animals

In total, 44 adult male Long-Evans rats (Charles River, Italy) were used in this study, of which 37 animals were subjected to surgery (300–430 g at the time of surgery) and seven were left unoperated. For the animals receiving surgeries, 27 animals were used for behavioral assessment, while 10 rats were used for spine density analysis only. All the rats were housed in pairs in a controlled enriched environment, with constant humidity (55 ± 5%), temperature (21 ± 1°C), and a 12-h light cycle (lights on at 7 p.m.). Food and water were available ad libitum. All experimental protocols followed the European Community Council Directive 2010/63, the Norwegian Experiments on Animals Act, and were approved by the Norwegian Animal Research Authority before initiation. Surgeries and the following behavioral assessments were done in batches of five to seven animals, each containing representatives for all three groups (GH, aGH, and control).

Viral vectors

Three recombinant adeno-associated viruses (rAAVs) 1/2 chimeric pseudotypes were used to either overexpress GH and GFP, mutated antagonizing (mutated) GH (aGH) and GFP, or GFP only (generous gift from Ki Ann Goosens, MIT). The construction of the viral vectors is described in more detail in Meyer et al. (2014), while a summary is presented here: Three cassettes were synthesized (Epoch Life Science), including one cassette containing the coding region of the rat *GH* gene (GeneBank Accession number U62779.1). Another cassette contained the rat *GH* gene with a single amino acid substitution at position 120 (*rGH-G120R*) to produce mutant GH protein with antagonist activity on the GH receptor. Both the cassettes contained internal ribosome entry site (IRES) and GFP. The third cassette only contained IRES and GFP. The cassettes were flanked by EcoRI and BGIII, and subcloned into pFB-AAV-CMV-SC40pa (V032) AAV gateway plasmid from Virotek (Hayward, CA), with AAV1/2 chimeric pseudotyping, yielding the three contstructs: pAAV-CMV-GH-IRES-GFP, pAAV-CMV-aGH-IRES-GFP, and pAAV-CMV-IRES-GFP. The purified viruses were suspended in PBS, making the titers 2.46×10^{12} vg/mL for the control and GH AAV, and 2.42×10^{12} vg/mL for the aGH AAV.

Stereotaxic surgeries

All the surgeries were conducted under analgesia and deep isoflurane gas anesthesia. The animals ($n = 37$) were weighed and fully anesthetized in an induction chamber, before being placed on a heating plate (Agnthos; 37°C) on a stereotaxic frame (David Kopf Instruments). Buprenorphine (0.05 mg/kg) and Meloxicam (2 mg/kg) were given subcutaneously as analgesics, both before surgery and postsurgery. Simplex eye ointment was applied on the eyes to prevent dehydration. Nontraumatic ear bars positioned at the bones in the ear cavity were used to fixate the head. During surgery, the isoflurane concentration was adjusted according to reflexes, respiration rate, and oxygen saturation (Kent Scientific). Before incision, the skin was disinfected with 70% ethanol. The skin was cut open and holes were drilled at the appropriate locations on each hemisphere. Rats were randomly assigned to receive either pAAV-CMV-GH-IRES-GFP, pAAV-CMV-aGH-IRES-GFP, or pAAV-CMV-IRES-GFP. The viruses were injected with a sterile 2 µL Hamilton Syringe (Hamilton Company) using a pressure pump (KD Scientific). The rats received four injections of 0.4 µL virus solution (0.2 µL/min) in each hemisphere in the dorsal hippocampal area CA1 according to the injection coordinates calculated anteroposteriorly (AP), mediolaterally (ML) from bregma, and dorsoventrally (DV) from dura: AP −3.0 mm, ML ± 1.2 mm, DV 2.3 mm; AP −3.5 mm, ML ± 2.2 mm, DV 2.2 mm; AP −4.0 mm, ML ± 2.4 mm, DV 2.4 mm; AP −4.4 mm, ML ± 3.5 mm, DV 2.8 mm. The needle was left at the site of injection for 5 min after each injection to allow diffusion of the virus before slow retraction. After the last injection, the skin was sutured and the animals were allowed to recover with a warm water bottle in their home cages.

Behavioral tasks

Spontaneous location recognition tasks

Two weeks after surgery, 22 operated and seven unoperated rats were habituated to an empty open field arena (1 × 1 m with 60 cm walls), 15 min per day for 5 d. A white cue card (21.0 × 29.7 cm) on one of the black walls served as a local cue. Items in the room (cabinets, boxes) served as distal cues and remained constant throughout the experiment. After habituation, all rats participated in two main variations of the task (square and circle arenas), consisting of a sample phase and a test phase separated by either 3 or 24 h. In the sample phase, the rats explored novel objects which were secured in place by blue-tack. In the following test phase, one object was put in a novel location while the other object remained in the familiar location, both secured by blue-tack, and using copies of identical objects to avoid transfer of smell. The animal's natural preference for exploring the displaced object was manually scored by two blind observers in Ethovision XT 11.5, using video tracking. Object exploration was defined as rat directing its nose toward the object at a distance of 2 cm or less. Standing on the object with the nose clearly pointing away from the object was not counted as object exploration. The preference for the displaced object was calculated by the discrimination ratio, that is, the difference in time spent with the object placed in the novel location and the object in the familiar location divided on the sum of the time spent with both of them. A score of 1 indicates that the animals only spent time near the object in the novel location, while a score of −1 means that the animals visited only the familiar object location. We analyzed the first 3 min of the 5 min test phase as the animals explored the objects the most during these first minutes. This is in line with reports from other labs using this task to describe the preference for displaced objects during the first 2–3 min (Dix and Aggleton 1999; Larkin et al. 2014). To avoid familiarization to the objects, the animals explored new sets of unique objects in each task variation. Between trials, the arena and the objects were cleaned with water and 70% ethanol. Objects that were used included blue tea light holders (6.5 cm in diameter × 3.5 cm

height), serum bottles (7.5 cm × 3.5 cm × 15 cm) with blue corks, clear plastic water bottles (6 cm in diameter × 14 height) covered with green tape, Falcon 50 mL Centrifuge tubes (3.5 cm in diameter × 11.5 height), and standing petri dishes on metal plates covered in green, blue, and orange tape (about 2 × 6 × 9 cm).

In the square version of the task, the familiar 1 × 1 m open field box was used. In the sample phase, two identical objects were located in random corners next to each other 10 cm from the walls (Figs. 5A, 6A–F). In the test phase, one object was relocated to the diagonally and opposing corner of the box. The animals were allowed to explore the arena with the objects for 5 min in the test phase before they were put back to their home cages. To avoid exploration bias for any preferred corner in the data, all four corners were used in each condition (familiar/novel) an equal amount of times in a pseudorandomized order (Fig. 6A,C). The order of task variations was square 3 h, square 24 h, circle 3 h, and circle 24 h.

In the circular version of the task, animals were first given one habituation session for 10 min to the cylindrical arena (90 cm in diameter, 60 cm high) before they were put back to their home cages. In the sample phase, three identical objects (A, B, C) were located in the arena (Fig. 6G–I). Object A was located the furthest away from the other two objects. The rats were allowed to explore the three objects for 10 min in the sample phase before they were moved back to their home cages. After a delay of 3 or 24 h, the animals were put back to the circular arena for the test phase. For the task with 3 h delay, the objects in the sample phase were situated in largest distance to each other (120° between object A and the other two objects, object B and C), while for the most challenging condition, we used 24 h delay between trials and a smaller separation between the objects (40°). In the test phase, only two identical copies of the objects (A, D) were assessable (Fig. 5D). The object location for object A in the test phase was identical to the location for object A in the sample phase, making this a familiar location, while object D was placed between the former locations of the objects in the sample phase, objects B and C, resulting in a novel location.

Morris water maze task

Rats transfected with virus ($n = 27$) were trained in a water maze (2 m in diameter, filled with 50 cm opaque water, about 23°C), for five consecutive days to find a submerged platform located southwest (SW). Each training day consisted of eight trials. The trials were divided into two sessions of four trials each, separated by at least 3 h. The first trial of each day was a single reinforcement probe trial, in which the rats were searching for the hidden platform location for 60 sec before the platform was raised to an available position. Then, another 60 sec were provided for the rats to locate the platform. During the other seven trials of the day, the platform remained in the raised and available position, 1 cm below opaque water. If the rat failed to locate the platform within 120 sec, it was manually guided to the platform by the experimenter. After each trial, the rats were allowed to rest for 30 sec on the platform. The overall memory performance was measured during a probe trial on day 6. The starting positions (South, East, North, West) were counterbalanced across the trials. After each training session (four trials), the rats were put to dry under a heating lamp. One week after the last training session, the rats received an additional 2 d (day 12 and 13) of reversal training with the platform located in the quadrant opposite to the previous goal. Learning the new platform location was measured on the probe trial the subsequent day (day 14).

Balance test

After the water maze tasks, the animals were subjected to a balance beam test to rule out any motor or balance effects of the treatment which could influence the water maze performance. We used a 60 cm long and 3 cm broad ruler placed on plastic shelves, 40 cm high off ground. The animals were placed in the middle and left balancing on the ruler for maximum 1 min.

Perfusion and sectioning

All the rats were deeply anesthetized with isoflurane gas before given Buprenorphine (0.05 mg/kg) and a lethal dose of Pentobarbital (100 mg/kg). The rats were transcardially perfused with physiological PBS and then a 4% paraformaldehyde in PBS solution (pH 7.4) at 80 mL/min using a peristaltic pump (World Precision Instruments). The brains were submerged in a 4% paraformaldehyde solution for additional fixation before 2% dimethyl sulfoxide and 20% glycerol (DMSO) at 4°C. The rats used for spine analysis ($n = 10$) were perfused with ice-cold physiological PBS before brain tissue was stored in a 4% paraformaldehyde solution for 1 wk and then in dimethyl sulfoxide (DMSO) until the brain was sectioned. The brains were cut coronally on Leica CM1950 cryostat (Leica Biosystems), with 40 µm thick sections with six series, in which the first series was put directly on Super Frost glass slides for Cresyl violet (Nissl) staining (Sigma-Aldrich), while the other sections were put on DMSO for immunohistochemistry and stored at −20°C. The brains for spine analysis were cut in 100 µm thick sections and stored at 4°C.

Immunohistochemistry

To assess the viral transfection in the brains from all the animals used in behavioral testing, the GFP expression in the tissue was amplified using a free-floating immunohistochemistry protocol. The 40 µm thick sections were washed with 0.01 M PBS for 5 min repeated six times (later washed three times between the steps), before put on ice-cold methanol at −20°C for 10 min to disturb the integrity of the cell membrane. The sections were washed for 5 min three times. The sections were transferred to a blocking buffer (1% BSA, 0.2% Triton-X, in 0.01 M PBS) for 1 h, then incubated with primary antibody anti-Chicken GFP Polyclonal antibody, 1:2000 dilution (ThermoFischer # A10262) overnight at room temperature. Then, the sections were incubated in secondary antibody Goat anti-Chicken IgY Alexa Fluor 488, 1:200 dilution (ThermoFischer # A-11039) for 2 h and mounted using ProLong DAPI antifade (ThermoFischer # P36941). For the GFP immunohistochemistry of the 100 µm thick sections, the tissues were stained with primary and secondary antibodies for GFP as described above, but with longer blocking time (2 h), higher concentrations for the anti-Chicken GFP Polyclonal antibody (1:1000), and higher concentration (1:100) and longer incubation time (4 h) for the Goat anti-Chicken IgY Alexa Fluor 488.

For phosphorylated Signal transducer and activator of transcription 5 (p-Stat5) immunohistochemistry, representative sections from animals used in the behavioral tests were used ($n = 15$ in four GH rats, $n = 12$ in three aGH rats, $n = 12$ in three control rats). Sections were transferred to a blocking buffer with 5% normal goat serum (Sigma-Aldrich), and 0.3% Triton-X in 0.01 M PBS for 1 h, and incubated with primary antibody anti-Rabbit p-Stat5 (1:200 dilution, Cell Signal # 9314) overnight at 4°C. Consequently, the sections were incubated with secondary antibody anti-Rabbit IgG Alexa Fluor 546 Conjugate (1:200, Termofisher # A-11071) for 2 h and mounted using ProLong DAPI antifade (ThermoFischer #P36941). The fluorescence in the tissue was imaged by a fluorescence microscope Axio Zoom V.16 (Carl Zeiss). Positive p-Stat5 labeled DAPI cells were manually counted blinded for treatment in an area of 0.5 mm^2 per section in immediate proximity to the injection sites, using Zen 2 Lite Software.

Spine analysis

For analyzing the effects of the GH treatment on spine density, we looked at 100 µm thick sections after GFP immunohistochemistry and DAPI labeling in 10 rats ($n = 3$ GH, $n = 3$ aGH, $n = 4$ control). These sections were from animals that were not used in behavioral tests. Images of neurons were obtained from a confocal microscope Zeiss LSM 780 with ZEN 2012 black edition imaging software. An eGFP contrast filter and 488 nm wavelength argon laser were used to gather a *Z*-stack of laser scan images (1756 × 1756 pixels) averaged four times, with an average optimal *Z* distance at 0.6× optical zoom, and a 100× oil objective. The *Z*-stack images were analyzed with ImageJ (NIH). The resolution of the stack image

was increased by a factor of 3 in the X and Y directions with the Transform J Scale plug-in, and the spines were counted using the Cell Counter plug-in to manually mark spines. Spines from apical dendrites of CA1 pyramidal cells were defined as in the following review (von Bohlen Und Halbach 2009), and sampled between 100 and 200 µm from the pyramidal layer, where the density of the spines is relatively uniform (Megias et al. 2001), when the dendrites were clearly traceable. The spine density was averaged by dividing the number of spines on the length of the dendritic segment and calculated on cell level ($n = 64$ dendritic segments in 15 neurons from GH animals, $n = 75$ dendritic segments from 22 neurons in aGH animals, and $n = 49$ dendritic segments in eight neurons in control animals). The spines were further classified based on their morphology as either filopodia, immature or mature spines. All analysis was performed blind to the virus treatment, as K.G.H. performed the surgeries and histology, while A.O. and A.L. did the work on spine density measurement and classification.

Experimental design and statistical analysis

All of the data is presented as mean ± SEM. Statistical analysis was performed in SPSS (IBM Corporation) and MATLAB (Mathworks) with $\alpha = 0.05$. Water maze data was analyzed first by testing for effect of platform Zone and Group × Zone interaction by a two-way analysis of variance (ANOVA). If significant Group × Zone effects were found, time in the target platform zone was evaluated by one-way ANOVA followed by orthogonal comparisons between the groups. The data in the SLR tasks was analyzed using one-way ANOVA and paired *t*-test. For the histology, the p-Stat5 positive cells were analyzed using ANOVA followed by *t*-tests. Nonparametric tests (Jonckheere–Terpstra test, Mann–Whitney U) were chosen for spine density analysis due to lack of normal distribution in the data set and low number of animals, while spine classification was analyzed by ANOVA and post-hoc contrast *t*-tests. The position of the animals in the water maze was sampled using Dacq acquisition system (Axona Ltd). The performance in the task was calculated by measuring the mean latency to the platform location (sec), time in zone (sec), and plotting occupancy maps for heat map visualization of the swimming path in MATLAB. Videos from the SLR tasks were recorded and analyzed using EthoVision Software (Noldus). Graphs for illustrations were made using GraphPad Prism version 7.09 (GraphPad Software).

Acknowledgments

We thank Dr. Ki Ann Goosens (Massachusetts General Hospital/Harvard Medical School) for contributing the AAVs used. We also thank Angel Moldes-Anaya for contributing to the pilot studies and for great discussions, Fanny Stette for assistance with p-Stat5 immunohistochemistry, and Håvar Marsteen for helping with the water maze training. We thank Torkel Hafting and Heikki Tanila for comments on earlier versions of the manuscript. This work was supported by the Northern Norway Regional Health Authority (grant number SFP1165-14) and the Norwegian Research Council (grant number 230413).

Author contributions: V.H.B., K.B.K., and K.G.H. designed the experiment. K.G.H. performed all surgeries. K.G.H. and K.B.K. ran the behavioral experiments. K.G.H. did the histology and immunohistochemistry. A.O. and A.L. performed spine density analysis. V.H.B. and K.G.H. analyzed all behavioral data and wrote the manuscript.

References

Åberg D. 2010. Role of the growth hormone/insulin-like growth factor 1 axis in neurogenesis. *Endocr Dev* **17:** 63–76. doi:10.1159/000262529

Åberg ND, Brywe KG, Isgaard J. 2006. Aspects of growth hormone and insulin-like growth factor-I related to neuroprotection, regeneration, and functional plasticity in the adult brain. *ScientificWorldJournal* **6:** 53–80. doi:10.1100/tsw.2006.22

Albarran-Zeckler RG, Brantley AF, Smith RG. 2012. Growth hormone secretagogue receptor (GHS-R1a) knockout mice exhibit improved spatial memory and deficits in contextual memory. *Behav Brain Res* **232:** 13–19. doi:10.1016/j.bbr.2012.03.012

Ashpole NM, Sanders JE, Hodges EL, Yan H, Sonntag WE. 2015. Growth hormone, insulin-like growth factor-1 and the aging brain. *Exp Gerontol* **68:** 76–81. doi:10.1016/j.exger.2014.10.002

Baker LD, Barsness SM, Borson S, Merriam GR, Friedman SD, Craft S, Vitiello MV. 2012. Effects of growth hormone-releasing hormone on cognitive function in adults with mild cognitive impairment and healthy older adults: results of a controlled trial. *Arch Neurol* **69:** 1420–1429. doi:10.1001/archneurol.2012.1970

Bartke A. 2008. Growth hormone and aging: a challenging controversy. *Clin Interv Aging* **3:** 659–665. doi:10.2147/CIA.S3697

Basu A, McFarlane HG, Kopchick JJ. 2017. Spatial learning and memory in male mice with altered growth hormone action. *Horm Behav* **93:** 18–30. doi:10.1016/j.yhbeh.2017.04.001

Bekinschtein P, Kent BA, Oomen CA, Clemenson GD, Gage FH, Saksida LM, Bussey TJ. 2013. BDNF in the dentate gyrus is required for consolidation of "pattern-separated" memories. *Cell Rep* **5:** 759–768. doi:10.1016/j.celrep.2013.09.027

Berry KP, Nedivi E. 2017. Spine dynamics: are they all the same? *Neuron* **96:** 43–55. doi:10.1016/j.neuron.2017.08.008

Birzniece V, Sata A, Ho KK. 2009. Growth hormone receptor modulators. *Rev Endocr Metab Disord* **10:** 145–156. doi:10.1007/s11154-008-9089-x

Brun VH, Ytterbø K, Morris RG, Moser MB, Moser EI. 2001. Retrograde amnesia for spatial memory induced by NMDA receptor-mediated long-term potentiation. *J Neurosci* **21:** 356–362. doi:10.1523/JNEUROSCI.21-01-00356.2001

Burton KA, Kabigting EB, Clifton DK, Steiner RA. 1992. Growth hormone receptor messenger ribonucleic acid distribution in the adult male rat brain and its colocalization in hypothalamic somatostatin neurons. *Endocrinology* **131:** 958–963. doi:10.1210/endo.131.2.1353444

Chen WY, Wight DC, Wagner TE, Kopchick JJ. 1990. Expression of a mutated bovine growth hormone gene suppresses growth of transgenic mice. *Proc Natl Acad Sci* **87:** 5061–5065. doi:10.1073/pnas.87.13.5061

Chen WY, Wight DC, Mehta BV, Wagner TE, Kopchick JJ. 1991. Glycine 119 of bovine growth hormone is critical for growth-promoting activity. *Mol Endocrinol* **5:** 1845–1852. doi:10.1210/mend-5-12-1845

Chen DY, Stern SA, Garcia-Osta A, Saunier-Rebori B, Pollonini G, Bambah-Mukku D, Blitzer RD, Alberini CM. 2011. A critical role for IGF-II in memory consolidation and enhancement. *Nature* **469:** 491–497. doi:10.1038/nature09667

Cobb S, Lawrence JJ. 2010. Neuromodulation of hippocampal cells and circuits. In *Hippocampal microcircuits* (ed. Vassils Cutsurdis BG, Cobb S, Vida I), pp. 617. Springer, New York, USA.

Deijen JB, de Boer H, van der Veen EA. 1998. Cognitive changes during growth hormone replacement in adult men. *Psychoneuroendocrinology* **23:** 45–55. doi:10.1016/S0306-4530(97)00092-9

Diano S, Farr SA, Benoit SC, McNay EC, da Silva I, Horvath B, Gaskin FS, Nonaka N, Jaeger LB, Banks WA, et al. 2006. Ghrelin controls hippocampal spine synapse density and memory performance. *Nat Neurosci* **9:** 381–388. doi:10.1038/nn1656

Dix SL, Aggleton JP. 1999. Extending the spontaneous preference test of recognition: evidence of object-location and object-context recognition. *Behav Brain Res* **99:** 191–200. doi:10.1016/S0166-4328(98)00079-5

Donahue CP, Kosik KS, Shors TJ. 2006. Growth hormone is produced within the hippocampus where it responds to age, sex, and stress. *Proc Natl Acad Sci* **103:** 6031–6036. doi:10.1073/pnas.0507776103

Eichenbaum H. 2017. The role of the hippocampus in navigation is memory. *J Neurophysiol* **117:** 1785–1796. doi:10.1152/jn.00005.2017

Enhamre E, Carlsson A, Grönbladh A, Watanabe H, Hallberg M, Nyberg F. 2012. The expression of growth hormone receptor gene transcript in the prefrontal cortex is affected in male mice with diabetes-induced learning impairments. *Neurosci Lett* **523:** 82–86. doi:10.1016/j.neulet.2012.06.050

Furigo IC, Metzger M, Teixeira PD, Soares CR, Donato J Jr. 2017. Distribution of growth hormone-responsive cells in the mouse brain. *Brain Struct Funct* **222:** 341–363. doi:10.1007/s00429-016-1221-1

Gisabella B, Farah S, Peng X, Burgos-Robles A, Lim SH, Goosens KA. 2016. Growth hormone biases amygdala network activation after fear learning. *Transl Psychiatry* **6:** e960. doi:10.1038/tp.2016.203

Grönbladh A, Johansson J, Nöstl A, Nyberg F, Hallberg M. 2013. GH improves spatial memory and reverses certain anabolic androgenic steroid-induced effects in intact rats. *J Endocrinol* **216:** 31–41. doi:10.1530/JOE-12-0315

Kim E, Grover LM, Bertolotti D, Green TL. 2010. Growth hormone rescues hippocampal synaptic function after sleep deprivation. *Am J Physiol Regul Integr Comp Physiol* **298:** R1588–R1596. doi:10.1152/ajpregu.00580.2009

Kwak MJ, Park HJ, Nam MH, Kwon OS, Park SY, Lee SY, Kim MJ, Kim SJ, Paik KH, Jin DK. 2009. Comparative study of the effects of different growth hormone doses on growth and spatial performance of

hypophysectomized rats. *J Korean Med Sci* **24:** 729–736. doi:10.3346/jkms.2009.24.4.729
Lai Z, Roos P, Zhai O, Olsson Y, Fhölenhag K, Larsson C, Nyberg F. 1993. Age-related reduction of human growth hormone-binding sites in the human brain. *Brain Res* **621:** 260–266. doi:10.1016/0006-8993(93)90114-3
Larkin MC, Lykken C, Tye LD, Wickelgren JG, Frank LM. 2014. Hippocampal output area CA1 broadcasts a generalized novelty signal during an object-place recognition task. *Hippocampus* **24:** 773–783. doi:10.1002/hipo.22268
Le Greves M, Steensland P, Le Greves P, Nyberg F. 2002. Growth hormone induces age-dependent alteration in the expression of hippocampal growth hormone receptor and N-methyl-D-aspartate receptor subunits gene transcripts in male rats. *Proc Natl Acad Sci* **99:** 7119–7123. doi:10.1073/pnas.092135399
Le Grevès M, Zhou Q, Berg M, Le Grevès P, Fhölenhag K, Meyerson B, Nyberg F. 2006. Growth hormone replacement in hypophysectomized rats affects spatial performance and hippocampal levels of NMDA receptor subunit and PSD-95 gene transcript levels. *Exp Brain Res* **173:** 267–273. doi:10.1007/s00221-006-0438-2
Leutgeb JK, Leutgeb S, Moser MB, Moser EI. 2007. Pattern separation in the dentate gyrus and CA3 of the hippocampus. *Science* **315:** 961–966. doi:10.1126/science.1135801
Li E, Kim DH, Cai M, Lee S, Kim Y, Lim E, Hoon Ryu J, Unterman TG, Park S. 2011. Hippocampus-dependent spatial learning and memory are impaired in growth hormone-deficient spontaneous dwarf rats. *Endocr J* **58:** 257–267. doi:10.1507/endocrj.K11E-006
Lobie PE, García-Aragón J, Lincoln DT, Barnard R, Wilcox JN, Waters MJ. 1993. Localization and ontogeny of growth hormone receptor gene expression in the central nervous system. *Brain Res Dev Brain Res* **74:** 225–233. doi:10.1016/0165-3806(93)90008-X
Lobie PE, Zhu T, Graichen R, Goh EL. 2000. Growth hormone, insulin-like growth factor I and the CNS: localization, function and mechanism of action. *Growth Horm IGF Res* **10:** S51–S56. doi:10.1016/S1096-6374(00)80010-6
Mahmoud GS, Grover LM. 2006. Growth hormone enhances excitatory synaptic transmission in area CA1 of rat hippocampus. *J Neurophysiol* **95:** 2962–2974. doi:10.1152/jn.00947.2005
Maruff P, Falleti M. 2005. Cognitive function in growth hormone deficiency and growth hormone replacement. *Horm Res* **64:** 100–108. doi:10.1159/000089325
Matsuzaki M. 2007. Factors critical for the plasticity of dendritic spines and memory storage. *Neurosci Res* **57:** 1–9. doi:10.1016/j.neures.2006.09.017
Megias M, Emri Z, Freund TF, Gulyás AI. 2001. Total number and distribution of inhibitory and excitatory synapses on hippocampal CA1 pyramidal cells. *Neuroscience* **102:** 527–540. doi:10.1016/s0306-4522(00)00496-6
Meyer RM, Burgos-Robles A, Liu E, Correia SS, Goosens KA. 2014. A ghrelin-growth hormone axis drives stress-induced vulnerability to enhanced fear. *Mol Psychiatry* **19:** 1284–1294. doi:10.1038/mp.2013.135
Molina DP, Ariwodola OJ, Linville C, Sonntag WE, Weiner JL, Brunso-Bechtold JK, Adams MM. 2012. Growth hormone modulates hippocampal excitatory synaptic transmission and plasticity in old rats. *Neurobiol Aging* **33:** 1938–1949. doi:10.1016/j.neurobiolaging.2011.09.014
Molina DP, Ariwodola OJ, Weiner JL, Brunso-Bechtold JK, Adams MM. 2013. Growth hormone and insulin-like growth factor-I alter hippocampal excitatory synaptic transmission in young and old rats. *Age (Dordr)* **35:** 1575–1587. doi:10.1007/s11357-012-9460-4
Morris RG, Garrud P, Rawlins JN, O'Keefe J. 1982. Place navigation impaired in rats with hippocampal lesions. *Nature* **297:** 681–683. doi:10.1038/297681a0
Moser MB, Trommald M, Andersen P. 1994. An increase in dendritic spine density on hippocampal CA1 pyramidal cells following spatial learning in adult rats suggests the formation of new synapses. *Proc Natl Acad Sci* **91:** 12673–12675. doi:10.1073/pnas.91.26.12673
Nakazawa K, McHugh TJ, Wilson MA, Tonegawa S. 2004. NMDA receptors, place cells and hippocampal spatial memory. *Nat Rev Neurosci* **5:** 361–372. doi:10.1038/nrn1385
Nieves-Martinez E, Sonntag WE, Wilson A, Donahue A, Molina DP, Brunso-Bechtold J, Nicolle MM. 2010. Early-onset GH deficiency results in spatial memory impairment in mid-life and is prevented by GH supplementation. *J Endocrinol* **204:** 31–36. doi:10.1677/JOE-09-0323
Nyberg F. 2000. Growth hormone in the brain: characteristics of specific brain targets for the hormone and their functional significance. *Front Neuroendocrinol* **21:** 330–348. doi:10.1006/frne.2000.0200
Nyberg F, Hallberg M. 2013. Growth hormone and cognitive function. *Nat Rev Endocrinol* **9:** 357–365. doi:10.1038/nrendo.2013.78
Ozcan AS. 2017. Filopodia: a rapid structural plasticity substrate for fast learning. *Front Synaptic Neurosci* **9:** 12. doi:10.3389/fnsyn.2017.00012
Palacios-Filardo J, Mellor JR. 2018. Neuromodulation of hippocampal long-term synaptic plasticity. *Curr Opin Neurobiol* **54:** 37–43. doi:10.1016/j.conb.2018.08.009
Pan W, Yu Y, Cain CM, Nyberg F, Couraud PO, Kastin AJ. 2005. Permeation of growth hormone across the blood-brain barrier. *Endocrinology* **146:** 4898–4904. doi:10.1210/en.2005-0587
Pascual-Lucas M, Viana da Silva S, Di Scala M, Garcia-Barroso C, González-Aseguinolaza G, Mulle C, Alberini CM, Cuadrado-Tejedor M, Garcia-Osta A. 2014. Insulin-like growth factor 2 reverses memory and synaptic deficits in APP transgenic mice. *EMBO Mol Med* **6:** 1246–1262. doi:10.15252/emmm.201404228
Ramis M, Sarubbo F, Sola J, Aparicio S, Garau C, Miralles A, Esteban S. 2013. Cognitive improvement by acute growth hormone is mediated by NMDA and AMPA receptors and MEK pathway. *Prog Neuropsychopharmacol Biol Psychiatry* **45:** 11–20. doi:10.1016/j.pnpbp.2013.04.005
Richards BA, Frankland PW. 2017. The persistence and transience of memory. *Neuron* **94:** 1071–1084. doi:10.1016/j.neuron.2017.04.037
Sathiavageeswaran M, Burman P, Lawrence D, Harris AG, Falleti MG, Maruff P, Wass J. 2007. Effects of GH on cognitive function in elderly patients with adult-onset GH deficiency: a placebo-controlled 12-month study. *Eur J Endocrinol* **156:** 439–447. doi:10.1530/eje.1.02346
Schneider-Rivas S, Rivas-Arancibia S, Vazquez-Pereyra F, Vázquez-Sandoval R, Borgonio-Pérez G. 1995. Modulation of long-term memory and extinction responses induced by growth hormone (GH) and growth hormone releasing hormone (GHRH) in rats. *Life Sci* **56:** PL433–PL441. doi:10.1016/0024-3205(95)00171-2
Shimizu E, Tang YP, Rampon C, Tsien JZ. 2000. NMDA receptor-dependent synaptic reinforcement as a crucial process for memory consolidation. *Science* **290:** 1170–1174. doi:10.1126/science.290.5494.1170
Sonntag WE, Csiszar A, deCabo R, Ferrucci L, Ungvari Z. 2012. Diverse roles of growth hormone and insulin-like growth factor-1 in mammalian aging: progress and controversies. *J Gerontol A Biol Sci Med Sci* **67:** 587–598. doi:10.1093/gerona/gls115
Studzinski AL, Barros DM, Marins LF. 2015. Growth hormone (GH) increases cognition and expression of ionotropic glutamate receptors (AMPA and NMDA) in transgenic zebrafish (Danio rerio). *Behav Brain Res* **294:** 36–42. doi:10.1016/j.bbr.2015.07.054
Sun LY, Bartke A. 2014. Tissue-Specific GHR Knockout Mice: metabolic Phenotypes. *Front Endocrinol (Lausanne)* **5:** 243. doi:10.3389/fendo.2014.00243
Sun LY, Al-Regaiey K, Masternak MM, Wang J, Bartke A. 2005. Local expression of GH and IGF-1 in the hippocampus of GH-deficient long-lived mice. *Neurobiol Aging* **26:** 929–937. doi:10.1016/j.neurobiolaging.2004.07.010
Toogood AA, Shalet SM. 1998. Ageing and growth hormone status. *Baillieres Clin Endocrinol Metab* **12:** 281–296. doi:10.1016/S0950-351X(98)80023-2
Vander Weele CM, Saenz C, Yao J, Correia SS, Goosens KA. 2013. Restoration of hippocampal growth hormone reverses stress-induced hippocampal impairment. *Front Behav Neurosci* **7:** 66. doi:10.3389/fnbeh.2013.00066
von Bohlen Und Halbach O. 2009. Structure and function of dendritic spines within the hippocampus. *Ann Anat* **191:** 518–531. doi:10.1016/j.aanat.2009.08.006
Warburton EC, Barker GR, Brown MW. 2013. Investigations into the involvement of NMDA mechanisms in recognition memory. *Neuropharmacology* **74:** 41–47. doi:10.1016/j.neuropharm.2013.04.013
Xu T, Yu X, Perlik AJ, Tobin WF, Zweig JA, Tennant K, Jones T, Zuo Y. 2009. Rapid formation and selective stabilization of synapses for enduring motor memories. *Nature* **462:** 915–919. doi:10.1038/nature08389
Zhao Z, Liu H, Xiao K, Yu M, Cui L, Zhu Q, Zhao R, Li GD, Zhou Y. 2014. Ghrelin administration enhances neurogenesis but impairs spatial learning and memory in adult mice. *Neuroscience* **257:** 175–185. doi:10.1016/j.neuroscience.2013.10.063

Received June 28, 2019; accepted in revised form October 29, 2019.

Hippocampal growth hormone modulates relational memory and the dendritic spine density in CA1

Kamilla G. Haugland, Anniken Olberg, Andreas Lande, et al.

Learn. Mem. 2020, **27:**
Access the most recent version at doi:10.1101/lm.050229.119

A

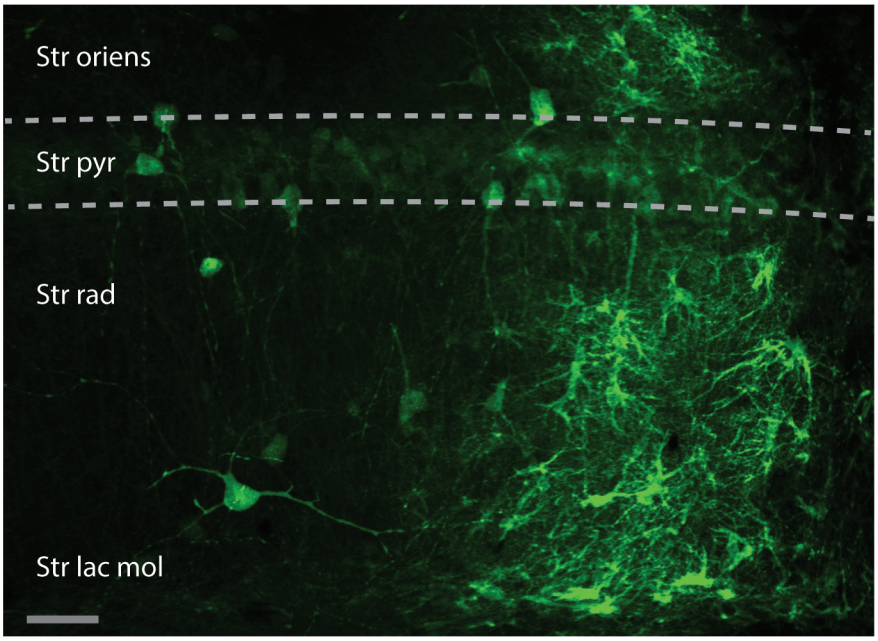

Supplementary Figure 1: Recombinant adeno-associated viruses (rAAVs) transfected also non-pyramidal cells. A) In addition to pyramidal cells, non-pyramidal cells were labeled in close proximity to the viral injections in CA1. The dotted line represents the pyramidal layer. Non-pyramidal cells were labeled above the pyramidal layer, in stratum oriens, and below in stratum radiatum and stratum lacunosum-moleculare. Scale bar 50 µm.

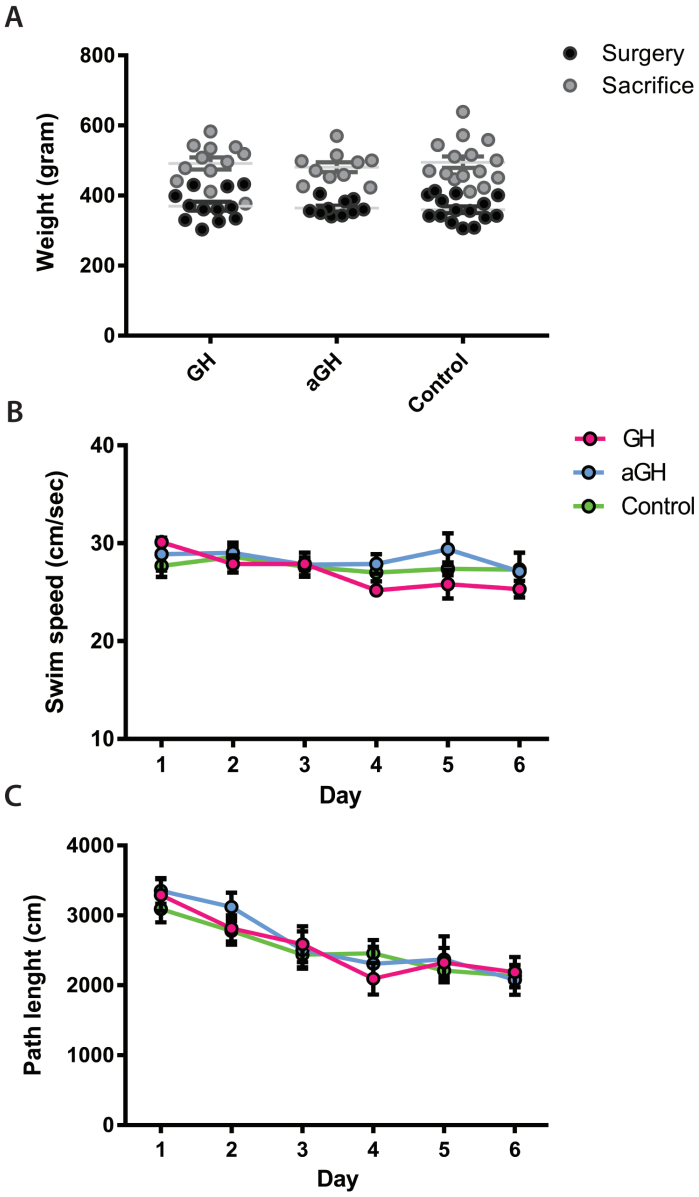

Supplementary Figure 2: The growth hormone (GH) manipulations did not affect the weight of the animals, nor swim speed or path length in the water maze. A) Weights of all animals before surgery (black) and at the day of sacrifice (grey). Each dot represents an individual value. The mean value is indicated in light grey lines. Dark grey lines indicate SEM. B) Swim speed in the water maze on day 1 to 6 revealed no differences between the groups. Mean values for the GH group (pink), the antagonizing GH (aGH) group (blue), and the control group (green). Black lines indicate SEM. C) Path length in the water maze during acquisition showed no significant differences between the groups.

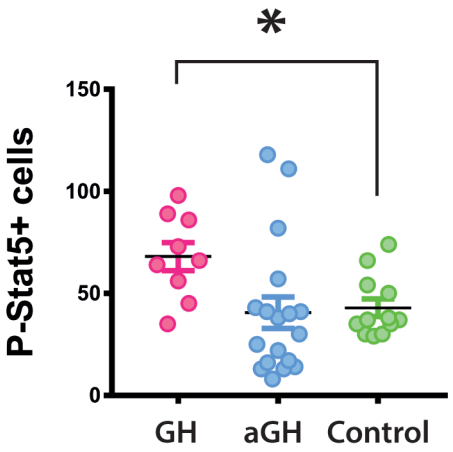

Supplementary Figure 3: Quantification of activated growth hormone receptors by p-Stat5 in pilot experiments in rats receiving five-fold higher virus titers. As for the standard dose used in all other presented data, rats treated with AAV expressing growth hormone (GH) had more p-Stat5 positive DAPI cells (ANOVA $F(2,36) = 3.68$, $p = 0.035$, t-test $p = 0.02$), but the antagonizing GH (aGH) group did not show a significant decrease. Count numbers are not directly comparable to Figure 2E as a smaller counting window was used.

All statistics for manuscript Haugland et al. 2019

Figure no	Test used	Page	n		df	p-value
			exact number	defined as		
p-Stat5						
2E	One-way ANOVA of number of p-Stat5 positive DAPI celles	5	15,12,12	cells	F(2,36) = 6.34	**0.004**
	Bonferroni's comparison between GH and control	5	15,12	cells	t(36) = 2.59	**0.013 (1-tailed)**
	Bonferroni's comparison between aGH and control	5	12,12	cells	t(36) = 0.70	0.48 (1-tailed)
Suppl 3	One-way ANOVA of number of p-Stat5 positive DAPI celles	5	9,18,12	cells	F(2.36) = 3.68	**0.035**
	Bonferroni's comparison between GH and control	5	9,18	cells	t(36) = 2.61	**0.020 (1-tailed)**
	Bonferroni's comparison between aGH and control	5	18,12	cells	t(36) = 0.25	0.49 (1-tailed)
SPINE DENSITY STATISTICS					All t values are absolute values	
3C	Jonckheere-Terpstra Test neuron level	6	22, 8, 15	neurons	JT = 530	**<0.001**
	Mann-Whitney U aGH vs control	6	22, 8	neurons	Z = 1.92	**0.03 (1-tailed)**
	Mann-Whitney U control vs GH	6	8, 15	neurons	Z = 2.58	**0.005 (1-tailed)**
	Jonckheere-Terpstra Test animal level	6	4, 3, 3	rats	JT= 32	**0.003**
3D	One-way ANOVA, percentage of filopodial-like spines	6	22, 8, 15	neurons	F(2,42) = 0.79	0.46
	One-way ANOVA, percentage of immature spines	6	22, 8, 15	neurons	F(2,42) = 23.7	**<0.001**
	Post-hoc contrast t-test GH vs control	6	8, 15	neurons	t (42) = 6.36	**0.036 (1-tailed)**
	Post-hoc contrast t-test aGH vs control	6	22, 8	neurons	t (42) = 11.4	**<0.001 (1-tailed)**
3D	One-way ANOVA, percentage of mature spines	6	22, 8, 15	neurons	F(2,42) = 21.3	**<0.001**
	Post-hoc contrast t-test GH vs control	6	8, 15	neurons	t (42) = 11.84	**0.003 (1-tailed)**
	Post-hoc contrast t-test aGH vs control	6	22, 8	neurons	t (42) = 8.12	**0.019 (1-tailed)**
WATER MAZE STATISTICS						
	No difference between merged control groups in water maze	7				
	Two-way ANOVA Zone x Group interaction Day 6	7	7, 6	rats in each group	F(3,33) = 0.24	0.87
	Two-way ANOVA Zone x Group interaction Day 12	7	7, 6	rats in each group	F(3,33) = 0.50	0.68
	Two-way ANOVA Zone x Group interaction Day 13	7	7, 6	rats in each group	F(3,33) = 1.64	0.20
	Two-way ANOVA Zone x Group interaction Day 14	7	7, 6	rats in each group	F(3,33) = 0.24	0.87
4A	Repeated measures ANOVA effect of Day 1-5	7	13, 8, 8	rats in each group	F(4,104) = 40.97	**<0.001**
4A	Repeated measures ANOVA Day x Group interaction Day 1-5	7	13, 8, 8	rats in each group	F(8, 104) = 1.76	0.094
4A	One-way ANOVA Latency Day 1	7	13, 8, 8	rats in each group	F(2,26) = 1.42	0.260
4B	Two-way ANOVA effect of SW target Zone	7	13, 8, 8	rats in each group	F(3,78) = 29.11	**<0.001**
4B	Two-way ANOVA SW Zone x Group interaction	7	13, 8, 8	rats in each group	F(6,78) = 3.59	**0.003**
4B	One-way ANOVA of time in SW zone	7	13, 8, 8	rats in each group	F(2,26)=4.61	**0.019**
4B	Post-hoc orthogonal comparison GH vs control	7	8, 13	rats in each group	t(26) = 0.34	0.370 (1-tailed)
4B	Post-hoc orthogonal comparison aGH vs other two groups	7	8, 21	rats in each group	t(26)=2.95	**0.004 (1-tailed)**
4D	Repeated measures ANOVA effect of Day 12-13	7	13, 8, 7	rats in each group	F(1,25) = 10.80	**0.003**
4D	Repeated measures ANOVA Day x Group interaction Day 12-13	7	13, 8, 7	rats in each group	F(2,25) = 1.30	0.291
4E	Two-way ANOVA effect of Zone	7	13, 8, 8	rats in each group	F(3,78) = 10.92	**<0.001**
4E	Two-way ANOVA Zone x Group interaction	7	13, 8, 8	rats in each group	F(6,78) = 0.48	0.82
4E	One-way ANOVA, only time in platform zone (south west)	7	13, 8, 8	rats in each group	F(2,26) = 0.28	0.76
4F	Two-way ANOVA effect of Zone	7-8	13, 8, 8	rats in each group	F(3,78) = 8.74	**<0.001**
4F	Two-way ANOVA Zone x Group interaction	7-8	13, 8, 8	rats in each group	F(6,78) = 2.54	**0.027**
4F	One-way ANOVA of time in old platform zone (south west)	7-8	13, 8, 8	rats in each group	F(2,26) = 1.96	0.162
4F	One-way ANOVA of time in new platform zone (north east)	7-8	13, 8, 8	rats in each group	F(2,26) = 3.64	**0.041**
4F	Post-hoc orthogonal comparison GH vs control (north east)	7-8	8, 13	rats in each group	t(26)=0.50	0.310 (1-tailed)
4F	Post-hoc orthogonal comparison aGH vs other two groups (north east)	7-8	8, 21	rats in each group	t(26)=2.69	**0.006 (1-tailed)**
4G	Two-way ANOVA effect of Zone	8	13, 8, 8	rats in each group	F(3,75) = 22.98	**<0.001**
4G	Two-way ANOVA Zone x Group interaction	8	13, 8, 8	rats in each group	F(3,75) = 1.25	0.292
SPONTANEOUS LOCATION RECOGNITION (SLR) STATISTICS						
	Comparison between unoperated and AAV controls before groups were merged					
	Student's t test of discrimination ratio, condition: square arena & 3 hours	8	6, 6	rats in each group	t(10) = 0.21	0.84 (2-tailed)
	Student's t test of discrimination ratio, condition: square arena & 24 hours	8	6, 7	rats in each group	t(11) = 0.36	0.73 (2-tailed)
	Student's t test of discrimination ratio, condition: circular arena & 3 hours (no unoperated controls for condition circular arena & 24 hours)	8	5, 6	rats in each group	t(9) = 0.21	0.84 (2-tailed)
5B	**Condition square arena, 3 hours delay**					
	Paired samples t-test, time with novel and familiar obj, GH group	9	8	rats in each group	t(7) = 3.78	**0.004 (1-tailed)**
	Paired samples t-test, time with novel and familiar obj, aGH group	9	8	rats in each group	t(7) = 3.41	**0.006 (1-tailed)**
	Paired samples t-test, time with novel and familiar obj, control group	9	12	rats in each group	t(11) = 2.50	**0.015 (1-tailed)**
	One-way ANOVA of discrimination ratio	9	8, 8, 12	rats in each group	F(2,25) = 1.16	0.330
5C	**Condition square arena, 24 hours delay**					
	Paired samples t-test, time with novel and familiar obj, GH group	9	8	rats in each group	t(7) = 2.56	**0.019 (1-tailed)**
	Paired samples t-test, time with novel and familiar obj, aGH group	9	8	rats in each group	t(7) = 1.23	0.129 (1-tailed)
	Paired samples t-test, time with novel and familiar obj, control group	9	13	rats in each group	t(12) = 0.01	0.496 (1-tailed)
	One-way ANOVA of discrimination ratio (DR)	9	8, 8, 13	rats in each group	F(2,26) = 3.36	**0.050**
	Post-hoc orthogonal comparison of DR, aGH vs control group	9	8, 13	rats in each group	t(26) = 0.12	0.878 (2-tailed)
	Post-hoc orthogonal comparison of DR, GH vs the other two groups	9	8, 8, 13	rats in each group	t(26) = 2.59	**0.016 (2-tailed)**
5E	**Condition circular arena, 3 hours delay**					
	Paired samples t-test, time with novel and familiar obj, GH group	10	8	rats in each group	t(7) = 1.27	0.123 (1-tailed)
	Paired samples t-test, time with novel and familiar obj, aGH group	10	8	rats in each group	t(7) = 0.30	0.378 (1-tailed)
	Paired samples t-test, time with novel and familiar obj, control group	10	13	rats in each group	t(12) = 0.04	0.483 (1-tailed)
	One-way ANOVA of discrimination ratio (DR)	10	8, 8, 13	rats in each group	F(2,26) = 0.70	0.507

5F	**Condition circular arena, 24 hours delay**					
	Paired samples t-test, time with novel and familiar obj, GH group	10	8	rats in each group	t(7) = 1.69	0.068 (1-tailed)
	Paired samples t-test, time with novel and familiar obj, aGH group	10	8	rats in each group	t(7) = 0.20	0.423 (1-tailed)
	Paired samples t-test, time with novel and familiar obj, control group	10	6	rats in each group	t(5) = 0.16	0.439 (1-tailed)
	One-way ANOVA of discrimination ratio (DR)	10	8, 8, 6	rats in each group	F(2,19) = 0.43	0.659
6C	One-way ANOVA of exploration time in all four corners sample phase before 3 h dela	8	16, 16, 13, 13	object corners	F(3,54) = 0.64	0.592
no figure	One-way ANOVA of exploration time in all four corners sample phase before 24 h de	8	14, 14, 15, 15	object corners	F(3,54) = 1.18	0.328
6E	Two-way ANOVA of exploration time, Effect of Obj location, before 3 h delay	9	8, 8, 13	rats in each group	F(1,26) = 0.04	0.852
	Two-way ANOVA of exploration time, Group X Obj location interaction, before 3 h de	9	8, 8, 13	rats in each group	F(2,26) = 0.68	0.516
6F	Two-way ANOVA of exploration time, Effect of Obj location, before 24 h delay	9	8, 8, 13	rats in each group	F(1,26) = 0.06	0.813
	Two-way ANOVA of exploration time, Group X Obj location interaction, before 24 h c	9	8, 8, 13	rats in each group	F(2,26) = 1.84	0.178
6H	Two-way ANOVA of exploration time, Effect of Obj location, before 3 h delay	9	8, 8, 13	rats in each group	F(2,52) = 0.60	0.552
	Two-way ANOVA of exploration time, Group X Obj location interaction, before 3 h de	9	8, 8, 13	rats in each group	F(4,52) = 0.32	0.822
6I	Two-way ANOVA of exploration time, Effect of Obj location, before 24 h delay	9	8, 8, 6	rats in each group	F(2,38) = 0.57	0.570
	Two-way ANOVA of exploration time, Group X Obj location interaction, before 24 h c	9	8, 8, 6	rats in each group	F(4,38) = 1.05	0.385

OTHER						
Suppl 2A	Repeated measures ANOVA Weight X Group interaction	7	15,12,10	rats	F(2,34) = 0.67	0.519
Suppl 2B	Two-way ANOVA Swim speed X Group interaction	7	13,7,7	rats	F(5,120) = 1.07	0.387
Suppl 2C	Two-way ANOVA Path length X Group interaction	7	13,7,7	rats	F(5,120) = 0.43	0.929

Paper 3

Haugland, K.G, Knutsen, E., Kjelstrup, K.B., Brun, V.H.

Growth hormone modulates remapping in the hippocampal area CA1

Manuscript

Growth hormone modulates remapping in the hippocampal area CA1

Kamilla G. Haugland[1], Erik Kutsen[2], Kirsten B. Kjelstrup[1,3] and Vegard H. Brun[1,3]

[1] Department of Clinical Medicine, UiT – The Arctic University of Norway, 9019 Tromsø, Norway

[2] Department of Medical Biology, UiT – The Arctic University of Norway, 9019 Tromsø, Norway

[3] University Hospital of North Norway, 9019 Tromsø, Norway

Abstract

Growth hormone is a neuromodulator that can bind to receptors in the hippocampus and alter the synaptic plasticity. Decline in GH levels is associated with normal ageing, stress and disease, and mechanisms are proposed to involve the hippocampal circuit. To see how GH affects the neural code, we recorded single cells in the hippocampal area CA1 in male Long Evans rats with locally altered GH levels. The rats received injections of adeno-associated viruses to make the cells overexpress either GH or an antagonizing mutated GH (aGH). Place cells were recorded in both familiar and novel environments to allow the assessment of pattern separation in the neural representations, termed remapping. All the animals showed intact and stable place fields in the familiar environment. In the novel environment, the aGH treated animals had increased average firing rate, peak rate and information density, and reduced field size and sparseness. GH treated animals displayed more global remapping than controls when introduced to the novel environment. Only cells of control animals showed significant rate changes. Our results suggest that GH increases hippocampal sensitivity to novel information as their firing fields remapped more than controls. The increase in firing rate of aGH animals could reflect a compensatory mechanism of the network or lack of inhibition. Our findings confirm that GH is a significant neuromodulator in the hippocampus, affecting how place cells represent the environment. These results can have implications for understanding the mechanisms behind the reduced memory processes seen in GH-deficiency and normal ageing.

Introduction

The hippocampus has an enormous storage capacity with neural activity that represent previous experiences (Moser et al., 2015, Shapiro, 2001, Lisman et al., 2017, Eichenbaum, 2017, Colgin, 2020). The place cells of the hippocampus fire in a location-specific manner (O'Keefe and Dostrovsky, 1971), representing both spatial information (place field) and the current configuration of sensory input and internal state (firing rate). As the firing patterns of the place cells are flexible (Cobar et al., 2017), the cell activity can easily be adjusted to changes in the animal's experience (Cohen et al., 2017). A common approach to investigate the plasticity of place cells is therefore to record the neural activity when the animal is exploring different environments (Muller and Kubie, 1987, Thompson and Best, 1989, Leutgeb et al., 2005, Alme et al., 2014, Leutgeb et al., 2004). Place cells with a particular firing pattern in one environment may change the firing properties when the animal explores another environment, or significant parts of the environment is exchanged, a phenomenon known as remapping (Latuske et al., 2017, Colgin et al., 2008). The type of remapping with the greatest change in neural activity is referred to as global remapping (Muller and Kubie, 1987, Leutgeb et al., 2004, Leutgeb et al., 2005, O'Neill et al., 2008). In global remapping, the cell ensembles reorganize orthogonally, and such events are commonly observed when the animal visits a novel room. Another version of remapping is rate remapping, in which the place fields remain in the same location but the firing rates change (Allen et al., 2012, Ainge et al., 2012, Wood et al., 2000). This rate modulation is suggested to depend on nonspatial variables and is apparent with more subtle spatial changes, like when the animal explores a novel apparatus in a familiar room. Despite CA3 represent more pronounced changes in firing rate after changes in the shape of apparatus, also CA1 exhibit rate differences in similar conditions (Leutgeb et al., 2005). Rate remapping in CA1 is associated with on task demands (Sanders et al., 2019).

Although studies have described various types of remapping events as direct responses to changes in sensory information, remapping may also be dependent on the intrinsic plasticity of the hippocampus (Cobar et al., 2017). In such way, the plasticity of place cells could reflect the animals' awareness of changes in the environments. The activity of the place cells is especially sensitive to local modulation by neuromodulators (Atherton et al., 2015, Teles-Grilo Ruivo and Mellor, 2013, Brandon et al., 2014, Tran et al., 2008, Kentros et al., 2004). Neuromodulators primarily alter the dynamics of excitatory and inhibitory synaptic transmission, modifying synaptic processes and changing the resting membrane potential

(Edelmann et al., 2017, Palacios-Filardo and Mellor, 2019). Growth hormone (GH) is a local neuropeptide expressed in hippocampus with the ability to increases the spine density in CA1, as well as to enhance memory performance (Haugland et al., 2020). However, it remains unknown whether this increase in hippocampal plasticity affects the information processes displayed by changes in place cell firing. By using recombinant adeno-associated viruses (rAAV)s we can overexpress GH or an antagonist of GH receptor (aGH) to locally manipulate the levels of GH in the hippocampus. In this study we investigate how GH or the aGH affects hippocampal place cell firing when the animal explores a novel environment.

Methods

Subjects

In total, 23 male Long Evans rats (350 - 400 g at surgery) were housed in single cages after implantation, in a humidity and temperature-controlled environment. All animals were kept at 90 - 100% of free-feeding body weight and maintained on a 12-h light/ 12-h dark schedule. 12 animals were used for single-unit recordings while 11 were used to RT-qPCR. Single-unit recordings were conducted in the dark phase. The experiments were performed in accordance with the Norwegian Animal Welfare Act and the European Convention for the Protection of Vertebrate Animals used for the Experimental and Other Scientific Purposes.

Viruses

We provide a brief description of the viruses used in this study as this method is described in detail (Haugland et al., 2020). Three recombinant adeno-associated viruses (rAAVs) 1/2 chimeric pseudotypes (kindly provided by Ki Ann Goosens, MIT) were used to either overexpress GH and GFP, mutated antagonizing GH (aGH) and green fluorescent protein (GFP), or GFP only. The expression sequences were rAAV-CMV-GH-IRES-GFP, rAAV-CMV-aGH-IRES-GFP, or rAAV-CMV-IRES-GFP. Animals were randomly assigned to receive the different viruses and successful single unit recordings were made in 12 animals (GH: n = 3, aGH: n = 4, control: n = 5), while 11 animals were used for RT-qPCR (GH: n = 4, aGH: n = 4, control: n = 3). The rAAV-GFP-GH was constructed with the *Gh* gene (GeneBank Accession number U62779.1). The rAAV-GFP-aGH contained a *Gh* gene with a single amino acid substitution (rGH-G144R) to produce a mutant GH protein with antagonist

activity on the GH receptor. This mutation is equivalent to human G120R, and therefore also described as the 120R mutation of the GH.

Stereotaxic surgery

The rats were anesthetized in an induction chamber with isoflurane for surgery, and received subcutaneous buprenorphine and meloxicam to minimize postoperative discomfort. When fully anesthetized, the skull was fixed in a Kopf stereotaxic frame. The depth of anesthesia was monitored by heart rate and oxygen saturation (Kent Scientific, Torrington, CT), as well as clinically by regular reflex testing and breathing monitoring. The local anesthetic bupivacaine was given subcutaneously, and the skin was disinfected with 70 % ethanol before incision. Holes in the skull were drilled at appropriate locations on each hemisphere. The viruses were injected with a sterile 2 µl Hamilton Syringe (Hamilton Company, Bonaduz, Switzerland). The animals received four injections of 0.4 µl virus solution (0.2 µl/min) in each hemisphere in the dorsal hippocampus according to the injection coordinates calculated anteroposteriorly (AP), mediolaterally (ML) from bregma and dorsoventrally (DV) from dura: AP -3.0 mm, ML ± 1.2 mm, DV 2.3 mm; AP -3.5 mm, ML ± 2.2 mm, DV 2.2 mm; AP -4.0 mm, ML ± 2.4 mm, DV 2.4 mm; AP -4.4 mm, ML ±3.5 mm, DV 2.8 mm. The needle was left at the site of injection for 5 min after each injection to allow diffusion of the virus before slow retraction. After the virus injections, one or two microdrives were implanted above hippocampal CA1 (AP -3.5, ML +- 3.3, DV -1.5) each with a bundle of four tetrodes. The implant was secured to the skull with dental cement and histoacryl and screws were attached to the skull. After surgery, the animals recovered in their home cage and were closely monitored for three days post-surgery.

Recording procedures

The local field potentials (LFP) were recorded using tetrodes attached to microdives (Axona Ltd). Tetrodes were constructed from four twisted 17-um polyamide-coated platinum-iridium (90-10 %) wires (California Fine Wire). Before implantation, the electrode tips were plated with platinum to reduce electrode impedance to between 120 and 220 kΩ at 1 kHz.

Data collection started 1 week after implantation of the tetrodes. Rats were connected to an Axona data acquisition system (Axona Ltd) via a wire connecting the microdrive to a pre-amplifier to digitize the signals at 24-bit resolution and 48 kHz sampling rate. The signals

were then amplified by a system unit, which also contained a video tracker. The weight of the cable to the preamp was counterbalanced by wires attached to the ceiling with a counterweight. The unit activity was amplified between 4,000 - 14,000 times and highpass filtered with 360 Hz cutoff and lowpass filtered at 7 kHZ. For the EEG, the signals were band-passed with a lowpass filter with 500 Hz cutoff with a 4800 Hz resolution. An overhead camera recorded the position of the light-emitting diode (LED) on the head stage of the microdrive. The tetrodes were lowered daily in steps of 50 um between sessions until the hippocampus was reached. Recording started when the tetrodes were in CA1 with putative principal cells and theta modulation was present in the EEG.

Behavioral procedures

After recovering from the surgeries, the rats were habituated to a square arena (100 cm x 100 cm with 50 cm high walls) to become a familiar to the environment (Figure 2A). A cue card centered on one of the walls was used as a local cue. Dark curtains covered parts of the recording arena with distance cues. The animals were trained daily to forage for crumbs of cookies. Before a trial session in the box, the animal rested on a pedestal in a small pot with a blanket and a warm heating bottle (named pot sessions). After trials, the animal was allowed back to the pot. The apparatus was cleaned between each trial. When the animals were familiar with the box (>5 days of experience) and place cells were well separable during offline analysis, the rats were introduced to a novel environment consisting of a novel circular apparatus in the same room with the same floor.

The standard trial sequence started with a pot session (5 min), followed by two sessions in the familiar box (10 min) separated by 10 min, before the last pot session (5 min). When a sufficient number of single-units were separable, the trial sequence included a novel circle (10 min) in between the familiar box trials. The circle arena remained novel during the experiments as each animal only visited the circle 1-3 times. Each trial was typically separated by a few minutes to allow cleaning of the arenas, and clustering and inspection of recorded cells by the experimenter.

Spike sorting and place fields

Spike sorting was performed offline using graphical cluster-cutting software (TINT, Axona). The spikes were manually clustered in 2D projections of the multidimensional parameter space (consisting of waveform amplitudes and waveform energy), using autocorrelation and

cross-correlation functions as additional separation criteria. The cluster separation was assessed by calculating distance between spikes of different cells in Mahalonobis space (isolation distance). Clusters that remained stable across recording trails were regarded as the same unit.

Putative excitatory cells were distinguished from putative interneurons based by the width of the extracellular action potential, firing pattern (complex spikes) and average rate. Only active place cells with an average firing rate of minimum 0.25 Hz in at least one of the sessions, were included in the analysis.

To characterize place fields, a spike density function was estimated by convolving the spike train (sum of Dirac delta functions) with a smoothing kernel (2 s Blackman window, normalised to unit gain at zero frequency). The spike density function was sampled synchronously with a position tracker. The rate map was calculated as a weighted mean of the sampled spike density function, with weights given by Euclidian distance and a 30 cm wide Blackman window. The rate map was calculated for pixels of 5 x 5 cm visited by the rat. Field size was defined as the size of the largest cluster of neighboring pixels with firing rate above 20 % of the peak rate. The percentage of bursting was calculated as the number of bursts divided by number of bursts plus the number of single spikes. The spatial information (bits/spike) was calculated as

$$I = \sum_{i=1}^{N} p_i \frac{\lambda_i}{\lambda} log_2 \frac{\lambda_i}{\lambda}$$

in which I is the information density, λ_i is the mean firing rate in the i-th bin, and λ is the overall mean firing rate. p_i is the probability of the animal being in the i-th bin, as previously described (Skaggs et al., 1996). The sparseness (S) was calculated by dividing the squire mean rate (λ^2) by the mean square rate over all pixels (Skaggs et al., 1996).

$$S = \frac{\lambda^2}{\sum_i^N p_i (\lambda_i)^2}$$

Spatial correlation was estimated as the first order spatial autocorrelation of the place field maps between sessions, and measures the extent to which the firing rate in a pixel is predicted by the rates of the neighboring pixels.

The rate overlap between two recording trials was estimated by dividing, for each cell, the average firing rate in the less active enclosure by the average firing rate in the more active arena. The ratios were averaged for all the cells active in the arenas. The resulting overlap scores would be equal to 1 if the average firing rates were equal, while the score would be towards 0 if the cell was only active in one environment. The rate change was calculated by the absolute change in average firing rate between the environments.

Histology

The rats were deeply anesthetized with isoflurane gas and given Buprenorphine (0.05 mg/kg) and a lethal dose of pentobarbital (100 mg/kg), before perfused intracardially with PBS and 4 % formaldehyde at 80 ml/min using a peristaltic pump (World Precision Instruments, Sarasota, FL. The brains were extracted and stored in 4 % formaldehyde at 4 C. Before sectioning, the brains were quickly frozen and placed on a cryostat. 40 μm coronal sections were cut on Leica CM1950 cryostat (Leica Biosystems, Wetzlar, Germany) and mounted on superfrost objectglass. The trace of the tetrodes and the viral expression were detected in the fluorescence microscope using Axio Zoom V.16 (Carl Zeiss).

RNA Isolation, cDNA Synthesis and RT-qPCR

Rat brains were homogenized in 1 ml TRI Reagent® (Zymo Research) using the Precellys tissue homogenizers (MagNA Lyser Green Beads with ceramic beads (Roche), 6000 rpm, 1 x 20 sec). Total RNA was isolated from homogenized brains using the Direct-zol RNA MiniPrep (Zymo Research) kit according to the manufacturer's recommendation. RNA concentration was measured by Qubit (Thermo Fisher Scientific). DNA contamination was removed using 0.5U DNase I (Ambion) following heat inactivation. cDNA synthesis of DNase treated total RNA was performed with SuperScript™ IV Reverse Transcriptase (ThermoFisher Scientific). 2.5 μM of random hexamer primer (ThermoFisher Scientific) and 500 ng of template were used for the reaction (10 μl total reaction volume). RNA was denaturated at 65ºC for 5 min, and cDNA was synthesized at 53ºC for 10 min. cDNA was diluted 1:10 in nuclease free H_2O.

For RT-qPCR, 2.5 µl cDNA was mixed with 5.0 µl FastStart Essential DNA Green Master (Roche Life Science) and 2.5 µl forward and reverse primer mix (1 µM each). All primer sequences are provided in Supplementary Table 1. The LightCycler® 96 was used for quantification, and expression of *Gh* is presented as $2^{-\Delta Cq}$ using the geometric mean of *Hprt, B2m,* and *Actb* as internal reference.

Table 1:

Gene	**Forward primer**	**Reverse primer**
Hprt	AGCAGACGTTCTAGTCCTGTG	CAAAAGGGACGCAGCAACAG
B2m	ACTGAATTCACACCCACCGA	TACATGTCTCGGTCCCAGGT
Actb	GCAGATGTGGATCAGCAAGC	GCAGCTCAGTAACAGTCCGC
Gh1	AATTGCTTCGCTTCTCGCTG	AGTTTCTCATAGACGCGGTCC

Sanger sequencing

For verification of expression of wild type and antagonist *Gh* mRNA, Sanger sequencing across the mutated region of *Gh* was performed. 1 µl cDNA was used as input in a 20 µl PCR reaction, using the PrimeSTAR GXL DNA Polymerase (TaKaRa) according to the manufactures recommendations. PCR primers used were: GAC AAA GTG TAG GGG TGG CA (forward) and TTC ATG ACC CGC AGG TAG GT (reverse). PCR reactions were run on a 1% agarose gel, and the PCR bands at 510 nt were cut out of the gel and purified using the QIAquick Gel Extraction Kit (Qiagen). Samples were sequenced at the DNA sequencing core facility UNN using the Applied Biosystems 3130xl Genetic Analyzers. For sequencing, the forward PCR primers was used.

Experimental Design and Statistical analysis

All of the data is presented as mean ± SEM. The data was tested for normal distribution using Shapiro-Wilk normality test. If the data passed the normality test, parametric tests (ANOVA and t-test) were used for statistical analysis, while the nonparametric tests (Kruskal-Wallis test and Whitney test) were used if the data were not normalized. The place cell firing were analyzed using MATLAB (Mathworks, Natick, MA). Statistical analysis and graphs was made using GraphPad Prism version 7.09 (GraphPad Software, La Jolla, CA) with $\alpha = .05$.

Results

A total of 12 rats were used in this study, all receiving both viral injections and microdrive implantations. The histology revealed that the tetrodes in all animals were lowered into the dorsal CA1, among transfected cells shown by the expression of GFP (Figure 1A and C). The overall *Gh* mRNA in the animals were quantified by RT-qPCR, which revealed significantly increased levels of *Gh* in the GH and aGH group compared to controls (Figure 1B; One-way ANOVA $F(2,8) = 7.774$, $p = 0.0113$; unpaired two-tailed t-test GH-control, $p = 0.0205$, unpaired two-tailed t-test aGH-control, $p = 0.0034$). Since the RT-qPCR test was sensitive to both the GH and aGH mRNA's, we further sequenced the mRNAs of GH vs aGH (Figure 1 D) to verify the G144R mutation in the aGH gene, suggested to prevent activation of GH receptor after binding of the aGH ligand.

Increased place cell firing after overexpression of growth hormone antagonist in familiar environment

We examined the hippocampal place cell activity by recording cells in different environments, including a familiar box and a novel circle, in the same room. A total 224 place cells were included in the following analyses (control: n = 71, aGH: n = 124, GH: n = 31).

We first investigated the impact of GH modulations on place cells in a familiar environment. Recordings in the familiar environment were divided into two 10 min sessions separated by 10 min (Figure 2B). All of the groups displayed place cells that were active in the familiar environments (Figure 2C). Spatial correlation confirmed stable place fields across the familiar box trials (Figure 3C; GH r = 0.58, aGH r = 0.58, control r = 0.53; Kruskal-Wallis test, $p = 0.9195$). The average firing rate did not differ between the groups (Figure 2D; Kruskal-Wallis test, $p = 0.7095$), nor did the information content (bits/spike; Figure 2I; Kruskal-Wallis test, $p = 0.1412$), Nevertheless, the aGH significantly increased the peak rate (Figure 2E; Kruskal-Wallis test, $p < 0.0001$, Mann-Whitney test aGH-control, $p < 0.0001$), as well as the bursting (Figure 2F; Kruskal-Wallis test, $p = 0.0012$; Mann-Whitney test aGH-control $p = 0.0014$). In addition, place cells of the aGH animals displayed smaller field size (Figure 2G; Kruskal-Wallis test, $p = 0.0494$; Mann-Whitney test aGH-control $p = 0.04555$), and a reduction in the place field sparseness (Figure 2H; Kruskal-Wallis test, $p = 0.0022$; Mann-Whitney test aGH-control $p = 0.0024$).

Growth hormone affects place cell representations in a novel environment

As GH alters hippocampal plasticity (Molina et al., 2012, Kim et al., 2010, Molina et al., 2013, Haugland et al., 2020), we wanted to investigate if GH could modulate the place cell activity during the first experience to a novel environment (Figure 3A). After exploration in the familiar environment (F), the rats were introduced to a novel circular environment in the same room (N), before going back to the familiar environment (F'). The spatial correlation was high between the sessions of the familiar environments and did not differ between the groups (Figure 3C). Interestingly, the place cells of the GH animals changed their place field locations in the novel environment compared to their place field representation in the familiar environment. None of the cells had a positive spatial correlation, with an average spatial correlation of r = -0.036. In contrast, both aGH and controls exhibited only a reduced spatial correlation (aGH r = 0.211, control r = 0.263), with a significant difference between GH and control (Figure 3B; Kruskal-Wallis test, $p = 0.0055$; Mann-Whitney test $p = 0.0012$).

Both the rate overlap (Figure 3D) and the rate change (Figure 3E) were significantly different in the control group (Figure 3D; Mann-Whitney test $p = 0.0258$; Mann-Whitney test $p = 0.0359$, respectively) when comparing the respective values in the familiar environment sessions (F-F') and the familiar-to-novel environment (F-N). The changes observed in rate overlap and rate change indicate that only controls displayed rate remapping in the novel environment.

In the novel environment, aGH had showed higher average firing rates compared to the controls (Figure 3F; Kruskal-Wallis test, $p = 0.0194$; Mann-Whitney test $p = 0.0146$). Also the peak firing rate (Figure 3G; Kruskal-Wallis test, $p < 0.0001$; Mann-Whitney test $p = 0.0007$) and information was higher in the aGH animals (Figure 3K; Kruskal-Wallis test, $p < 0.0001$; Mann-Whitney test $p < 0.0001$), while the field size and sparseness was significantly lower than in the other groups (Figure 3I; Field Size: Kruskal-Wallis test in N, $p = 0.0098$; Mann-Whitney test aGH-Control in N, $p = 0.0014$; Figure 3J; Sparseness: Kruskal-Wallis test, $p < 0.0001$; Mann-Whitney test $p < 0.0001$). The peak firing rate of the aGH animals was high throughout the experiments, including both the familiar environment sessions and the novel environment (Kruskal-Wallis test of peak firing rate in F', $p < 0.0001$; Mann-Whitney test aGH-Control in F', $p < 0.0001$).

Discussion

Changes in sensory information can update the hippocampal representation of space, and this process depends on the intrinsic properties of the network and endocrine modulation. In our study we report that GH can adjust the place cell representation concerning both the firing rate and the place field. In the familiar environment, blockage of the GH receptor by aGH changed the place cell firing. The peak rate and bursting increased, while the field size and sparseness decreased. When the animal explored a novel arena in the same room, the place cells kept firing high, with increased average firing rate, peak rate and information, and decreased field size and sparseness. The control animals displayed changes in rate overlap and rate changes in the novel environment, indicating rate remapping. However, the GH cells tended to induce global remapping instead, as the GH place fields lacked spatial correlation between the familiar and the novel environment. Since we have previously demonstrated that GH enhances hippocampal plasticity by using the same approach to manipulate the GH levels locally in the hippocampus (Haugland et al., 2020), we believe that the observed changes in firing rate and spatial correlation is due to the changed plasticity in the hippocampus.

The intrinsic plasticity of the hippocampus is important and affects the computation of incoming information to the place cells (Debanne and Poo, 2010, Cobar et al., 2017, Buzsaki and Tingley, 2018). Neuromodulators are perfect candidates to change the neural signaling as they can modulate the spike frequency and synaptic properties, to alter the functional and behavioral outcome (Edelmann et al., 2017, Palacios-Filardo and Mellor, 2019). Although very little is known about the GH as a neuromodulator, a plausible action of GH is to enhance novelty inputs to the place cells, as our study provide evidence for the lack of spatial correlation of place fields in the novel vs the familiar environment after the GH modulation. In global remapping, the experience in each environment become organized in separate spatial maps such that smaller changes to feature with an environment can be detected (Solstad et al., 2014). GH may therefore induce pattern separation processes to make the animal aware of subtle changes in the environment. While the stabilization of place cell representation after global remapping is associated with sensory information from the EC (Miao et al., 2015, Rueckemann et al., 2016, Kanter et al., 2017, Schlesiger et al., 2018), rate remapping in CA1 is proposed to depend on the information originating in the EC3 (Middleton and McHugh, 2016). We found that aGH impairs rate remapping which may be due to reduced novelty inputs or increased consolidation processed during the exploration.

Although the mechanisms of GH modulations are elusive, the actions of GH are associated with the NMDA receptor (Le Greves et al., 2006, Studzinski et al., 2015). The NMDA receptor is important for long-term stabilization of place cells (McHugh et al., 1996, Kentros et al., 1998), and GH is known to enhance excitatory transmission through NMDA receptors in the CA1 (Molina et al., 2013, Molina et al., 2012). By increasing the plasticity in CA1, the GH may increase the sensitivity for new information. Contrarily, enhanced stability is suggested to associated with higher peak rate (Cohen et al., 2017), which is what we see in the aGH animals. The altered base-line firing could suggest that the threshold for new sensory inputs is higher. This could also explain why the place cells of the aGH animals keep bursting high in the familiar environment. As aGH decrease the spine density in the CA1 (Haugland et al., 2020), increased bursting may be a mechanism for compensating for the reduction of spines.

Interestingly, aGH provided increased average firing of the place cells in the novel environment similar to what is reported in aged animals (Wilson et al., 2003, Wilson et al., 2005, Wilson et al., 2006). We have previously reported memory deficiency of aGH animals in the Morris water maze, which also have been described in aged animals (Gallagher et al., 1993). Since aGH seems to reduce hippocampal plasticity, our findings are in line with recent report claiming that low-firing rate place cells are more plastic (Grosmark and Buzsaki, 2016).

The increased firing rate observed in the aGH animals may represent rigidity of encoding due to failure in the dentate gyrus to reduce the similarity of input patterns sufficiently. Upon entry to a novel environment, the balance of incoming sensory and stored information force the hippocampal network to either settle upon the previously stored representation or to create a new representation. In our previous study (Haugland et al., 2020) we reported that aGH animals failed to locate the hidden platform location the first day, but with one day of extra learning, they remembered. In this study, we found that the place cells with increased levels of GH tended to induce global remapping instead of rate remapping in the novel environment, with only subtle changes. A possible explanation for this could be that GH induce pattern separation processes, which may be a mechanism of the enhanced hippocampal-dependent memory functions. The hippocampal effects of GH could resemble the effects of acetylcholine (ACh), as high ACh enhance the magnitude of afferent inputs, making the circuits responding stronger to EC information, which provides a stronger attention and encoding for new information. ACh also decreases excitatory feedback which can reduce

interference during retrieval and consolidation (Dannenberg et al., 2017). More experiments are however required to identify the detailed mechanisms of the GH actions in the hippocampus.

Acknowledgement

We are very grateful for receiving the opportunity to conduct the last experiments at The University of Bergen in the laboratory of Professor Janne Grønli, Head of Bergen Stress and Sleep Group. We kindly thank you Janne, and Anne Marie Kinn Rød and Nina Harkestad.

Figure text

Figure 1 Overexpression of growth hormone or the antagonizing growth hormone in the dorsal hippocampus

A) Upper illustration: Sagittal view of the rat brain illustrating the viral injections by recombinant adeno-associated viruses (rAAV)s to provide overexpression of growth hormone (GH) or antagonizing GH (GH). The tetrodes were placed in between viral injections in the dorsal hippocampus. Lower panel: Three coronal sections of the dorsal hippocampus with blue dotted lines showing the anteroposterior positions. The orange arrow head points at the tetrode traces in each hippocampus. The green fluorescent protein (GFP) in green indicate viral transfection. Scale bar: 1000 μm
B) Gene expression of the growth hormone 1 (*gh1*), not sensitive to the aGH mutation, shows that both GH and aGH animals have elevated *gh1* expression compared to controls.
C) Tetrode traces and GFP expression in representatives for each group, the GH, aGH and the control, respectively. Scale bar: 1000 μm
D) Sequencing the coding sequence (CDS) the G114R mutation was verified in the aGH and not in the GH.

Figure 2 Growth hormone modulation on place cell firing the a familiar environment

A) Time line of the experiment. The animals received surgeries with both viral injections and microdrive implantation. After a recovery period of one week, the animals were habituated to a square box (1 x 1 meter) with a local cue. When the animals were familiar to the environment (> 5 days in the box), place cells were separable during off-line analysis, and after the three weeks of incubation time for viral transfections, the animals were subjected to experiments.
B) The stabilization experiments consisted of two visits to the familiar environment separated by a 10 min break.
C) Representable place cells in each of the groups, with red illustrating the maximum firing location of the cells (place fields) while dark blue indicate firing rates (Hz) towards zero. All of the groups display place cells with stable place fields in the first (F) and the second (F') familiar environment.

D) The average firing rate (Hz) in the familiar (F) environment did not differ between the groups (Kruskal-Wallis test, $p = 0.7095$)

E) The peak rate (HZ) was significantly higher in the aGH group (Kruskal-Wallis test, $p < 0.0001$; Mann-Whitney test aGH-Control, $p < 0.0001$).

F) The aGH increased the bursting (%) in the familiar environment Kruskal-Wallis test, $p = 0.0012$; Mann-Whitney test aGH-Control, $p = 0.0014$).

G) The field size (dm^2) was smaller in the aGH cells (Kruskal-Wallis test, $p = 0.0022$; Mann-Whitney test aGH-Control, $p = 0.0024$).

H) The aGH decreased the sparseness (Kruskal-Wallis test, $p = 0.0494$; Mann-Whitney test aGH-Control, $p = 0.0455$).

I) The information did not differ between the groups (Kruskal-Wallis test, $p = 0.1412$)

Figure 3 Growth hormone modulates remapping in the hippocampus

A) Upper panel: Experimental design consisting of the familiar environment and a novel environment. The animals were first allowed to explore the familiar environment (F) before visiting a novel environment (N), and ending the experiment with exploring the familiar environment (F') again. Lower panel: Representative place cells in each group with the maximum firing rate (Hz) shown in red and minimum firing rate shown in blue. In the growth hormone animals, the place fields changed their spatial location between the familiar and novel environments, while aGH and controls displayed place cells that both kept and changed their place fields in the novel environment.

B) Spatial correlation between the familiar and novel environment shows that the GH place cells exhibit no spatial correlation in their place fields (Kruskal-Wallis test, $p = 0.0055$; Mann-Whitney test aGH-Control, $p = 0.0012$).

C) The spatial correlation between the familiar environments describes a positive spatial correlation of the place fields for all the groups (Kruskal-Wallis test, $p = 0.9195$).

D) The rate overlap between the familiar and novel environment indicate that the place cells of the controls were the only ones to rate remap (Mann-Whitney test aGH-Control, $p = 0.0258$). The GH group is illustrated in pink, aGH in blue and control in green.

E) The change in firing rate (Hz) provide further indications of the control place cells rate remapped as these cells changed their firing rates significantly between the familiar and novel environments (Mann-Whitney test aGH-Control, $p = 0.0359$).

F) aGH cells exhibit increased firing rate (Hz) in the novel environment (Kruskal-Wallis test, $p = 0.0194$; Mann-Whitney test aGH-Control, $p = 0.0146$).

G) aGH cells had a higher peak firing rate (Hz) throughout the experiments, including the familiar and novel environments (Kruskal-Wallis test in N, $p < 0.0001$; Mann-Whitney test aGH-Control in N, $p = 0.0007$; Kruskal-Wallis test in F', $p < 0.0001$; Mann-Whitney test aGH-Control in F', $p < 0.0001$).

H) aGH cells increased the bursting (%) in both the familiar environments (Kruskal-Wallis test in F', $p < 0.0001$; Mann-Whitney test aGH-Control in F', $p < 0.0001$), although it was not a significant change in the novel environment Kruskal-Wallis test in N, $p = 0.0529$)

I) The field size (dm^2) decreased in the aGH cells in novel environment (Kruskal-Wallis test in N, $p = 0.0098$; Mann-Whitney test aGH-Control in N, $p = 0.0014$).

J) The sparseness decreased the aGH cells in the novel environment.

K) aGH increased the information (bits/spike) in the novel environment.

References

AINGE, J. A., TAMOSIUNAITE, M., WORGOTTER, F. & DUDCHENKO, P. A. 2012. Hippocampal place cells encode intended destination, and not a discriminative stimulus, in a conditional T-maze task. *Hippocampus,* 22**,** 534-43.

ALLEN, K., RAWLINS, J. N., BANNERMAN, D. M. & CSICSVARI, J. 2012. Hippocampal place cells can encode multiple trial-dependent features through rate remapping. *J Neurosci,* 32**,** 14752-66.

ALME, C. B., MIAO, C., JEZEK, K., TREVES, A., MOSER, E. I. & MOSER, M. B. 2014. Place cells in the hippocampus: eleven maps for eleven rooms. *Proc Natl Acad Sci U S A,* 111**,** 18428-35.

ATHERTON, L. A., DUPRET, D. & MELLOR, J. R. 2015. Memory trace replay: the shaping of memory consolidation by neuromodulation. *Trends Neurosci,* 38**,** 560-70.

BRANDON, M. P., KOENIG, J., LEUTGEB, J. K. & LEUTGEB, S. 2014. New and distinct hippocampal place codes are generated in a new environment during septal inactivation. *Neuron,* 82**,** 789-96.

BUZSAKI, G. & TINGLEY, D. 2018. Space and Time: The Hippocampus as a Sequence Generator. *Trends Cogn Sci,* 22**,** 853-869.

COBAR, L. F., YUAN, L. & TASHIRO, A. 2017. Place cells and long-term potentiation in the hippocampus. *Neurobiol Learn Mem,* 138**,** 206-214.

COHEN, J. D., BOLSTAD, M. & LEE, A. K. 2017. Experience-dependent shaping of hippocampal CA1 intracellular activity in novel and familiar environments. *Elife,* 6.

COLGIN, L. L. 2020. Five Decades of Hippocampal Place Cells and EEG Rhythms in Behaving Rats. *J Neurosci,* 40**,** 54-60.

COLGIN, L. L., MOSER, E. I. & MOSER, M. B. 2008. Understanding memory through hippocampal remapping. *Trends Neurosci,* 31**,** 469-77.

DANNENBERG, H., YOUNG, K. & HASSELMO, M. 2017. Modulation of Hippocampal Circuits by Muscarinic and Nicotinic Receptors. *Front Neural Circuits,* 11**,** 102.

DEBANNE, D. & POO, M. M. 2010. Spike-timing dependent plasticity beyond synapse - pre- and post-synaptic plasticity of intrinsic neuronal excitability. *Front Synaptic Neurosci,* 2**,** 21.

EDELMANN, E., CEPEDA-PRADO, E. & LESSMANN, V. 2017. Coexistence of Multiple Types of Synaptic Plasticity in Individual Hippocampal CA1 Pyramidal Neurons. *Front Synaptic Neurosci,* 9**,** 7.

EICHENBAUM, H. 2017. The role of the hippocampus in navigation is memory. *J Neurophysiol,* 117**,** 1785-1796.

GALLAGHER, M., BURWELL, R. & BURCHINAL, M. 1993. Severity of spatial learning impairment in aging: development of a learning index for performance in the Morris water maze. *Behav Neurosci,* 107**,** 618-26.

GROSMARK, A. D. & BUZSAKI, G. 2016. Diversity in neural firing dynamics supports both rigid and learned hippocampal sequences. *Science,* 351**,** 1440-3.

HAUGLAND, K. G., OLBERG, A., LANDE, A., KJELSTRUP, K. B. & BRUN, V. H. 2020. Hippocampal growth hormone modulates relational memory and the dendritic spine density in CA1. *Learn Mem,* 27**,** 33-44.

KANTER, B. R., LYKKEN, C. M., AVESAR, D., WEIBLE, A., DICKINSON, J., DUNN, B., BORGESIUS, N. Z., ROUDI, Y. & KENTROS, C. G. 2017. A Novel Mechanism for the Grid-to-Place Cell Transformation Revealed by Transgenic Depolarization of Medial Entorhinal Cortex Layer II. *Neuron,* 93**,** 1480-1492 e6.

KENTROS, C., HARGREAVES, E., HAWKINS, R. D., KANDEL, E. R., SHAPIRO, M. & MULLER, R. V. 1998. Abolition of long-term stability of new hippocampal place cell maps by NMDA receptor blockade. *Science,* 280**,** 2121-6.

KENTROS, C. G., AGNIHOTRI, N. T., STREATER, S., HAWKINS, R. D. & KANDEL, E. R. 2004. Increased attention to spatial context increases both place field stability and spatial memory. *Neuron,* 42**,** 283-95.

KIM, E., GROVER, L. M., BERTOLOTTI, D. & GREEN, T. L. 2010. Growth hormone rescues hippocampal synaptic function after sleep deprivation. *Am. J. Physiol Regul. Integr. Comp Physiol,* 298**,** R1588-R1596.

LATUSKE, P., KORNIENKO, O., KOHLER, L. & ALLEN, K. 2017. Hippocampal Remapping and Its Entorhinal Origin. *Front Behav Neurosci,* 11**,** 253.

LE GREVES, M., ZHOU, Q., BERG, M., LE GREVES, P., FHOLENHAG, K., MEYERSON, B. & NYBERG, F. 2006. Growth hormone replacement in hypophysectomized rats affects spatial performance and hippocampal levels of NMDA receptor subunit and PSD-95 gene transcript levels. *Exp. Brain Res,* 173**,** 267-273.

LEUTGEB, S., LEUTGEB, J. K., BARNES, C. A., MOSER, E. I., MCNAUGHTON, B. L. & MOSER, M. B. 2005. Independent codes for spatial and episodic memory in hippocampal neuronal ensembles. *Science,* 309**,** 619-23.

LEUTGEB, S., LEUTGEB, J. K., TREVES, A., MOSER, M. B. & MOSER, E. I. 2004. Distinct ensemble codes in hippocampal areas CA3 and CA1. *Science,* 305**,** 1295-8.

LISMAN, J., BUZSAKI, G., EICHENBAUM, H., NADEL, L., RANGANATH, C. & REDISH, A. D. 2017. Viewpoints: how the hippocampus contributes to memory, navigation and cognition. *Nat Neurosci,* 20**,** 1434-1447.

MCHUGH, T. J., BLUM, K. I., TSIEN, J. Z., TONEGAWA, S. & WILSON, M. A. 1996. Impaired hippocampal representation of space in CA1-specific NMDAR1 knockout mice. *Cell,* 87**,** 1339-49.

MIAO, C., CAO, Q., ITO, H. T., YAMAHACHI, H., WITTER, M. P., MOSER, M. B. & MOSER, E. I. 2015. Hippocampal Remapping after Partial Inactivation of the Medial Entorhinal Cortex. *Neuron,* 88**,** 590-603.

MIDDLETON, S. J. & MCHUGH, T. J. 2016. Silencing CA3 disrupts temporal coding in the CA1 ensemble. *Nat Neurosci,* 19**,** 945-51.

MOLINA, D. P., ARIWODOLA, O. J., LINVILLE, C., SONNTAG, W. E., WEINER, J. L., BRUNSO-BECHTOLD, J. K. & ADAMS, M. M. 2012. Growth hormone modulates hippocampal excitatory synaptic transmission and plasticity in old rats. *Neurobiol. Aging,* 33**,** 1938-1949.

MOLINA, D. P., ARIWODOLA, O. J., WEINER, J. L., BRUNSO-BECHTOLD, J. K. & ADAMS, M. M. 2013. Growth hormone and insulin-like growth factor-I alter hippocampal excitatory synaptic transmission in young and old rats. *Age (Dordr),* 35**,** 1575-87.

MOSER, M. B., ROWLAND, D. C. & MOSER, E. I. 2015. Place cells, grid cells, and memory. *Cold Spring Harb Perspect Biol,* 7**,** a021808.

MULLER, R. U. & KUBIE, J. L. 1987. The effects of changes in the environment on the spatial firing of hippocampal complex-spike cells. *J Neurosci,* 7**,** 1951-68.

O'KEEFE, J. & DOSTROVSKY, J. 1971. The hippocampus as a spatial map. Preliminary evidence from unit activity in the freely-moving rat. *Brain Res,* 34**,** 171-175.

O'NEILL, J., SENIOR, T. J., ALLEN, K., HUXTER, J. R. & CSICSVARI, J. 2008. Reactivation of experience-dependent cell assembly patterns in the hippocampus. *Nat Neurosci,* 11**,** 209-15.

PALACIOS-FILARDO, J. & MELLOR, J. R. 2019. Neuromodulation of hippocampal long-term synaptic plasticity. *Curr Opin Neurobiol,* 54**,** 37-43.

RUECKEMANN, J. W., DIMAURO, A. J., RANGEL, L. M., HAN, X., BOYDEN, E. S. & EICHENBAUM, H. 2016. Transient optogenetic inactivation of the medial entorhinal cortex biases the active population of hippocampal neurons. *Hippocampus,* 26**,** 246-60.

SANDERS, H., JI, D., SASAKI, T., LEUTGEB, J. K., WILSON, M. A. & LISMAN, J. E. 2019. Temporal coding and rate remapping: Representation of nonspatial information in the hippocampus. *Hippocampus,* 29**,** 111-127.

SCHLESIGER, M. I., BOUBLIL, B. L., HALES, J. B., LEUTGEB, J. K. & LEUTGEB, S. 2018. Hippocampal Global Remapping Can Occur without Input from the Medial Entorhinal Cortex. *Cell Rep,* 22**,** 3152-3159.

SHAPIRO, M. 2001. Plasticity, hippocampal place cells, and cognitive maps. *Arch Neurol,* 58**,** 874-81.

SKAGGS, W. E., MCNAUGHTON, B. L., WILSON, M. A. & BARNES, C. A. 1996. Theta phase precession in hippocampal neuronal populations and the compression of temporal sequences. *Hippocampus,* 6**,** 149-72.

SOLSTAD, T., YOUSIF, H. N. & SEJNOWSKI, T. J. 2014. Place cell rate remapping by CA3 recurrent collaterals. *PLoS Comput Biol,* 10**,** e1003648.

STUDZINSKI, A. L., BARROS, D. M. & MARINS, L. F. 2015. Growth hormone (GH) increases cognition and expression of ionotropic glutamate receptors (AMPA and NMDA) in transgenic zebrafish (Danio rerio). *Behav Brain Res,* 294**,** 36-42.

TELES-GRILO RUIVO, L. M. & MELLOR, J. R. 2013. Cholinergic modulation of hippocampal network function. *Front Synaptic Neurosci,* 5**,** 2.

THOMPSON, L. T. & BEST, P. J. 1989. Place cells and silent cells in the hippocampus of freely-behaving rats. *J Neurosci,* 9**,** 2382-90.

TRAN, A. H., UWANO, T., KIMURA, T., HORI, E., KATSUKI, M., NISHIJO, H. & ONO, T. 2008. Dopamine D1 receptor modulates hippocampal representation plasticity to spatial novelty. *J Neurosci,* 28**,** 13390-400.

WILSON, I. A., GALLAGHER, M., EICHENBAUM, H. & TANILA, H. 2006. Neurocognitive aging: prior memories hinder new hippocampal encoding. *Trends Neurosci,* 29**,** 662-670.

WILSON, I. A., IKONEN, S., GALLAGHER, M., EICHENBAUM, H. & TANILA, H. 2005. Age-associated alterations of hippocampal place cells are subregion specific. *J. Neurosci,* 25**,** 6877-6886.

WILSON, I. A., IKONEN, S., MCMAHAN, R. W., GALLAGHER, M., EICHENBAUM, H. & TANILA, H. 2003. Place cell rigidity correlates with impaired spatial learning in aged rats. *Neurobiol. Aging,* 24**,** 297-305.

WOOD, E. R., DUDCHENKO, P. A., ROBITSEK, R. J. & EICHENBAUM, H. 2000. Hippocampal neurons encode information about different types of memory episodes occurring in the same location. *Neuron,* 27**,** 623-33.

Figure 1

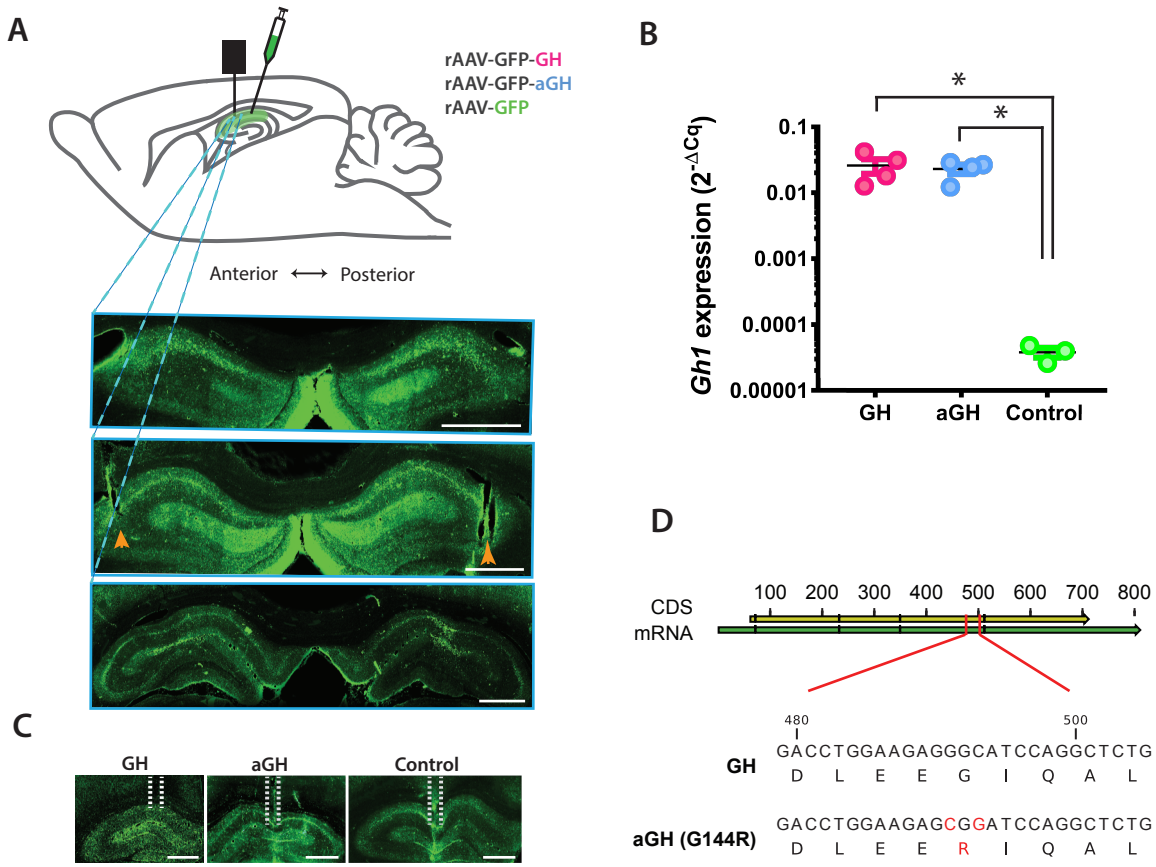
A
rAAV-GFP-GH
rAAV-GFP-aGH
rAAV-GFP
Anterior ⟷ Posterior
B
Gh1 expression (2-ΔCq)
0.1
0.01
0.001
0.0001
0.00001
*
*
GH
aGH
Control
C
GH
aGH
Control
D
CDS
mRNA
100 200 300 400 500 600 700 800
480
500
GH
GACCTGGAAGAGGGCATCCAGGCTCTG
D L E E G I Q A L
aGH (G144R)
GACCTGGAAGAGCGGATCCAGGCTCTG
D L E E R I Q A L

Figure 2

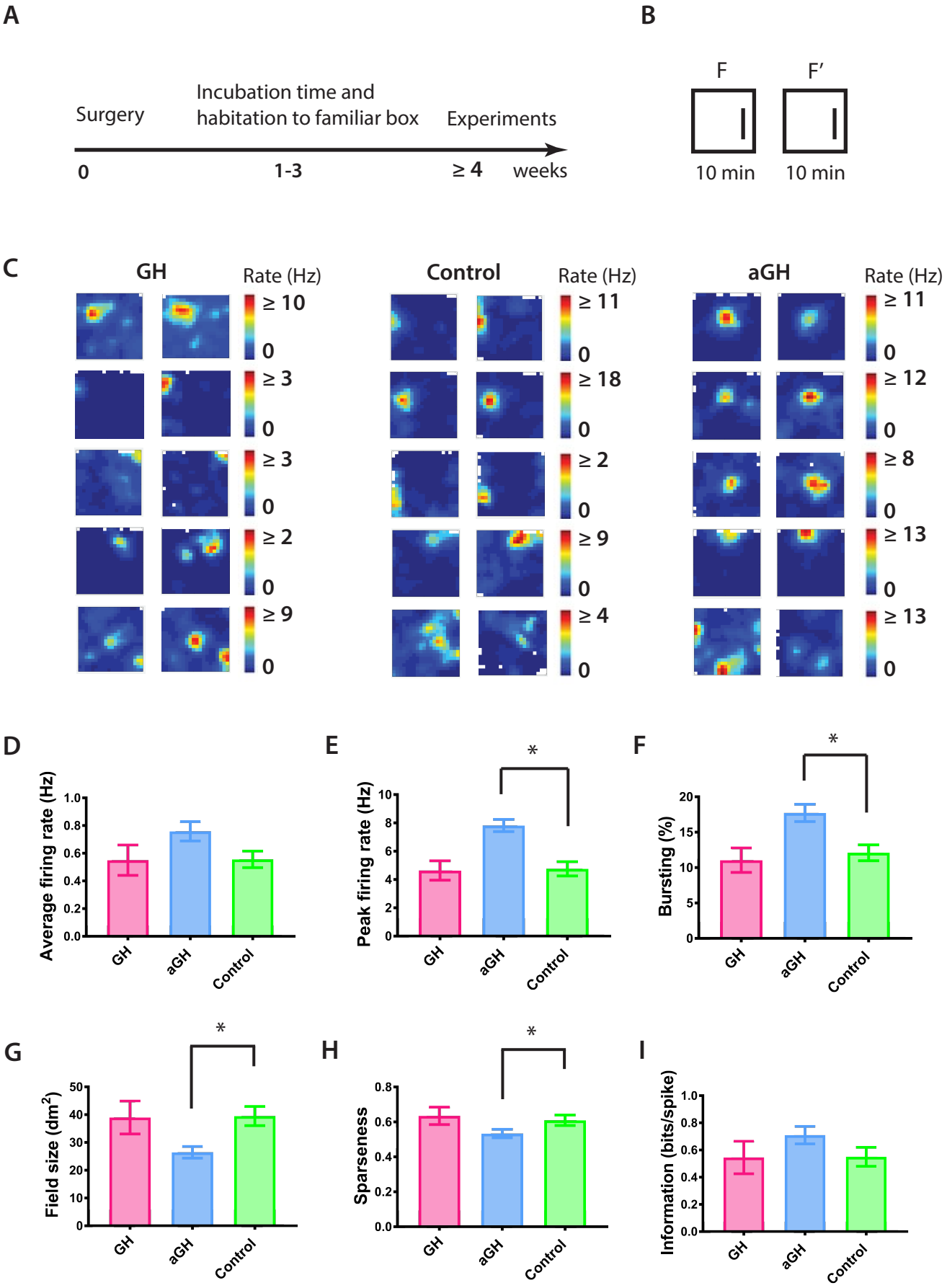
A
Surgery
Incubation time and habitation to familiar box
Experiments
0
1-3
≥ 4
weeks
B
F
F'
10 min
10 min
C
GH
Rate (Hz)
≥ 10
0
≥ 3
0
≥ 3
0
≥ 2
0
≥ 9
0
Control
Rate (Hz)
≥ 11
0
≥ 18
0
≥ 2
0
≥ 9
0
≥ 4
0
aGH
Rate (Hz)
≥ 11
0
≥ 12
0
≥ 8
0
≥ 13
0
≥ 13
0
D
Average firing rate (Hz)
1.0
0.8
0.6
0.4
0.2
0.0
GH
aGH
Control
E
*
Peak firing rate (Hz)
10
8
6
4
2
0
GH
aGH
Control
F
*
Bursting (%)
20
15
10
5
0
GH
aGH
Control
G
*
Field size (dm2)
50
40
30
20
10
0
GH
aGH
Control
H
*
Sparseness
0.8
0.6
0.4
0.2
0.0
GH
aGH
Control
I
Information (bits/spike)
1.0
0.8
0.6
0.4
0.2
0.0
GH
aGH
Control

Figure 3

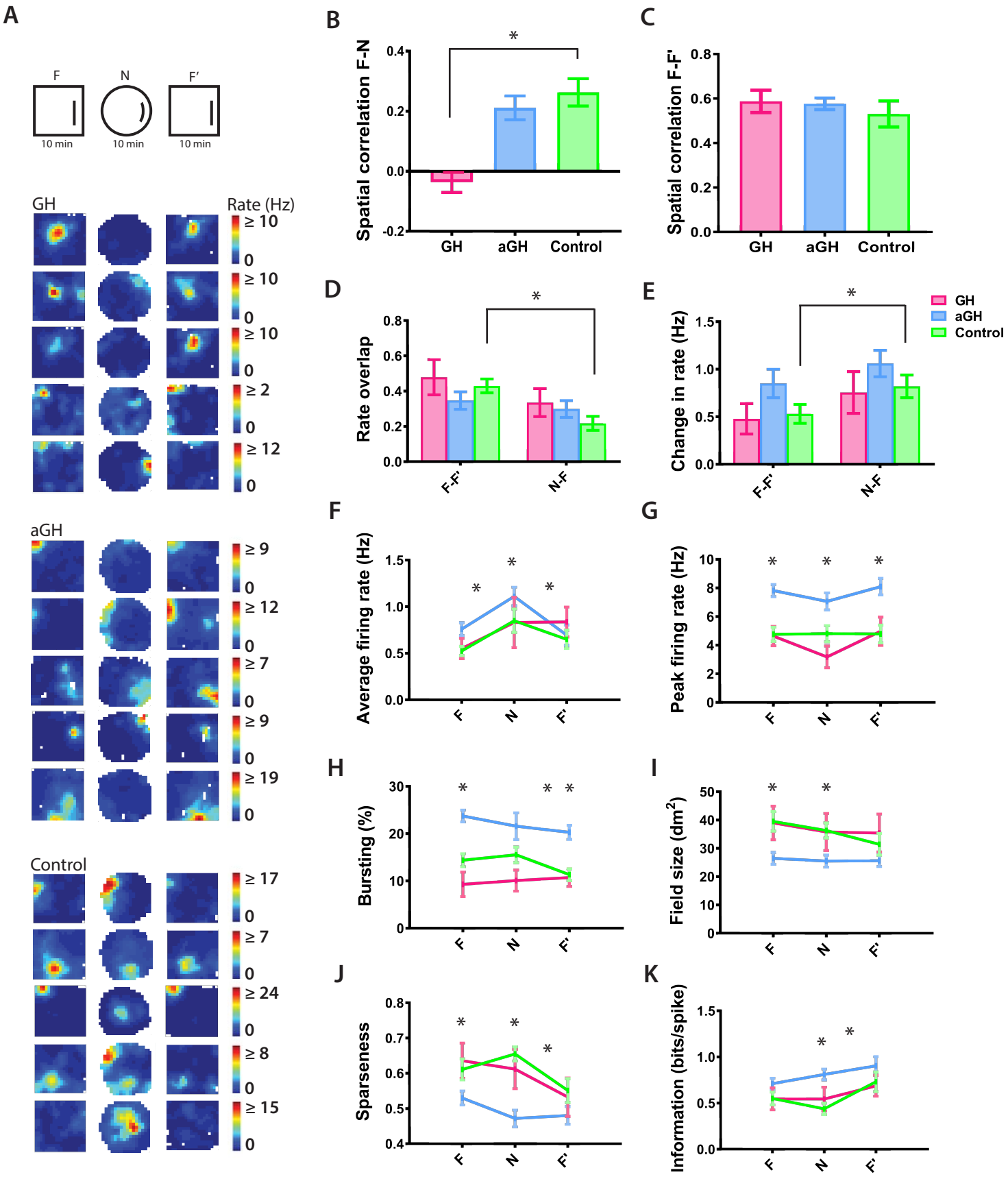
A
F
N
F'
10 min
10 min
10 min
GH
Rate (Hz)
≥ 10
0
≥ 10
0
≥ 10
0
≥ 2
0
≥ 12
0
aGH
≥ 9
0
≥ 12
0
≥ 7
0
≥ 9
0
≥ 19
0
Control
≥ 17
0
≥ 7
0
≥ 24
0
≥ 8
0
≥ 15
0
B
Spatial correlation F-N
0.4
0.2
0.0
-0.2
*
GH
aGH
Control
C
Spatial correlation F-F'
0.8
0.6
0.4
0.2
0.0
GH
aGH
Control
D
Rate overlap
0.8
0.6
0.4
0.2
0.0
*
F-F'
N-F
E
Change in rate (Hz)
1.5
1.0
0.5
0.0
*
F-F'
N-F
GH
aGH
Control
F
Average firing rate (Hz)
1.5
1.0
0.5
0.0
*
*
*
F
N
F'
G
Peak firing rate (Hz)
10
8
6
4
2
0
*
*
*
F
N
F'
H
Bursting (%)
30
20
10
0
*
*
*
F
N
F'
I
Field size (dm²)
50
40
30
20
10
0
*
*
F
N
F'
J
Sparseness
0.8
0.7
0.6
0.5
0.4
*
*
*
F
N
F'
K
Information (bits/spike)
1.5
1.0
0.5
0.0
*
*
F
N
F'

All statistics for manuscript Haugland et al. 2021

Figure no	Test used	n		df	p-value	
		exact number	defined as			
qPCR				All t values are absolute values		
IB	One-Way ANOVA with Bonferroni Post Hoc	4, 4, 3	animals	F(2,8) = 7.774	**0.0113**	*passed normaity test
IB	Unpaired two-tailed t-test GH - Control	4, 3	animals	t(3,343) = 5	**0,0205**	
IB	Unpaired two-tailed t-test aGH - Control	4, 3	animals	t(5,236) = 5	**0,0034**	
Place cell firing in familiar environment						
2D	**Average firing rate**					
2D	Kruskal-Wallis test	29, 119, 69	neurons	K = 0.6864	0.7095	*Not passed normaility test
2D	Mann-Whitney test two-tailed aGH - Control	119, 69	neurons	U = 3864	0.0524	
2E	**Peak firing rate**					
2E	Kruskal-Wallis test	29, 119, 69	neurons	K = 28.38	**<0.0001**	
2E	Mann-Whitney test two-tailed aGH - Control	119, 69	neurons	U = 23.84	**<0.0001**	
2F	**Bursting**					
2F	Kruskal-Wallis test	29, 119, 69	neurons	K = 13.38	**0.0012**	
2F	Mann-Whitney test two-tailed aGH - Control	119, 69	neurons	U = 2963	**0.0014**	
2G	**Field size**					
2G	Kruskal-Wallis test	29, 119, 69	neurons	K = 12.250	**0.0022**	
2G	Mann-Whitney test two-tailed aGH - Control	119, 69	neurons	U = 3820	**0.0024**	
2H	**Sparseness**					
2H	Kruskal-Wallis test	29, 119, 69	neurons	K = 6.016	**0.0494**	
2H	Mann-Whitney test two-tailed aGH - Control	119, 69	neurons	U = 3387	**0.0455**	
2I	**Information**					
2I	Kruskal-Wallis test	29, 119, 69	neurons	K = 3.915	0.1412	
Place cell firing in novel environment						
	Spatial correlation in FAM-NOV					
3B	Kruskal-Wallis test of 1-way ANOVA NOV-FAM	15, 49, 65	neurons	K = 10.4	**0.0055**	
	Mann-Whitney test two-tailed GH - Control	15, 49, 65	neurons	W = 168.5	**0.0012**	
3C	**Spatial correlation in FAM-FAM'**					
3C	Kruskal-Wallis test of 1-way ANOVA FAM-FAM	15, 49, 65	neurons	K = 0.1679	0.9195	
3D	**Rate overlap**					
3D	Mann-Whitney test one-tailed paired Control NF - FF	41, 34	neurons	W = 248	**0.0258**	
3D	Mann-Whitney test one-tailed paired aGH NF - FF	49, 41	neurons	W = 9	0.4719	
3D	Mann-Whitney test one-tailed paired GH NF - FF	9, 7	neurons	W = 9	0.2188	
3E	**Asolute rate difference**					
3E	Mann-Whitney test one-tailed paired Control NF - FF	41, 34	neurons	W = -230	**0.0359**	
3E	Mann-Whitney test one-tailed paired aGH NF - FF	49, 41	neurons	W = -89	0.2184	
3E	Mann-Whitney test one-tailed paired GH NF - FF	9, 7	neurons	W = -6	0.3438	
3D	**Average firing rate**					
3D	Kruskal-Wallis test of 1-way ANOVA NOV	29, 119, 69	neurons	K = 7.885	**0.0194**	
3D	Kruskal-Wallis test of 1-way ANOVA FAM'	29, 119, 69	neurons	K = 3.931	0.1401	
3D	Mann-Whitney test two-tailed aGH - Control NOV	119, 69	neurons	U = 1793	**0.0146**	
3D	Mann-Whitney test two-tailed Control FAM- NOV	69, 69	neurons	U = 2043	0.5541	
3D	Mann-Whitney test two-tailed Control NOV-FAM	69, 69	neurons	U = 1749	0.4761	
3D	Mann-Whitney test two-tailed aGH FAM-NOV	119, 119	neurons	U = 3222	**0.0010**	
3D	Mann-Whitney test two-tailed aGH NOV-FAM'	119, 119	neurons	U = 1790	**<0.0001**	
	Mann-Whitney test two-tailed GH FAM-FAM'	29, 29	neurons	U = 287.5	0.1964	
3E	**Peak firing rate**					
3E	Kruskal-Wallis test of 1-way ANOVA NOV	29, 119, 69	neurons	K = 18.88	**<0.0001**	
3E	Kruskal-Wallis test of 1-way ANOVA FAM'	29, 119, 69	neurons	K = 23.99	**<0.0001**	
3E	Mann-Whitney test two-tailed GH - Control NOV	29, 69	neurons	U = 393	0.0951	
3E	Mann-Whitney test two-tailed aGH - Control NOV	119, 69	neurons	U = 1581	**0.0007**	
3E	Mann-Whitney test two-tailed aGH - Control FAM	119, 69	neurons	U = 1963	**<0.0001**	
3E	Mann-Whitney test two-tailed aGH NOV-FAM'	119, 119	neurons	U = 3761	0.2271	
3E	Mann-Whitney test two-tailed aGH FAM-NOV	119, 119	neurons	U = 3877	0.1246	
3E	Mann-Whitney test two-tailed GH FAM-NOV	29, 29	neurons	U = 175	0.1067	
3E	Mann-Whitney test two-tailed GH NOV-FAM'	29, 29	neurons	U = 155	0.1455	
3F	**Bursting**					
3F	Kruskal-Wallis test of 1-way ANOVA NOV	29, 119, 69	neurons	K = 5.879	0.0529	
3F	Kruskal-Wallis test of 1-way ANOVA FAM'	29, 119, 69	neurons	K = 22.45	**<0.0001**	
3F	Mann-Whitney test two-tailed aGH - Control FAM'	119, 69	neurons	U = 2107	**<0.0001**	
3F	Mann-Whitney test two-tailed aGH FAM-FAM'	119, 119	neurons	U = 6139	0.3010	
3F	Mann-Whitney test two-tailed control FAM-FAM'	69, 69	neurons	U = 1916	0.4691	
3F	Mann-Whitney test two-tailed control NOV-FAM'	69, 69	neurons	U = 1403	**0.0134**	
3G	**Field size**					
3G	Kruskal-Wallis test of 1-way ANOVA NOV	29, 119, 69	neurons	K = 9.252	**0.0098**	
3G	Kruskal-Wallis test of 1-way ANOVA FAM'	29, 119, 69	neurons	K = 197	0.8375	
3G	Mann-Whitney test two-tailed aGH - Control NOV	29, 69	neurons	U = 1622	**0.0014**	
3H	**Sparseness**					
3H	Kruskal-Wallis test of 1-way ANOVA NOV	29, 119, 69	neurons	K = 23.7	**<0.0001**	
3H	Kruskal-Wallis test of 1-way ANOVA FAM'	29, 119, 69	neurons	K = 2.77	0.2504	
3H	Mann-Whitney test two-tailed aGH - Control NOV	119, 69	neurons	U = 1248	**<0.0001**	
	Mann-Whitney test two-tailed Control NOV-FAM'	69, 69	neurons	U = 1436	**0.0213**	
	Mann-Whitney test two-tailed Control FAM-NOV	69, 69	neurons	U = 1949	0.3069	
	Mann-Whitney test two-tailed aGH FAM-NOV	119, 119	neurons	U 3836	0.0999	
	Mann-Whitney test two-tailed aGH FAM-FAM'	119, 119	neurons	U = 5893	0.1288	
	Mann-Whitney test two-tailed control FAM-FAM'	69, 69	neurons	U = 1791	0.1880	
	Mann-Whitney test two-tailed GH FAM-FAM'	29, 29	neurons	U = 276.5	0.1377	

3I **Information**

Kruskal-Wallis test of 1-way ANOVA NOV	29, 119, 69	neurons	K = 24.26	**<0.0001**
Kruskal-Wallis test of 1-way ANOVA FAM'	29, 119, 69	neurons	K = 1.732	0.4205
Mann-Whitney test two-tailed aGH - Control NOV	119, 69	neurons	U = 1237	**<0.0001**
Mann-Whitney test two-tailed control NOV-FAM'	69, 69	neurons	U = 1461	**0.0297**
Mann-Whitney test two-tailed aGH NOV-FAM'	119, 119	neurons	U = 3786	0.2547
Mann-Whitney test two-tailed aGH FAM-FAM'	119, 119	neurons	U = 5930	0.1485
Mann-Whitney test two-tailed control FAM-FAM'	69, 69	neurons	U =1774	0.1624